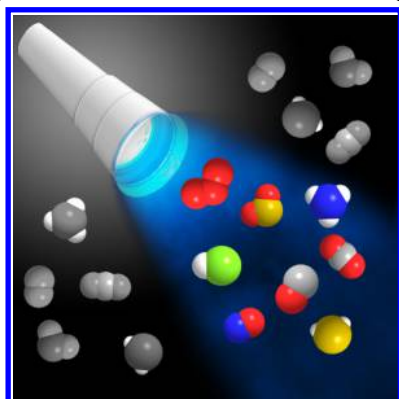# Recent Progress on the Development of Chemosensors for Gases

Xin Zhou,[†,‡] Songyi Lee,[†] Zhaochao Xu,*[,§] and Juyoung Yoon*[,†]

[†]Department of Chemistry and Nanoscience, Ewha Womans University, Seoul 120-750, Republic of Korea

[‡]Research Center for Chemical Biology, Department of Chemistry, Yanbian University, Yanjii 133002, People's Republic of China

[§]Key Laboratory of Separation Science for Analytical Chemistry, Dalian Institute of Chemical Physics, Chinese Academy of Sciences, 457 Zhongshan Road, Shahekou, Dalian, Liaoning, People's Republic of China

CONTENTS

1. INTRODUCTION

In the past few decades, the development of chemosensors has become an important research topic in supramolecular analytical chemistry, and as a result, it has attracted the continuous interest of academic researchers in chemistry and biology.[1−27] Chemosensors are chemical systems that convert chemical stimuli into some form of response that can be easily detected, such as a fluorescent or color change or an electronic signal. Numerous reports have demonstrated that chemosensors can be used as simple and sensitive detecting tools for a variety of analytes, which cannot be detected by utilizing traditional methods, especially when they are located in extreme and complicated environmental or biological systems.

A greatly growing demand exists for sensors that detect and monitor gases over the broad range of often-regulated concentrations in environmental and biological systems. The many uses of sensors of this type include monitoring air quality, detecting volatile organic compounds,[28,29] diagnosing clinical diagnosis gases,[30−32] detecting toxic gases including chemical-warfare agents,[33−36] and controlling fossil fuel combustion products arising from industrial sources and automobile engines.[37−39] Generally, the most common and typical methods that have been developed for the purpose of detecting gases and volatile compounds are mainly based on high-performance liquid chromatography (HPLC) and gas chromatography (GC).[40−42] However, it is well known to us that these techniques are time consuming and quite expensive. Thus, simple and convenient methods for this purpose are in great

demand. Consequently, the development of chemosensors for gases is considered to be a significant goal in science.

Numerous investigations related to the topic of gas sensing have been carried out to date. These efforts have been summarized in several excellent reviews focusing on sensor materials or targeting gases.[28,43−48] For example, Wenger recently compiled a scholarly review on the topic of "Vapochromism in Organometallic and Coordination Complexes: Chemical Sensors for Volatile Organic Compounds", which was written from the perspective of a coordination chemist.[28] Potyrailo presented a thorough review on "Materials and Transducers Toward Selective Wireless Gas Sensing", which summarizes recent progress on wireless gas sensors.[43] A review by Llobet covers recent progress made on the development of gas sensors based on carbon nanomaterials,[44] and a review on gas sensors based on nanostructured oxide semiconductor materials was written by Ho.[48] Recent progress on development of fluorescent sensors for sensing and imaging biological hydrogen sulfide was reviewed by Chang,[49] and Yoon summarized recent progress that has been made in studies of fluorescent sensors for the detection of reactive oxygen and nitrogen species.[5] Despite their large number and complete coverage, these reviews focus only on specific topics, and consequently, no comprehensive review has appeared presenting the state-of-the-art view of gas chemosensors from a holistic perspective.

In this review, we attempt to describe investigations of gas chemosensors carried out in recent decades in a systematic and inclusive manner. The coverage of this topic is divided into three sections according to the different types of chemosensors, including those that are based on newly designed fluorescent organic molecules, semiconducting oxides, as well as nanomaterials. In each section, discussion is organized to cover the different characteristics and/or sources of the gases, exemplified by those involved in environmental exhausts (CO_2, SO_2, NOx, VOCs), biological signaling (H_2S, NO, $^1O_2$), and toxic uses (nerve gases, sulfur mustard). In addition, design strategies, sensing mechanisms and performances, and related applications of chemosensors are also discussed in detail. The goal of the current review is to present comprehensive coverage of recent progress that has been made in studies targeted at the design and development of chemosensors for gases and, by doing so, to stimulate future research studies in this rapidly expanding multidisciplinary area.

2. CHEMOSENSORS BASED ON FLUORESCENT MOLECULES

Because of their simplicity, sensitivity, and especially non-destructive detection capabilities, fluorescence-based detecting techniques have emerged as an essential tool for sensing targeted analytes in the environment and in vivo.[1−13] The main hurdle for fluorescent techniques is how to construct fluorescent sensors with high selectivity, sensitivity, and stability. In the past decades, the development of fluorescent sensors based on organic molecules has drawn attention due to their various advantages, including easy synthesis, structural controllability, high fluorescence quantum yields, and biocompatibility. To date, the construction of fluorescent sensors has become a new multidisciplinary research field involving organic synthesis, analytical chemistry, and biology. Herein, we present a survey on recent progress in emerged fluorescent sensors used for the detection of gases which are widely distributed in the environment and in the biological system.

2.1. Sensors for Environment Exhaust Gases

2.1.1. Sensors for CO_2. Carbon dioxide (CO_2) is a major public concern with widespread discussion because of its role in global greenhouse warming.[50] Moreover, CO_2 is also quite critical to the modern agricultural, food, environmental, oil, and chemical industries. However, it is well known that it is dangerous for living beings to stay at high concentration levels of CO_2.[51] Therefore, the importance and prevalence of such a gas (CO_2) provides an incentive for development of new methods that can be used for the rapid and selective detection and monitoring of this relatively inert gas both in the gaseous and in the liquid phases. Some traditional detection methods, such as electrochemical and infrared spectroscopic techniques, are usually employed for CO_2 sensing and detection; however, these methods are believed to be expensive and time consuming. Hence, the development of chemosensors for determining the concentration level of CO_2 is of great interest.

2.1.1.1. pH Indicator-Based Sensors. This strategy of using pH indicators was first employed in the construction of fluorescent sensors for CO_2. As described in Figure 1, CO_2
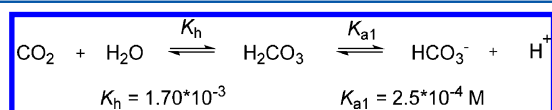
Figure 1. Hydration equilibrium constant (K_h) and the first acid dissociation constant (K_{a1}) of carbonic acid.

displays a reversible equilibrium between its gas form and carbonic acid (H_2CO_3). The hydration equilibrium constant of H_2CO_3 is $K_h = 1.70 \times 10^{-3}$ at room temperature. In contrast, the first acid dissociation constant for the dissociation of H_2CO_3 into hydrogen carbonate (HCO_3^-) is $K_{a1} = 2.5 \times 10^{-4}$ M. Since its ionization in water is incomplete, H_2CO_3 is a weak acid. It thus gives a fluorescent response with pH indicators. Early fluorescent sensors for CO_2 were based on this strategy.

The most common pH indicator used for sensing CO_2 is 1-hydroxypyrene-3,6,8-trisulfonate (HPTS), as shown in Figure 2
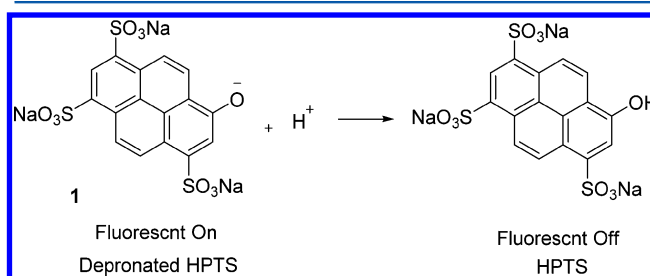
Figure 2. Structures of pH indicator (**1**) as a CO_2 sensor.

as indicator **1**. For instance, Sampathkumaran et al. reported the development of a sol−gel fluorescent sensor for detecting CO_2 with a sensitivity below the amount in the atmosphere (ca. 387 ppm) (Figure 2).[52] In this work, a sol−gel fluorescent sensor was modified into silica-doped matrix with **1** by spin coating on glass slides. The fluorescent intensity of this indicator (513 nm) was quenched by CO_2 as a result of protonations of the anionic form.

Diketopyrrolo-pyrrole (DPP) has been actively utilized as a core for various chemosensors since it not only acts as a core for conjugating system but also contains an acidic NH group,[53,54] resulting in colorimetric and fluorescent responses
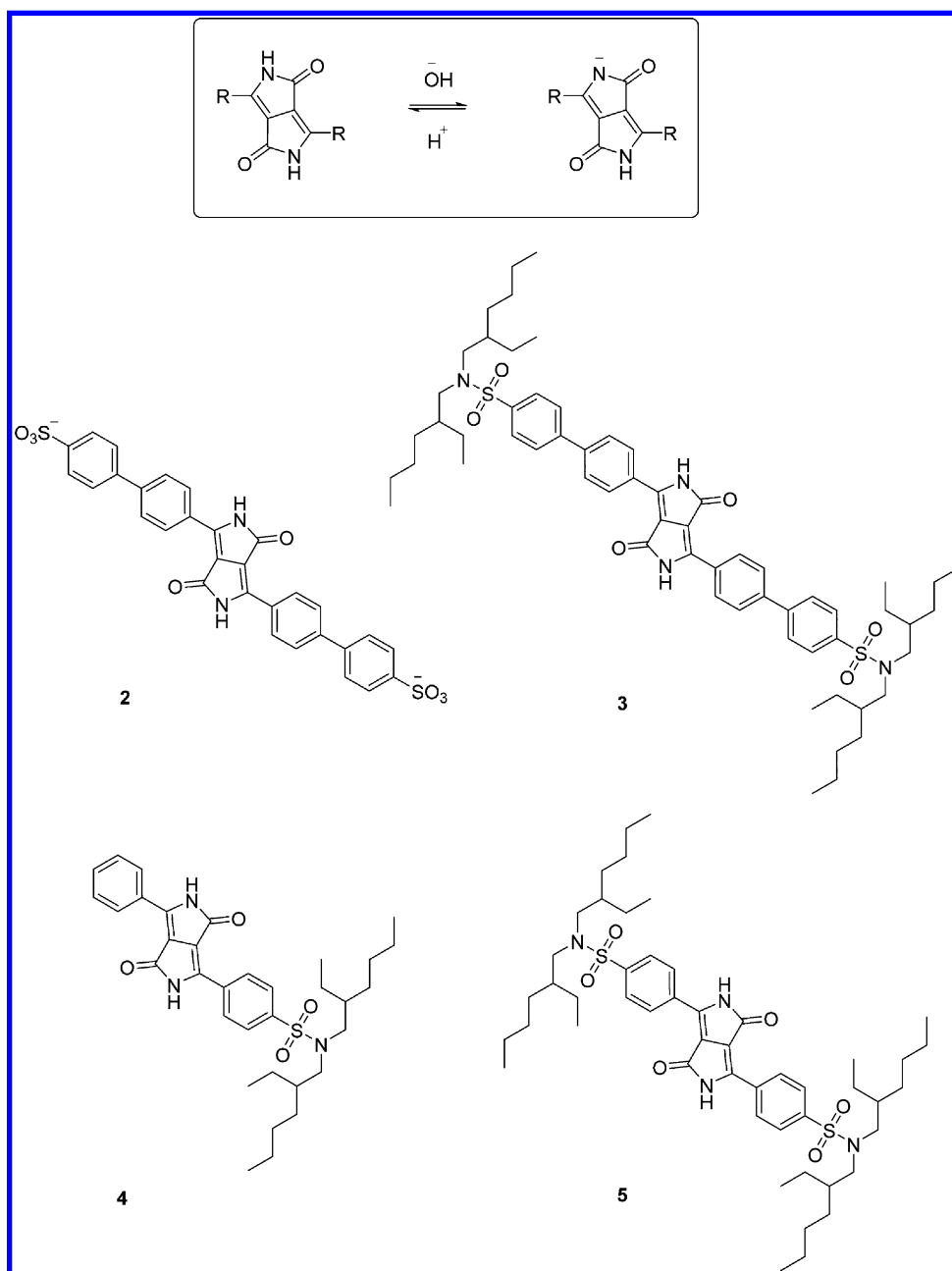
Figure 3. Structures of pH indicator (DPP) and DPP-based CO$_2$ sensors **2–5**.
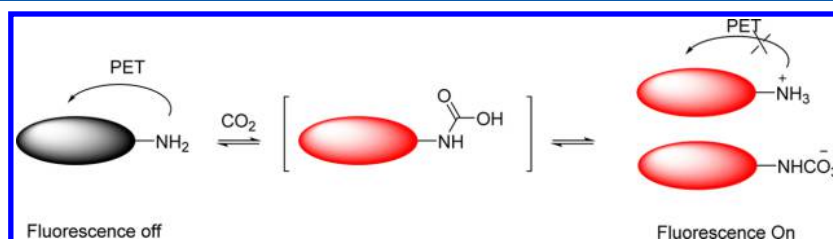
Figure 4. Strategy of PET-based chemosensor for CO$_2$.

to pH values, as shown in Figure 3. Borisov et al. reported the commercially available DPP-based pH-sensitive indicator for sensing CO$_2$.[55] As shown in Figure 3, sensors **2–5** showed strong absorbance and gave emissions in their neutral and deprotonated forms. Furthermore, the performance of these sensors was evaluated for their application as CO$_2$ sensors. The

absorption and emission spectra of the deprotonated forms showed a red shift (over 100 nm) compared to their neutral forms, resulting in a blue color in the absence of CO$_2$ and a pink color in the presence of CO$_2$ with a concomitant fluorescence color change from deep red to orange.

C
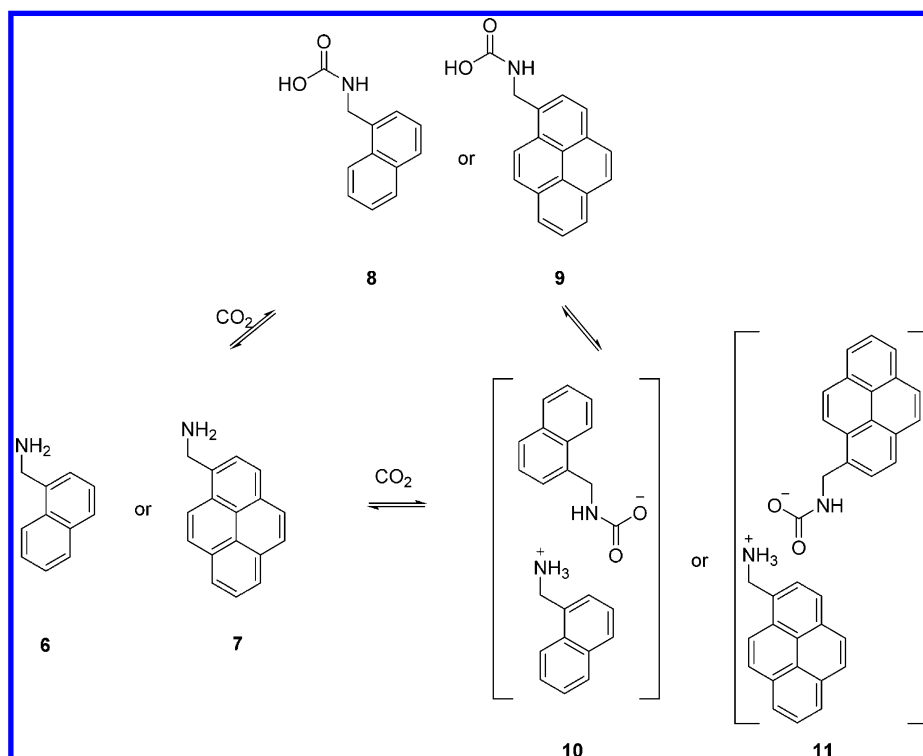
Figure 5. Structures of sensors (**6, 7**) and their reversible covalent bonding of CO_2.

2.1.1.2. Amine-Based Sensors. Another strategy was developed based on the chemical reaction between amine and CO_2 in which CO_2 is a weak electrophile that can react with an active basic amine to form corresponding carbamate salt and ammonium salt. On the basis of this chemical mechanism, a series of fluorescent sensors has been achieved to date. One approach is directly inserting an amine group (reaction group) into the conjugated fluorophore as shown in Figure 4. In this case, the sensor is nonfluorescent or weakly fluorescent since the fluorescence of the sensor is quenched by the amine group through a photoinduced electron transfer (PET) process. Upon reaction with CO_2, the basic amine group forms a carbamate salt and a positively charged ammonium group, resulting in suspension of the PET process, after which a turn-on fluorescent response is predictable.

Rudkevich et al. performed a detailed investigation on the reversible reaction of CO_2 with sensors **6** and **7** in polar aprotic solvents.[56] As shown in Figure 5, bubbling CO_2 to solutions of sensors in polar aprotic solvent did not change their absorbance but caused a great fluorescence enhancement, thus indicating CO_2 entrapment. In contrast, free sensors **6** and **7** only gave weak fluorescence under such conditions. Moreover, NMR titrations demonstrated formation of the 1:1 sensor−CO_2 adducts, carbamic acids **8** and **9**, as well as partial precipitation as carbamate salts **10** and **11**, respectively.

Sijbesma et al. investigated the reaction between CO_2 and optically pure chiral diamines ((*R,R*)-**12** or (*S,S*)-**12**), Figure 6.[57] This strategy for monitoring CO_2 is also based on the reversible carbamate formation mechanism. The corresponding diamine/diol complex was utilized in a reaction with CO_2 and demonstrated a strong color change as well as a helical twisting power. Moreover, this sensing platform showed a continuous reversible response for CO_2 monitoring based on the equilibrium complexation of **12** with CO_2.
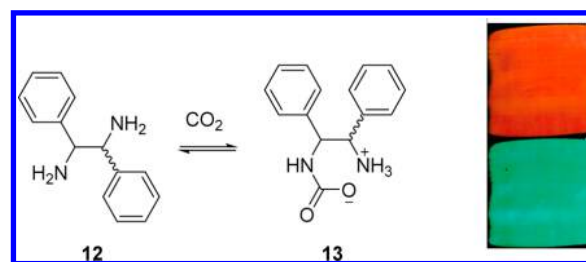
Figure 6. Structures of CO_2-responsive chiral dopants **12**. (Right) CLC film before (top) and after (bottom) exposure to CO_2 for 1 h.

Besides the above-mentioned strategy, another way for constructing a CO_2 sensing system was developed on the basis of altering the photophysical effect of the fluorescent indicator with an aggregation-induced emission (AIE). It has been well demonstrated that bubbling CO_2 or other gases through an amine results in the formation of a corresponding carbamate ionic liquid (CIL) and causes an enhancement of polarity and viscosity.[58,59] It can eventually change the fluorescence of the AIE effect. On the basis of this mechanism, Tang et al. first used hexaphenylsilole (**14**) as a fluorescent sensor in the construction of a CO_2 sensing system. Sensor **14** is nonfluorescent in solutions initially but emits high fluorescence as aggregates.[60,61] As shown in Figure 7, dipropylamine (DPA) can react with CO_2 to form carbamic acid (CA), eventually forming a viscous and polar carbamate ionic liquid (CIL) accompanied by a logarithmic increase in the viscosity of the DPA solution. After bubbling with CO_2, the **14** mixture gave a high strong green emission. Its viscosity and polarity increased along with an increase of CO_2, which enabled quantitation of the gas over the whole concentration range (0−100%). More interestingly, bubbling large volumes of CO_2 through **14** solutions in diethylamine (DEA), butylamine (BA), piperidine

Figure 7. (a) Structure of 1,1,2,3,4,5-hexaphenylsilole (**14**). (b) Formation of carbamate ionic liquid (CIL) by bubbling CO_2.

Figure 8. (a) Structure of tetraphenylethene (**15**) and 5-amino-1-pentanol (APN). (b) Formation of ionic liquid (IL) by bubbling CO_2.

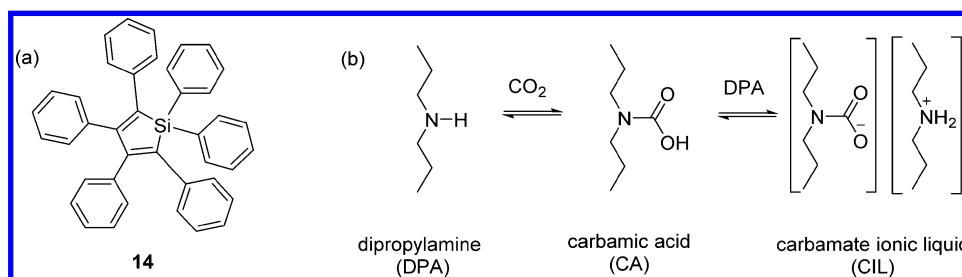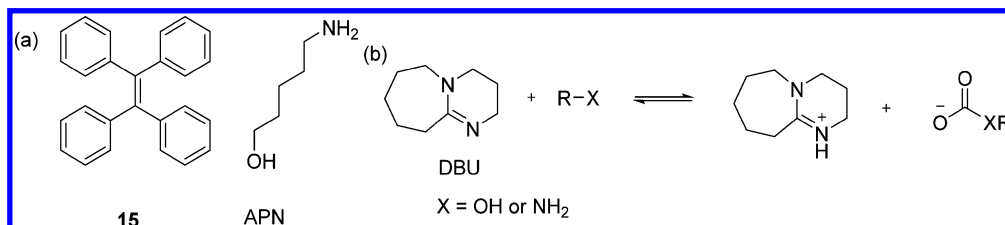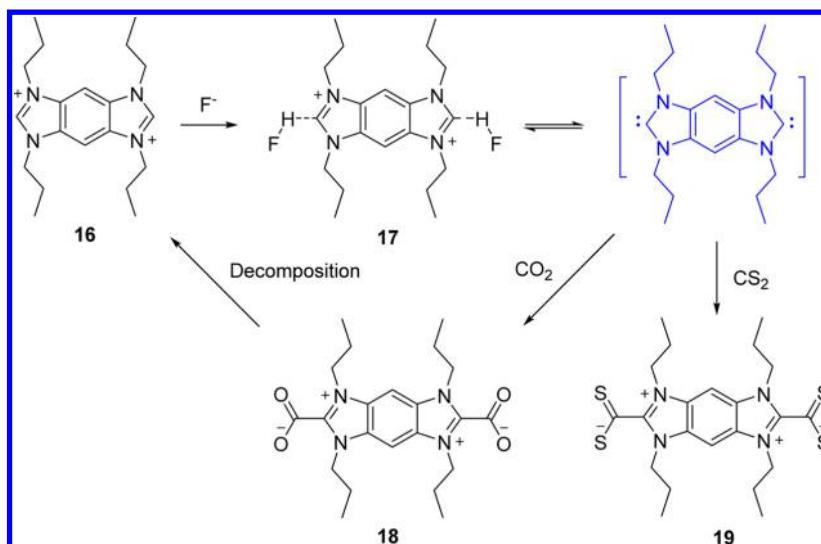**Figure 9.** Proposed reaction scheme for **16** with F⁻ followed upon exposure of CO_2 or CS_2.

(PA), and pyridine (Py) caused no obvious change in the fluorescence of **14**.

By using a similar approach, Wang and Guo et al. prepared a liquid system based on a traditional AIE compound tetraphenylethene (**15**), Figure 8.[51] Additionally, the sensing materials produced by mixing DBU and APN with different volume ratios were investigated. The results indicated that the **15**-containing mixture of DBU and APN with a ratio of 1:1, v/v, retained its transparency and showed high fluorescence immediately after CO_2 bubbling.

2.1.1.3. Deprotonation-Assisted Sensors. This effective strategy was first explored by Gunnlaugsson and co-workers by using naphthalimide amine derivatives,[62] in which fluoride-induced deprotonation of the amine moiety and the reaction with CO_2 could be monitored by changes in color and fluorescence. As a general approach, sensors with an active proton can undergo a deprotonation process in the presence of an anion through a strong R−H⁺···X⁻ hydrogen bond, resulting in forming the corresponding carbenes or negatively charged nitrogen species. Such types of species can act as good

nucleophiles for CO_2, which are regarded as the basis of the molecular recognition behaviors along with their electrostatic effects.

Recently, we successfully constructed a series of fluorescence and colorimetric sensors for detection of CO_2. We first developed a CO_2 sensor by using tetrapropyl benzobisimidazolium salts in conjunction with a specific organic-soluble N-heterocyclic carbene (NHC) precursor, sensor **16**, Figure 9.[63] **16** showed an absorption at 290 nm in acetonitrile solution. After addition of of F⁻ its absorption band shifted to 344 nm, and an efficient fluorescence quenching was also observed, which indicated the formation of strong (C−H)⁺···F⁻ bonds. When the solution was treated with 3.0 equiv of F⁻ followed by bubbling with increasing volumes of CO_2, the intensity of its absorption at 290 nm increased and so did its corresponding fluorescent emission. Moreover, this obvious fluorescent enhancement showed a good linear relationship with the CO_2 concentration. Thus, this approach can be regarded as an effective and novel method for CO_2 detection. The CO_2 detection limit of this method was calculated to be as low as

30 ppm. The sensing mechanism was further studied using NMR spectra (^{1}H, ^{13}C, and ^{19}F), MS spectra, and DFT calculations. Collectively, these data provided strong support for the hypothesis that F^- may activate the imidazolium group and then yield the free carbene species in solution. The main fundamental contribution of such a unique method is that it allows for direct reaction with CO_2 or CS_2 without recourse to an external base. The corresponding $NHC-CO_2$ is not stable and quickly undergoes decomposition in the presence of water to form an imidazolium salt. However, one disadvantage of this sensor is that the NHCs employed are not strong chromophores. Thus, there is still a room in this area to find more active sensors with highly nucleophilic nitrogen centers for improved CO_2 sensors.

Sessler and co-workers constructed two colorimetric- and fluorescence-based CO_2 sensors based on N-fused compounds **20** and **21**, Figure 10.[38] Such analogues were reported to be
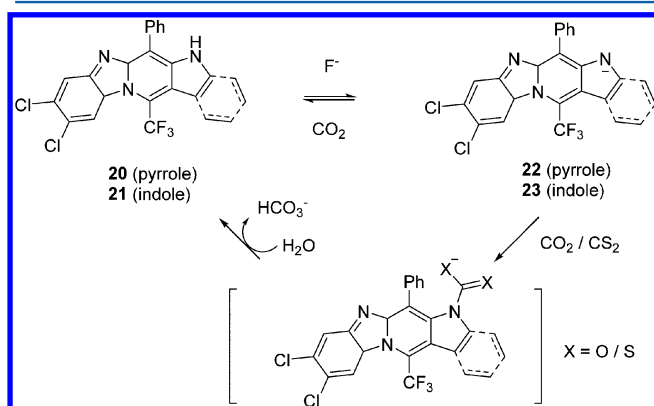
Figure 10. Proposed reactions that occur when **19** and **20** are treated first with F^- and then either CO_2 or CS_2.

highly fluorescent.[64] As mentioned above, these sensors could be easily deprotonated by F^- and displayed distinct colorimetric and fluorescent responses. Upon addition of F^-, the characteristic absorption band of **21** decreased and its fluorescent intensity quenched. When the deprotonated adduct (**23**) was exposed to CO_2 gas, both absorption and fluorescence changed dramatically. The detection limit for CO_2 was calculated to be 0.41 μM.

As mentioned above, active carbene and arylamine were successfully used for CO_2 sensing based on a novel F^- activated strategy. We further developed a fluorescent or colorimetric CO_2 sensing sol−gel system by employing other acidic nitrogen amides and based on a similar anion-activated strategy. We prepared a new naphthalimide-based sensor **24**, Figure 11, and realized the ideal functions of both sensing and capture of CO_2.[39] This system contains a cholesterol moiety and a carbamate ester linker. As expected, upon addition of F^- in a DMSO solution of the sensor, colorimetric and ratiometric fluorescent responses were observed, including a color change from colorless to orange and a fluorescent color change from blue (462 nm) to weak orange (572 nm). Moreover, these changes were absolutely reversed after addition of CO_2. The mechanism of this sensing process was further demonstrated by NMR (^{1}H and ^{13}C) titrations. Notably, **24** shows a very low critical gelation concentration (CGC) of 0.18 wt % in DMSO. Therefore, it can serve as a gel-based sensing platform and provide an optical response upon exposure to anions and CO_2. As described, **24** formed a stable organic gel with a red-shift

green emission, which is ascribed to hydrogen bonding interactions and $\pi-\pi$ stacking from donor−acceptor interactions between the vicinal naphthalene rings (J aggregation). This gel gradually collapsed and completely transformed into a homogeneous solution within 1 h. Upon bubbling with CO_2, the corresponding solution turned viscous and in due course gel-like rafts emerged. By using this sol−gel transition sensing system, a capturing efficiency of 30.1% was calculated.

We further extended this strategy to other common anion sensors with an amide moiety. As shown in Figure 12, a new bis-pyrene derivative **27** was synthesized, in which pyrene groups were treated as a fluorescent report unit and connected urea group as the reacted group.[65] This sensor displayed sensitive and selective responses toward cyanide and F^-, accompanied by unique colorimetric and turn-on fluorescent changes. We demonstrated that this sensor can be regarded as a unique anion-activated CO_2 sensing system. As shown in Figure 12, the addition of F^- changed the solution color to deep red, along with its fluoroescent color changing to high yellow. Also, upon bubbling of CO_2 it showed simple colorimetric and fluorescent changes.

2.1.2. Sensors for SO_2. Sulfur dioxide (SO_2) is a toxic gas with a pungent, irritating, and rotten smell. It has long been considered as a main air pollutant and the primary cause of acid rain along with nitrogen oxides (NOx), which cause significant environmental and public health problems. Nowadays, the increasing emission of SO_2 from the combustion of fossil fuels expands the risk of human exposure to SO_2. People exposed to SO_2 may suffer from respiratory diseases and cancers. Short-term overexposure of SO_2 causes inflammation and irritation, causing eye damage, coughing, and a feeling of chest tightness. Exposure to low concentrations (1−5 ppm) within a prolonged time is dangerous for persons with pre-existing heart and lung diseases. As reported, inhaled SO_2 can be rapidly hydrated into sulfite (SO_3^{2-}) and bisulfite (HSO_3^-) in neutral solutions (3:1 M/M).[66] On the other hand, SO_2 also showed its important role in regulating cardiovascular function. Moreover, sulfite is also well known as an antioxidant in the food industry to prevent bacterial growth at an early age. Therefore, there exists much interest in developing fluorescent sensors for such species. Indeed, a lot of good examples have been reported to date. The main design strategies regarding this kind of fluorescent sensor for SO_2 are mainly based on the nucleophilic reactivity of SO_2. In these cases, SO_2 and its derivatives selectively add to aldehydes/ketones or double bonds through Michael addition, leading to changes in the π conjugation of the sensors, resulting in fluorescent and colorimetric responses.

Chang et al. developed the fluorescent sensor **28** by using a commercial resorufin for sulfite detection, Figure 13.[67] In this case, sulfite can selectively react with the carbonyl carbon of the levulinate and yield a tetrahedral intermediate. This corresponding intermediate can next undergo an intermolecular cyclization to release the free resorufin moiety, resulting in an up to 57-fold fluorescence enhancement with a detection limit of 49 μM in aqueous solution. Guo et al. reported a coumarin-hemicyanine fluorescent sensor **30** for SO_3^{2-}/HSO_3^- detection.[68] The nucleophilic reaction of SO_3^{2-}/HSO_3^- on the double bond caused interruption of the conjugation of the sensor through a novel addition−rearrangement mechanism. As a result, a red emission of the coumarin−hemicyanine fluorophore at 633 nm shifted dramatically to the blue emission of coumarin fluorophore. With this sensor, as high as an 1110-fold enhancement of ratiometric signal was observed along with
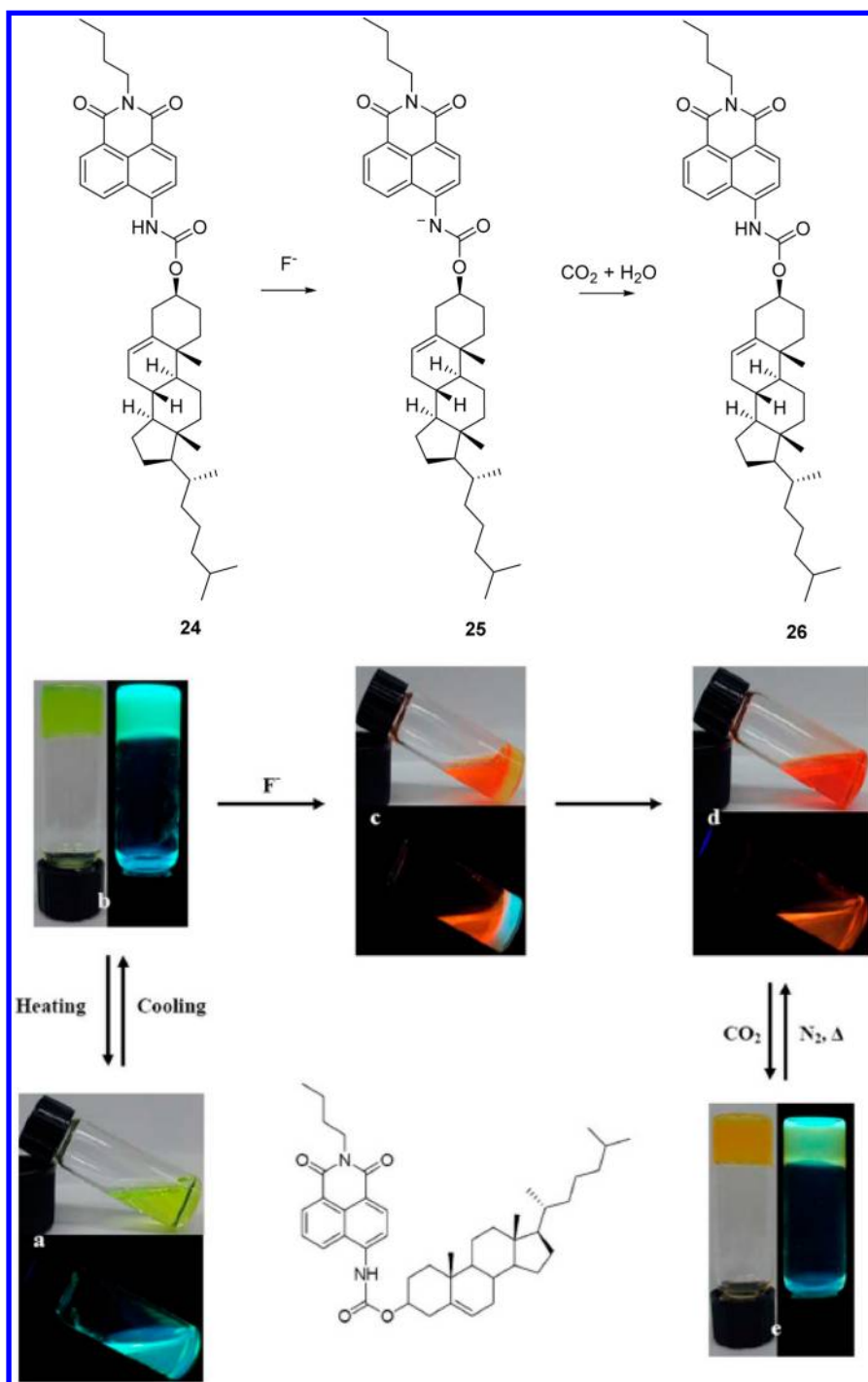
Figure 11. (Top) Proposed reactions that occur when **24** is treated first with F⁻ followed by CO_2. (Bottom) Multiple responses of **24** in DMSO under the stimulations of thermal, F⁻, and CO_2: (a) sol; (b) gel; (c) partial or (d) complete collapse of the gel induced by F⁻, (e) upon reaction with CO_2 in the presence of F⁻.
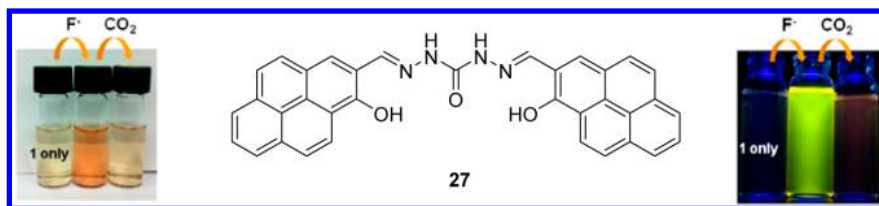
Figure 12. Structure of sensor **27** and its color and fluorescent changes after first addition of F⁻ and then CO_2.
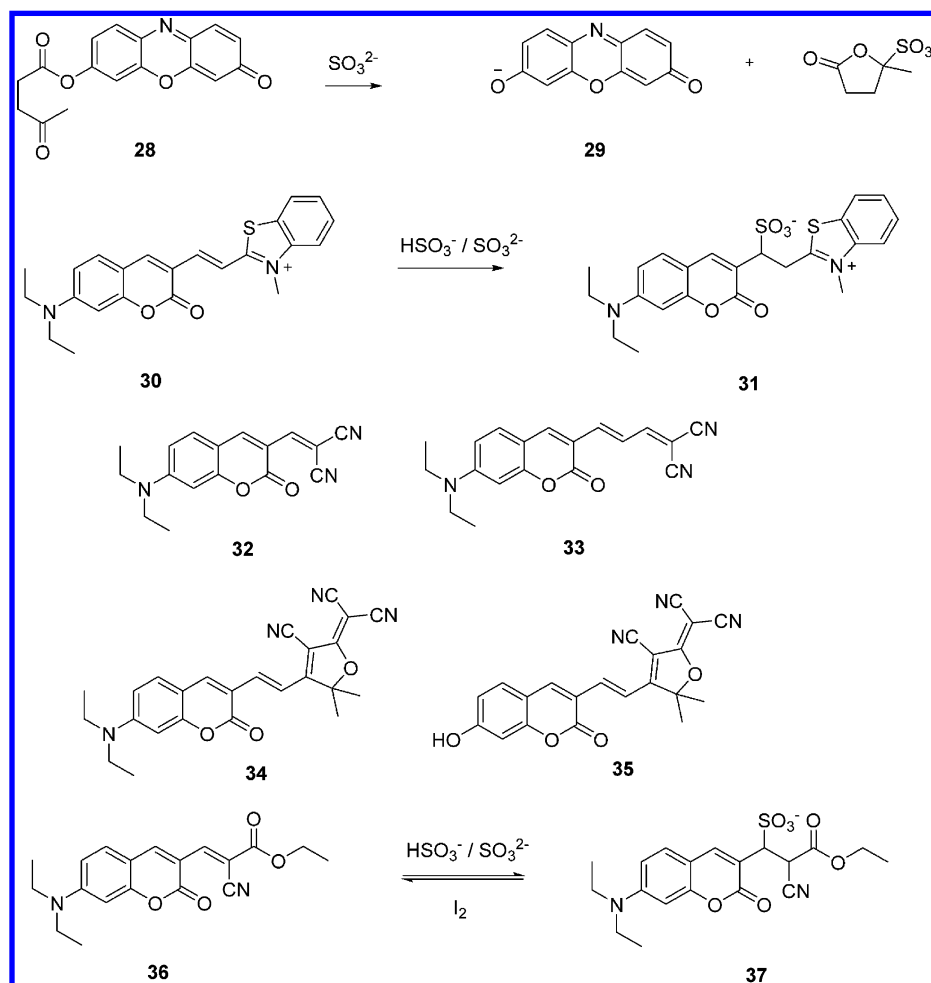
Figure 13. Structures of sensors for sulfite.

a detection limit of 0.38 μM. The sensor was also successfully applied to detect SO_3^{2-}/HSO_3^- in living HeLa cells. Li and Xu et al. reported fluorescent sensors **32** and **33** for the detection of sulfite. These sensors contain 7-diethylamine coumarin dye as the fluorophore, which conjugated with the cyano group through double bonds.[69] The sensors gave fluorescent responses toward SO_3^{2-}. In the presence of SO_3^{2-}, a Michael addition occurred at the α,β-unsaturated double bond, which caused colorimetric and ratiometric response of the sensors. A 232-fold fluorescent enhancement and a detection limit of 58 μM were observed in the case of **33**. This group continuously reported near-infrared fluorescent sensors **34** and **35** for the colorimetric and ratiometric detection of SO_2 derivatives.[70] The fluorescent ratio at two different wavelengths showed a 775-fold enhancement within 90 s in the presence of sulfite. The sensor was further used to detect SO_2 derivatives in U-2OS cells, and the detection limit was calculated to be as low as 0.27 nM. Zhou and Wu et al. found that this kind of Michael addition of sulfite with α,β - unsaturated ketone can be reversed in some certain cases.[71] They reported a reversible ratiometric fluorescent probe; in this case, they induced a conjugated ethyl cyanoacetate moiety in the unsaturated ketone moiety. This sensor showed high sensitivity and selectivity toward sulfite with a detection limit of 21 nM. Moreover, the sensing process could be reversed through a redox-based tandem reaction.

2.1.3. Sensors for O₃. Ozone (O_3) exposure is also a growing global problem. On one hand, ozone can protect living beings on the earth from the Sun's harmful UV radiation; on the other hand, tropospheric or ground-level ozone is toxic for human health. It has been demonstrated that O_3 can be produced endogenously in inflammatory and antibacterial responses of the immune system.[72] The main principle for the construction of fluorescent sensors is using but-3-enyl as a recognition group in which alkenes can be selectively cleaved by O_3 via ozonolysis.[73,74] By using this kind of strategy, Koide and co-workers reported a fluorescent sensor **38** for O_3.[75] In this case, sensor **38** showed no fluorescence initially. After reacting with O_3, a turn-on fluorescent response was observed upon exposure of O_3. The sensing mechanism is documented in Figure 14; in the first step, the sensor reacts with O_3 to yield the aldehyde intermediates **39** and **40**, which subsequently undergo β-elimination to form the product **41**. It was demonstrated that the sensing process of **38** toward O_3 was not interfered even in the presence of other ROS and physiologically relevant antioxidants. Moreover, another chemosensor **42** has been employed for sensing O_3 in living cells.[75] **42** also displayed weak fluorescence initially. After treatment with ozone gas, strong fluorescence signals were observed in living cells. In addition, **42** can detect O_3 in atmospheric samples. Using the same strategy, Ma et al. developed an off−on-type fluorescent sensor **44** for O_3.[76] This sensor uses a commercial resorufin as fluorescent reporting
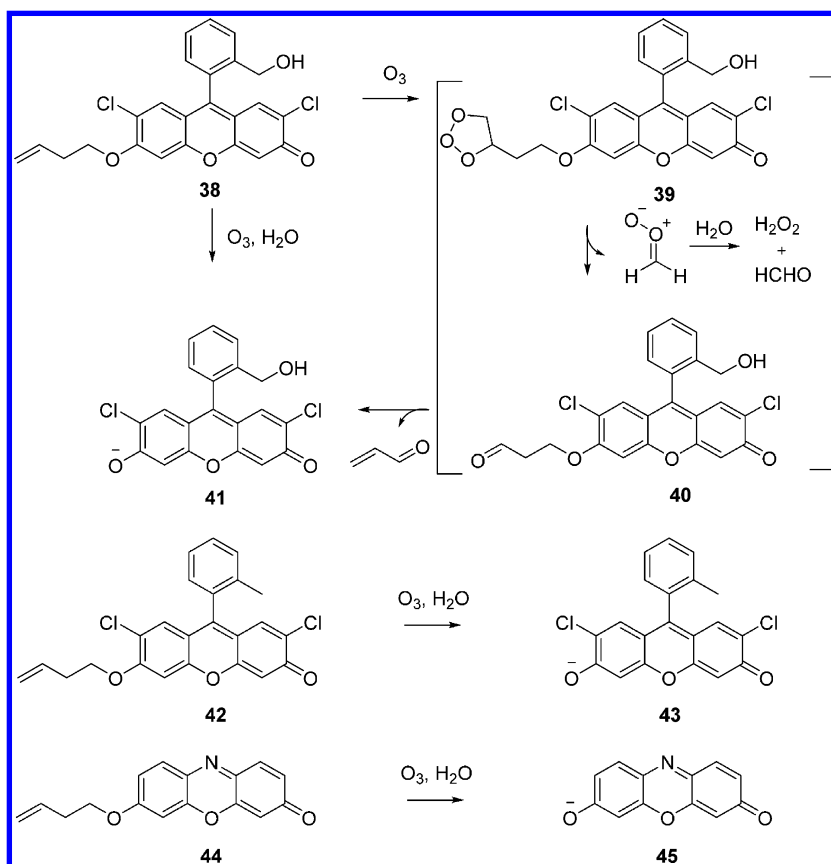
Figure 14. Structures of chemosensors for O_3 and their sensing mechanisms.
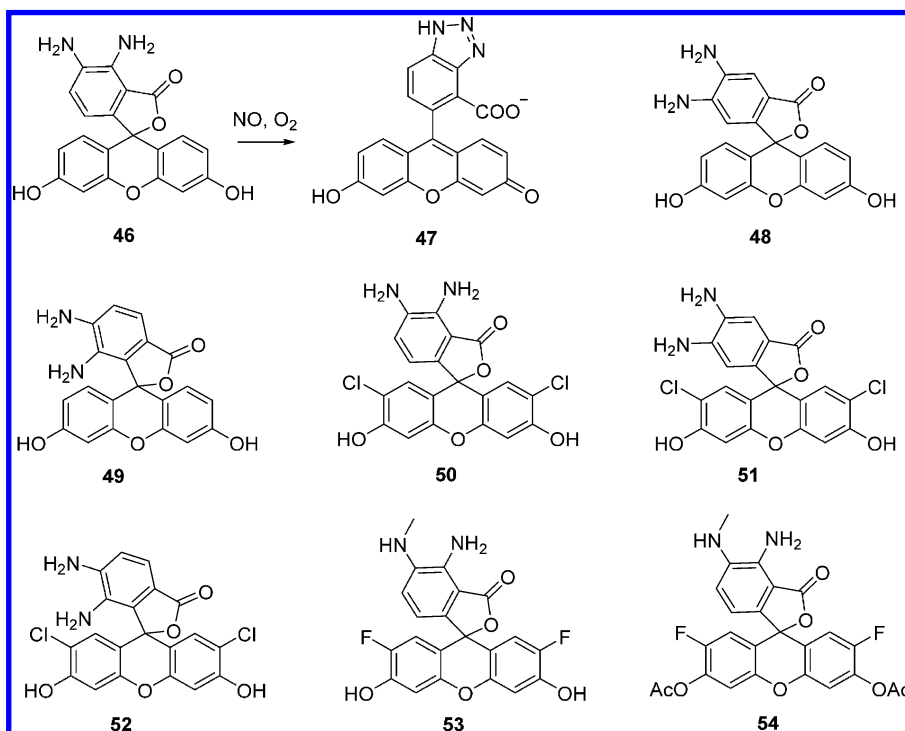
Figure 15. Structures of chemosensors for NO based on fluorescein and their sensing mechanisms.

unit. This sensor showed high sensitivity toward O_3 with a detection limit as low as 5.9 nM (0.056 mg/m^3) in air. Moreover, this sensor has been successfully employed in the fluorescence imaging of O_3 in HeLa cells.

2.2. Sensors for Biological Signaling Gases

2.2.1. Sensors for NO. Nitric oxide (NO), a gas produced by nitric oxide synthases and secreted from endothelial cells, is regarded as the first ubiquitous signaling molecule.[5] Endoge-

I
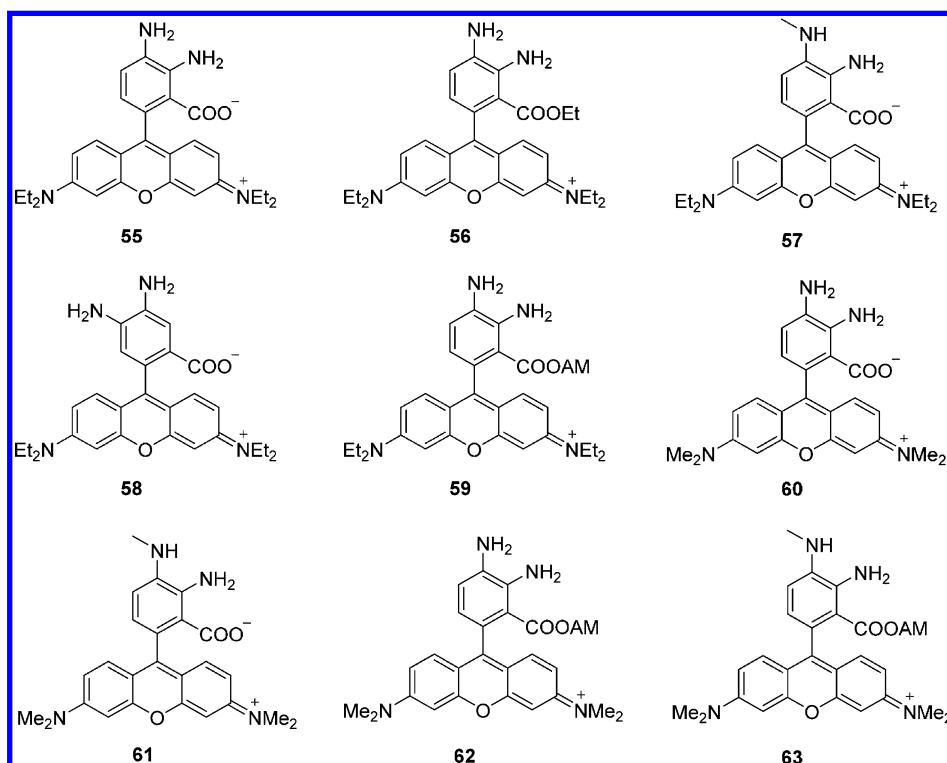
Figure 16. Structures of chemosensors for NO based on rhodamine dyes.

nous NO plays a key role in multiple processes in various physiological and pathological processes, such as regulating relaxation, and vasodilatation, as well as the cardiovascular, immune, central, and peripheral nervous systems.[77] However, uncontrolled NO secretion is known to be associated with the generation of reactive nitrogen species (RNS) that are responsible for many health problems including cancer, inflammation, endothelial dysfunction, and neurodegenerative diseases. However, the mechanisms of NO in these diverse biological processes are still not fully understood. One of the key requirements for studying the roles of NO is the availability of simple methods for sensitive and selective detection of this gas.

2.2.1.1. o-Phenylenediamine (OPD) Based NO Sensors.
Fluorescent sensors for NO containing *o*-phenylenediamine (OPD) moieties and fluorophores have been developed by Nagano's group and shown to be highly effective for visualizing this gas in vitro and in vivo. The sensing mechanism of these sensors involves the irreversible reaction of OPD with NO^+ or N_2O_3 to produce benzotriazole in association with an off–on fluorescence response caused by the disappearance of photo-induced electron transfer (PET) quenching of the fluorophores' excited state. Specifically, the sensor is nonfluorescent due to the PET effect from the electron-donating *o*-diamine moieties to the excited fluorophore. Reaction of NO with an *o*-diamine group leads to the formation of a triazole moiety, which does not serve as an electron donor in PET quenching.

Nagano et al. described a number of diamino-fluorescein-based NO fluorescent detectors that operate via a spirolactone ring-opening mechanism. The NO-promoted chemical transformation is a combination of the following two processes: an aromatic vicinal diamine that can react with NO in the aerobic condition, and a process that forms a triazole moiety in conjunction with spirolactone ring opening, which liberates a highly fluorescent tricyclic dienone. The fluorescence quantum

efficiencies of **46**–**52**, Figure 15, typical sensors designed by using this strategy, were observed to increase more than 100-fold upon reaction with NO, which was attributed to transformation to their highly green-fluorescent triazole forms. These sensors were found to display NO detection limits of 5 nM.[78]

However, the presence of the triazole proton in the products of the NO reactions causes undesirable variations in the fluorescence intensities in the neutral pH range. To solve this problem, Nagano and co-workers introduced a *N*-methylamino group into the NO sensor, exemplified by **53** and **54**.[79] The methylated sensors displayed greater sensitivity to NO due to their higher reaction rates with NO. As a result, fluorescence microscopy in association with these sensors could allow direct detection of intracellular production of NO. Indeed, the membrane permeating chemosensor **54** is transformed by intracellular esterases in living cell into the highly water-soluble dye **53**, which further reacts with NO produced by NO synthase (NOS) to form a fluorescent triazole. Consequently, **54** can be employed for imaging of NO in living systems with a high degree of temporal and spatial resolution.

Although their usefulness for studies of the function of NO has been demonstrated, *o*-phenylenediamine-fluorescein-based sensors lack some desirable characteristics, such as higher photostability, longer excitation wavelengths, and applicability over a wider pH range. In efforts aimed at addressing these problems, Nagano et al. developed membrane permeable, *o*-phenylenediamine-based fluorescent indicators **55**–**63** for NO detection, Figure 16.[80] For example, **63** displayed a turn-on fluorescent response to NO, associated with an 840-fold increase in emission intensity and a lower detection limit of 7 nM compared to sensors **46**–**54**. Moreover, the fluorescence mechanisms of **55**–**63** were not pH dependent above pH 4. Judging from NO standard curves calibrated by using indicators, the sensitivity of **61** to NO was twice than that of
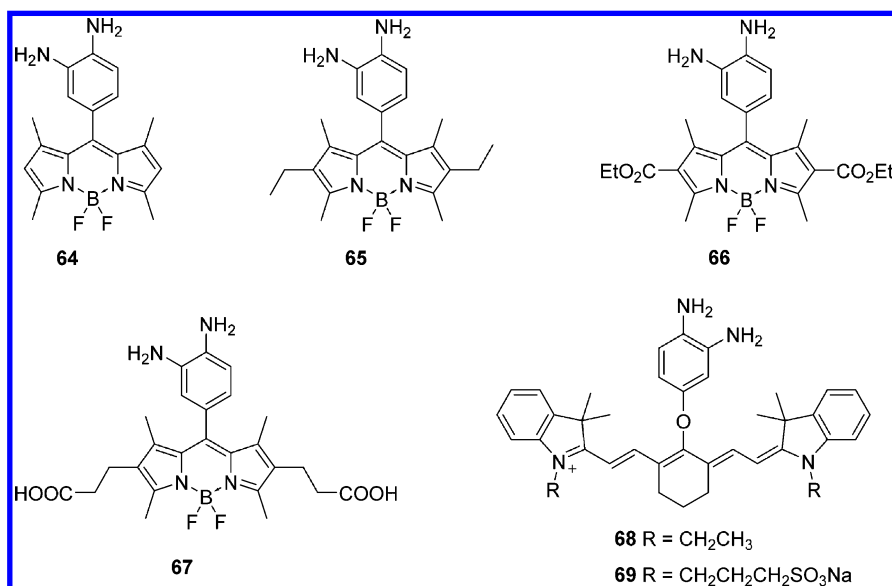
Figure 17. Structures of chemosensors for NO based on BODIPY and cyanine dyes.
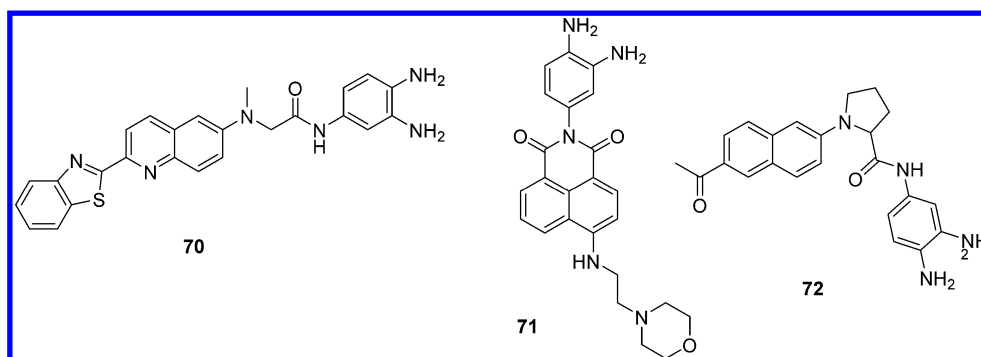
Figure 18. Structures of chemosensors for NO used in TPM imaging.
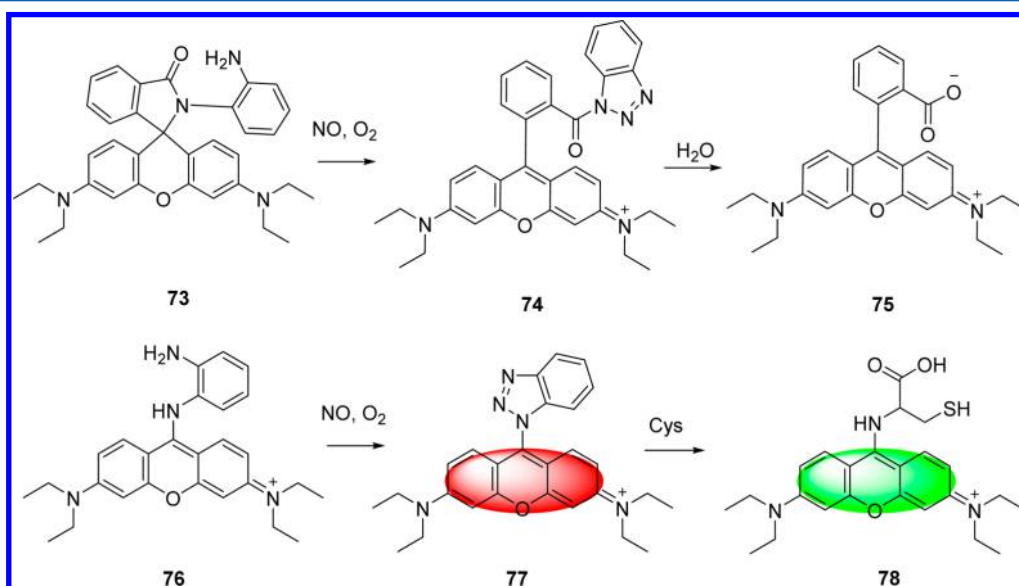
Figure 19. Structures of chemosensors for NO and their sensing mechanisms.

**55.** Finally, **63** was used to image NO detection in bovine aortic endothelial cells.

Using the same *o*-phenylenediamine cyclization strategy, Nagano et al. designed other NO fluorescent sensors **64−69**

with different emission properties, Figure 17. For example, sensor **67**, which contains the BODIPY fluorophore, was found to be a highly sensitive and selective sensor for NO.[81] **67** itself showed a low fluorescence efficiency of 0.002, whereas its
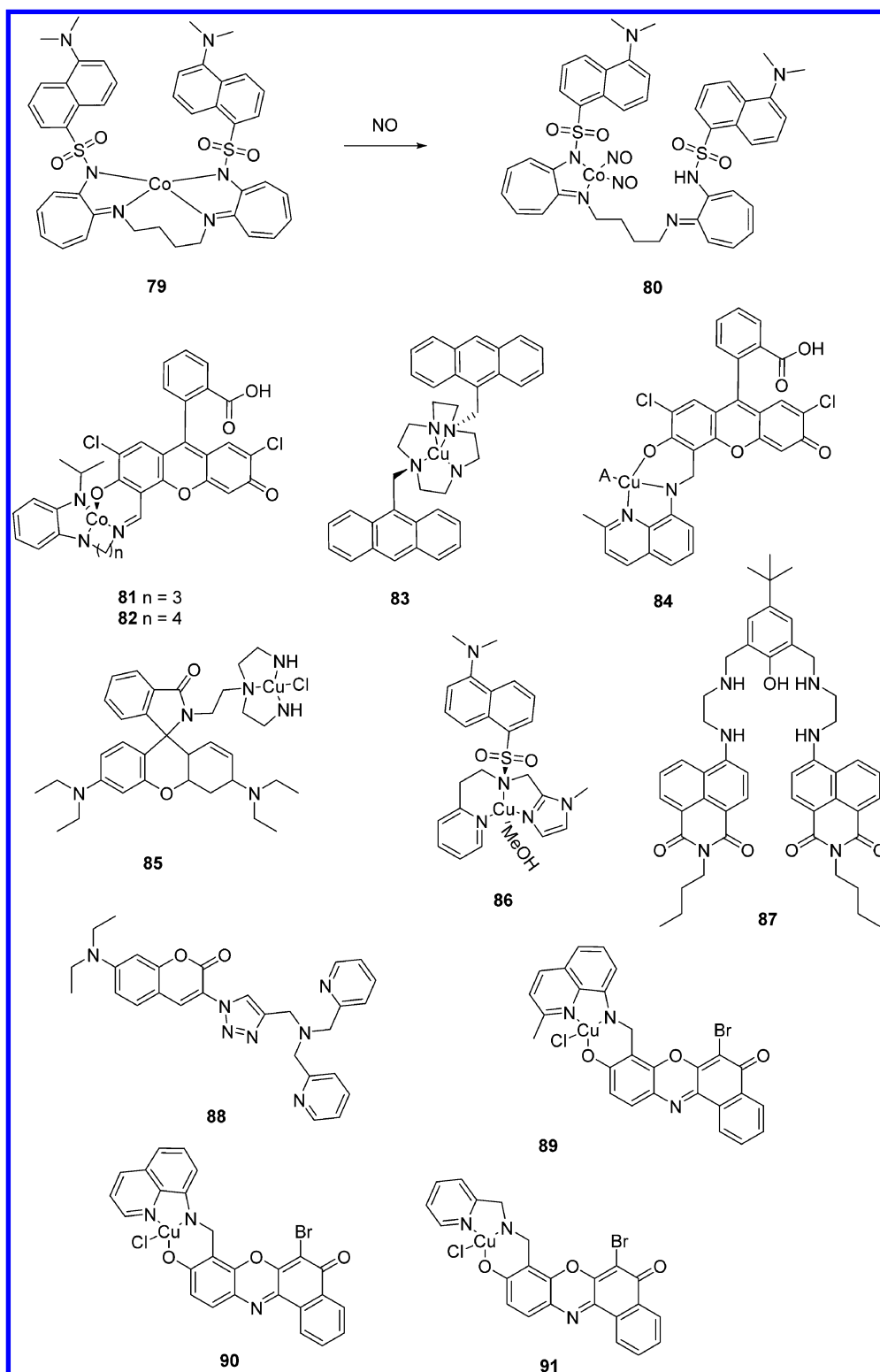
Figure 20. Structures of chemosensors for NO based on metal complexes.

triazole derivative, the product of the reaction of **67** with NO, emits strongly ($\varphi = 0.74$). Moreover, modification of the basic skeleton by the incorporation of sulfonate groups provided increased water solubility. In addition, near-infrared (NIR) NO sensors **68** and **69**, based on a tricarbocyanine fluorophore, were also reported by Nagano et al.[82] The efficiency of these NIR sensors' reactions with NO was at least 53 times higher than that of widely used NO sensors. Finally, the new sensors

were observed to function in isolated intact rat kidneys and to display lower interference from biological species.

Recently, the use of two-photon microscopy (TPM) has drawn emerging attention in the field of bioimaging due to its wonderful ability to circumvent several shortcomings.[83] Liu et al. devised the two-photon fluorescent NO sensor **70**, Figure 18.[84] This sensor displayed a 12-fold fluorescent enhancement toward NO. **70** showed a large two-photon action cross section
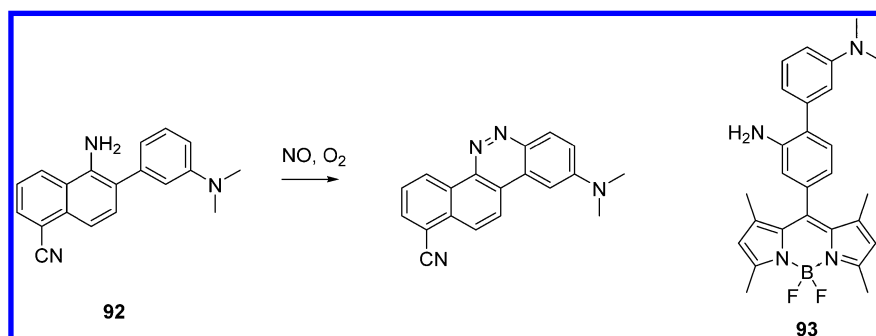
Figure 21. Structures of chemosensors for NO and their sensing mechanisms.

(52 GM) with excitation at 810 nm and a long wavelength emission. By utilizing TPM with **70**, detection of NO in live tissues at a depth of 90−180 μm for a long time range without photobleaching was possible. Xiao et al. reported the lysosome-targeted two-photon fluorescent sensor **71**, which contains the naphthalimide fluorophore and the lysosome targeting amino-ethyl-morpholine group.[85] **71** displayed selective fluorescence turn-on detection of NO, and it showed no obvious response to other ROS. The advantages of this sensor system are its low cytotoxity, favorable lysosomal localization, and efficient capture of endogenous NO in lysosomes of macrophage cells. Kim and Cho et al. reported the two-photon NO sensor **72** composed of an acedan as the signaling unit with a diamine moiety as the reaction site.[86] The sensor displayed 68-fold fluorescence enhancement toward NO within 5 min. Furthermore, **72** was employed in cells and tissues imaging to monitor NO in living tissues at a 100−180 μm depth for a longer time range than 1200 s.

In addition, the *o*-phenylenediamine group masked in the form of a lactam has also been developed as a reactive site for construction of turn-on-type fluorogenic sensors for NO. On the basis of this strategy, Xu and co-workers developed a fluorescent sensor **73** for highly sensitive detection of NO under normal physiological conditions.[87] The sensing mechanism was documented in Figure 19, which involves an initial NO-promoted diazotization of the diamino group followed by opening of the spirolactam ring to yield the fluorescent dye **74**, which further undergoes hydrolysis to yield rhodamine B and benzotriazole. **74** displayed a sensitivity of a 2400-fold fluorescence enhancement and a detection limit of 3.0 nM. Recently, Guo et al. constructed a novel fluorescent sensor **76**, in which a pyronin dye is conjugated with one amino group of a OPD moiety.[88] This sensor was found to sense NO selectively over other ROS/RNS as well as DHA, AA, and MGO. More interesting, triazole produced by the reaction of **76** with NO is further reacted with biothiols such as Cys and GSH and then yielded green-emitting aminopyronin **78** and red-emitting thiopyronin **77**, respectively. Moreover, with the help of cellular Cys and GSH, the sensor was able to detect exogenous and endogenous NO produced in mitochondria in different channels.

2.2.1.2. Metal−Ligand Complex Displacement-Based Approach. A metal complex displacement-based approach was also developed for the detection of NO by utilizing a transition metal complex system containing a coordinated fluorophore. In this case, the fluorescence of the complex is generally quenched by the partially filled d orbitals of the metal ion. However, NO forms metal−nitrosyl adducts with the metal ions by a pathway involving the liberation of the free

fluorophore. Lippard et al. utilized this displacement approach to develop a lot of sensors for fluorescent detection of NO. In this effort, a cobalt complex modified with a dansyl fluorophore **79** was prepared, Figure 20.[89] Studies with this sensor showed that the fluorescence from the Co^{2+} complex solution displayed a greater than 4-fold fluorescence enhancement in the presence of NO with a detection limit in the 50−100 μM range. Similarly, Co^{2+} complexes containing aminotroponiminate ligands linked to a derivative fluorescein moiety **81** and **82** also served as NO sensors.[90]

A related approach for the design of NO chemosensors takes advantage of the reduction of Cu^{2+} to Cu$^+$ by NO. Coordination of a fluorophore to the paramagnetic Cu^{2+} resulted in fluorescence quenching. Addition of NO promotes the conversion of Cu^{2+} to diamagnetic Cu$^+$, which cannot quench emission of the fluorophore. Ford et al. described a sensor of this type containing the complex **83**.[91] Complex **83** shows no fluorescence due to intramolecular quenching by paramagnetic Cu^{2+}. After addition of NO, fluorescence from the anthracene luminophores is enhanced owing to the intramolecular nitrosylation of an amino coordination site liberating the free ligand.

Another strategy involving NO-induced reaction of a coordinated ligand was used by Lippard et al. to design fluorescein-containing copper complex **84** for detection of the gas.[92] In comparison to Cu^{2+} complexes where NO triggered fluorescence enhancement that occurs via nitrosylation reaction to induce ligand dissociation from the reduced Cu$^+$ center, the fluorescein-based Cu^{2+} complexes react rapidly and specifically with NO to reduce the metal to the Cu$^+$ state. Duan et al. developed a rhodamine-based Cu^{2+} complex **85** for NO detection.[93] The detection mechanism of this sensor involves initial NO coordination to the square planar copper ion, subsequent reduction of Cu^{2+} to Cu$^+$, and simultaneous formation of NO$^+$. The NO$^+$ cation promoted opening of the spirolactam ring and nitrosylation. This sensor, which exhibited a 700-fold fluorescent enhancement in the presence of NO, has been employed to monitor intracellular NO.

Mondal and co-workers prepared Cu^{2+} complex **86** possessing a tridentate N-donor ligand with a pendant dansyl fluorophore.[94] The quenched emission from the dansyl group in **86** is restored upon exposure to NO, a phenomenon attributed to reduction of Cu^{2+} to Cu$^+$. Importantly, this Cu^{2+} complex has low cytotoxicity, and as a result, it can be employed for NO detection in living cells. Sensor **87**, a Cu^{2+} complex which contains a naphthalimide moiety, showed a fluorescent turn-on response for NO with an 8-fold fluorescent enhancement at 530 nm.[95] Moreover, LC-MS and IR analysis demonstrated that the reason for the fluorescence enhancement

was a consequence of NO-induced nitrosation along with the reduction of Cu^{2+} to Cu^+. Confocal fluorescence microscopy studies showed that this sensor can be utilized to image NO in living cells. Yao et al. developed the sensor **88**, which contains a coumarin group and a tripodal dipicolylamine ligand linked by a triazole bridge.[96] This sensor selectively binds Cu^{2+} with strong quenching of its fluorescence. After reaction, coumarin-chelated Cu^{2+} was reduced, forming a Cu^+ coumarin complex in association with an increase in fluorescence intensity at 499 nm. Moreover, this sensor was highly sensitive toward NO over other ROS/RNS. Finally, the Cu^{2+} complex exhibited low cytotoxicity and was employed for detection of NO in living cells.

Lippard et al. developed some benzoresorufin-based copper complexes **89–91** for fluorescent detecting NO.[97] These sensors displayed 1.5–4.8-fold emission enhancements in response to NO. Moreover, the fluorescent sensing mechanism was further explained using density functional theory calculations. Finally, sensors were further utilized for detecting HNO and NO in HeLa cells and RAW 264.7 macrophages.

2.1.1.3. Sensors Based on Other Strategies. In addition to the approaches described above, other strategies have been utilized to design sensors for the detection of NO. In 2010, Anslyn et al. carried out studies with the 2-dimethlyamino-phenyl-5-cyano-1-naphthylamine fluorophore-containing sensor **92**, designed by exploiting a novel sensing mechanism, Figure 21.[98] The sensor is nonfluorescent, but it displayed a 1500-fold fluorescence enhancement at 550 nm upon NO treatment. Importantly, the sensor showed excellent selectivity for NO over other ROS/RNS. Furthermore, this sensor operates over a wide pH range and is applicable to NO bioimaging. To extend the strategy, Guo et al. developed a modified version of this platform for fluorescent NO detection, sensor **93**, which integrates 2-amino-3-o-dimethylaminobiphenyl (AD) as an NO binding group with a BODIPY fluorophore.[99] **93** was weakly fluorescent initially owing to the PET effect. In the presence of NO, a diazo product is produced through a reaction mechanism proposed previously by Anslyn. Because of the absence of the electron-donating amine group in the generated product, the turn-on fluorescence was observed due to the blocking of the PET quenching process. Moreover, this sensor was employed to sense NO selectively over ROS/RNS with a detection limit of 30 nM. The results of preliminary cell experiments indicate that this sensor has a potential use for imaging NO in biological systems.

2.2.2. Sensors for CO. Carbon monoxide (CO) is a toxic gas to humans when encountered in concentrations over 35 ppm. However, recent studies have demonstrated that CO serves as the second gas massager in the body which plays an important role in human normal biological functions.[100] CO has received a great deal of clinical attention as a biological regulator, for example, anti-inflammatiories, modulating in vasorelaxation, vascular smooth muscle, and tissue injury. Although CO plays a significant role in physiological processes and clinical trials, many aspects of its real and potential functions still need to be explored. To this end, the development of fluorescent sensors with the capability of real-time, spatial, and temporal tracking and monitoring of CO at the cellular level remains challenging.

Sancenón and co-workers developed carbon monoxide sensors based on binuclear rhodium derivatives.[101] Most CO sensors which were reported previously possessed poor color modulations and relatively large detection limits. To solve these

problems, Sancenón and co-workers used binuclear rhodium complexes which have the well-known ability of binding in axial sites. In the study they prepared and fully characterized *cis*-$[Rh_2(C_6H_4PPh_2)_2(O_2CCH_3)_2](HO_2CCH_3)_2$ (**1·**$(CH_3CO_2H)_2)$ (**94**)), Figure 22. A dramatic color change of
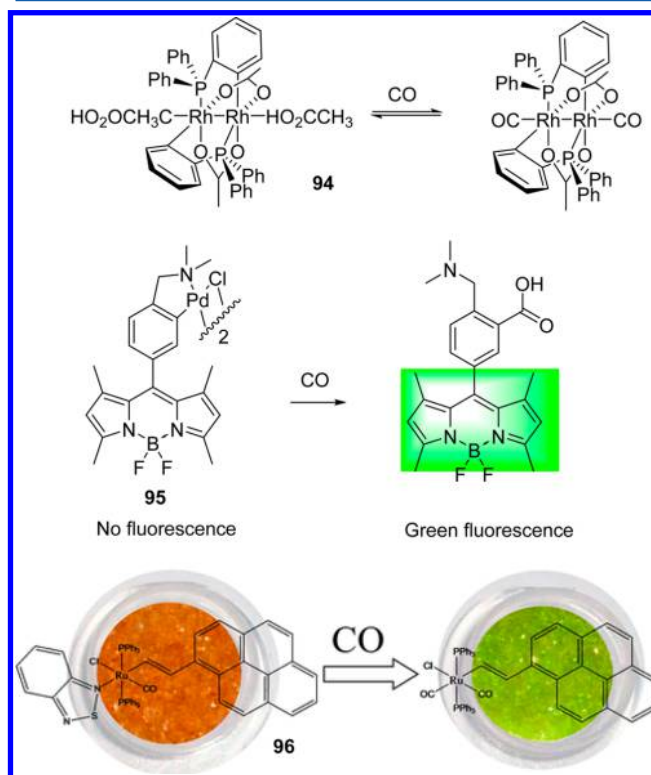
Figure 22. Structures of chemosensor **94–96** and its mechanism of CO responses.

the chloroform-containing **94** from violet to orange-yellow was observed. The color shifts come from an axial coordination by CO. In a typical test, the visible diffuse reflectance spectrum of silica gel containing **94** showed an absorption band at 554 nm. After bubbling of CO gas, a new band appeared at 398 nm. These changes were consistent with axial coordination by CO and the corresponding derivatives. In addition, the detection limit for CO in air was as low as 0.5 ppm.

The first single fluorescent sensor **95** for detecting CO in living cells was described by Chang et al.[102] **95** was demonstrated to be a turn-on fluorescent sensor that is selective for CO based on palladium-mediated carbonylation reactivity. The sensor is not itself fluorescent due to the heavy-atom effect of the coordinating palladium, resulting in fluorescence quenching of the BODIPY fluorophore. After binding CO, a carbonylation reaction takes place to release the reduced Pd(0) and the fluorescent BODIPY species. A 10-fold fluorescent enhancement was observed within 60 min after CO addition. The sensor showed high selectivity over a range of biologically relevant reactive small molecules that can also be utilized to detect CO both in aqueous buffers and in live cells.

Wilton-Ely and Martínez-Máñez et al. reported the first example of the design of a ruthenium(II) complex (**96**) for CO detection in the air.[103] This probe **96** showed exceptional sensitivity and selectivity for CO in the solid state with a color change observed by the naked eye at CO concentrations of 5 ppb. This probe also showed a turn-on fluorescent response

Table 1. Summary of Fluorescent H₂S Sensors Based on Reduction of Azide

	$\lambda_{ex}/\lambda_{em}$ (nm)	fluorescent enhancement	response time	detection limit	appliction in vivo
97	490/525	7-fold	60 min	5−10 μM	cell imaging with HEK293T cells
99	490/525	9-fold	60 min	5−10 μM	cell imaging with HEK293T cells
100	340/535	40-fold	3 min	1 μM	detection in blood using C57BL6/J mice
101	432/545	60-fold	45 min	1−5 μM	cell imaging with HeLa cells
102	625/750		20 min	0.08 μM	cell imaging with RAW 264.7 cells[a]
103	363/548	21-fold	120 min	5−10 μM	TPM imaging with HeLa cells[b]
104	760/480	40-fold	60 min	0.02 μM	TPM imaging with HeLa cells
105	750/420	9-fold	60 min	0.2 μM	TPM imaging with HeLa cells and fresh rat hippocampal slices
107	750/464	9-fold	60 min	0.4 μM	TPM imaging with HeLa cells and fresh rat hippocampal slices

[a]Ratio fluorescence imaging. [b]Two-photon fluorescence microscope imaging.
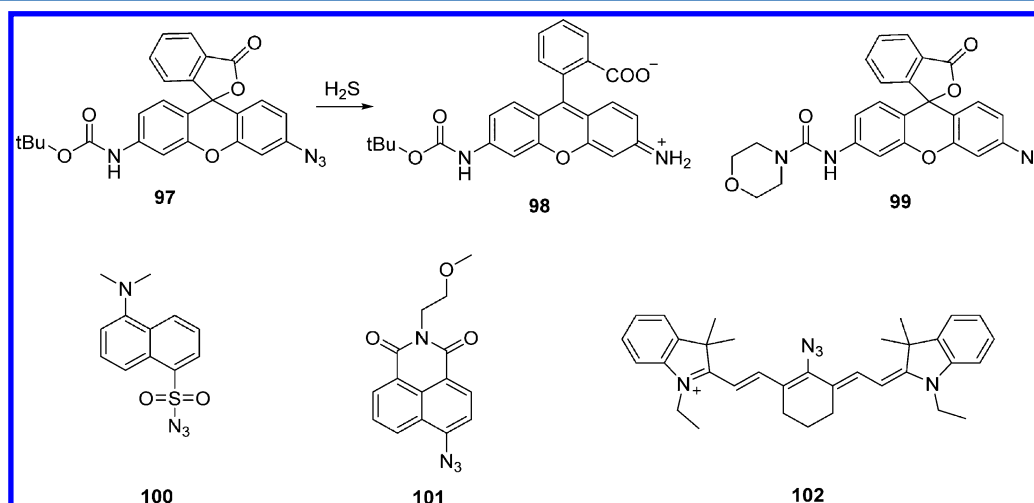
Figure 23. Fluorescent sensors based on H₂S underwent reduction of azides.

toward CO both in air and in solution with even greater sensitivity (1 ppb). Moreover, this probe showed exceptionally high selectivity for CO over aqueous vapor, making it of potential applications in a domestic setting. Finally, this probe was successfully immobilized on a cellulose strip; this immobilization system makes it able to be applied in a simple optoelectronic device as a numerical reading and/or an alarm.

2.2.3. Sensors for H₂S. Hydrogen sulfide (H₂S), which has an unpleasant smell like rotten eggs, is toxic to biological systems. However, recent studies have established that this reactive species is of importance in maintaining normal functions in physiology.[104] It is now recognized to be the third essential physiological mediator and cellular signaling species behind nitric oxide (NO) and carbon monoxide (CO).[105,106] Endogenous H₂S has been found in high concentrations (10−600 μM) in the brain and at a typical concentration of 10−100 μM in the blood of humans.[107,108] Recent studies have demonstrated the significance of endogenous H₂S in a number of physiological and pathological processes, such as antiapoptosis, anti-inflammation, and antioxidative effects.[109,110] On the other hand, abnormal levels of endogenous H₂S are associated with the symptoms of Alzheimer's disease, diabetes, and liver cirrhosis.[111−113] To better understand the biological roles of H₂S in complicated biological systems, recent studies have focused on the development of fluorescent sensors for H₂S, Table 1.[114] A key challenge facing these efforts stems from the comparatively high concentrations of biological thiols in cells. To date, a number of excellent investigations leading to the development of fluorescent sensors for H₂S have been carried out recently.[49]

The strategies for the design of the fluorescent sensors developed to date are generally based on the following strategies, including reduction of azides to amines, nucleophilic addition reactions, and copper sulfide precipitation.

2.2.3.1. Reduction of Azides to Amines. One approach to sensing H₂S takes advantage of the selective reduction of a fluorophore-tethered azide to an amine group by H₂S. One advantage of using this approach is the highly selective nature of the H₂S-promoted reaction over other biothiols. Using this approach, Chang and co-workers devised two rhodamine-based sensors masked by azide groups (**97** and **99**), Figure 23.[115] The two sensors, which exist in closed lactone forms, display no fluorescence. Upon reaction with H₂S, the azide is selectively reduced to form the corresponding amine with concomitant lactone ring opening in conjunction with bright fluorescent emission. The sensors showed high selectivity toward H₂S over other biothiols, ROS/RNS. In addition, they can be employed in biological applications to visualize changes in H₂S levels within living cells. Furthermore, by using the sensors, imaging of H₂S in vitro at concentrations as low as 5−10 μm can be achieved. However, some drawbacks exist with the use of these sensors. For example, approximately 1 h is required to complete the reduction reaction promoted by H₂S. This requirement may present problems in real-time detection because H₂S is metabolized rapidly.

Wang and co-workers described the interesting H₂S sensor **100** that is based on an azide reduction strategy. In this case, the azide moiety is directly attached to the sulfonyl group of a dansyl fluorophore. The sensor, which has no fluorescence initially, reacts rapidly with H₂S to form the dansyl sulfonamide

O
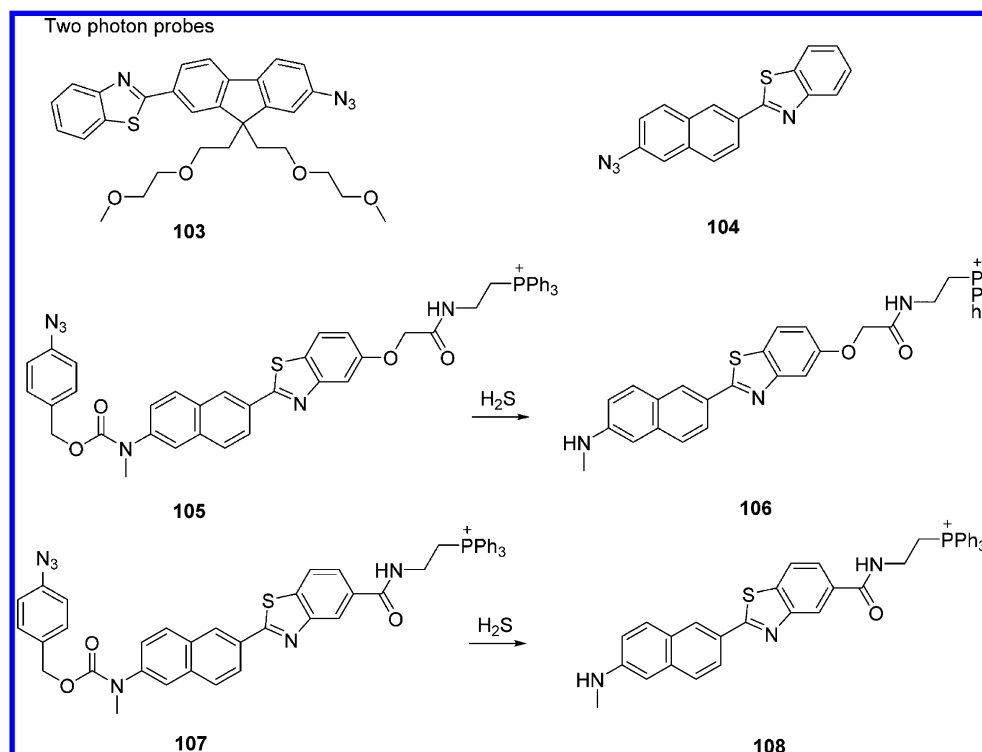
Figure 24. Structures of two photon sensors for H$_2$S.

with high fluorescence. Furthermore, a significant increase in fluorescence is observed, as is exemplified by the 40-fold enhancement in fluorescence observed with 25 μm H$_2$S in a phosphate buffer solution. Moreover, even at concentrations as low as 1 μM, H$_2$S is able to induce a noticeable change in the fluorescence intensity of this sensor. Most importantly, the response time of this sensor is only 3 min, a phenomenon attributed to the presence of the adjacent electron withdrawing from the sulfonyl group, which is claimed to enhance the reduction reactivity of the azide with H$_2$S. **100** can be utilized to detect H$_2$S in bovine serum at concentrations from 5 to 100 μM, suggesting that it is a promising platform for the design of related motifs for bioanalytical H$_2$S assays.

Pluth et al. developed the fluorescent sensor **101** containing a 4-azido-1,8-naphthalimide fluorophore, which is selective for the detection of H$_2$S over Cys, GSH, and other reactive sulfur, ROS/RNS.[116] The strategy utilized to design **101** involves masking a fluorogenic amine as an azide or a nitro group, and its liberation via H$_2$S-promoted reduction in association with turn on changes in fluorescence. Han et al. designed the fluorescence sensor **102** for cellular H$_2$S. The sensor possesses an azido−heptamethine−cyanine platform.[117] H$_2$S underwent a reduction reaction of the azide group in **102** to yield an amine along with a 40 nm fluorescent red shift. This sensor also displayed a high sensitivity with a detection limit of 80 nM. **102** was also employed to quantify H$_2$S in water as well as in fetal bovine serum. In addition, the sensor exhibited good cell permeability and was used in detection of H$_2$S in RAW264.7 macrophages.

Two-photon imaging has attracted increasing attention owing to its deep tissue penetration, efficient light detection, and reduced phototoxicity.[118] Cho reported the first two-photon fluorescent H$_2$S sensor **103**, Figure 24, which contained an azide-modified benzothiazole−fluorene moiety and displayed a 21-fold fluorescent enhancement in response to H$_2$S.

Furthermore, by using two-photon microscopy and **103**, H$_2$S could be selectively detected in live cells and living tissues at 90−190 μm depth.[119] In continuing studies, Cho and Kim devised the mitochondrial localized two-photon sensors, **105** and **107**.[120] Both sensors showed a marked fluorescent color change from blue to yellow in the presence of H$_2$S. Both of the sensors were employed in cell imaging in which **107** was brighter than those labeled with **105**. Finally, **107** was used for ratiometric detection of H$_2$S in live astrocytes and living brain slices. The results indicated that **107** displayed low cytotoxicity and minimum interference from other biologically relevant species. As a result, this sensor was used to further quantitatively analyze H$_2$S levels. In a related effort, Zhang developed the two-photon H$_2$S fluorescent sensor **104** bearing a naphthalene derivative and an azide group.[121] Sensor **104** displayed a high fluorescence enhancement for both one photon and two photon in response to H$_2$S. Moreover, a detection limit of 20 nM was observed, which is much lower than previously reported TP sensors. This two-photon sensor was applied to direct TP imaging of H$_2$S in living cells, demonstrating its practical application in the analysis of biological systems. Taken together, these new sensors illustrated the versatility of the azide moiety as a H$_2$S trigger.

2.2.3.2. Nucleophilic Addition. Employing another strategy, fluorescent sensors were designed to contain fluorescent reporters and H$_2$S trapping groups with two electrophilic reaction sites. The anticipated pathway in this design involves initial nucleophilic attack of H$_2$S to the sensor, resulting in the formation of a thiol, which then undergoes subsequent nucleophilic attack to a second electrophilic site. The process can generate a fluorescent molecule or inhibit PET, resulting in an observable fluorescence response. One of the main concerns would be avoiding reactions with biothiols, which can result in low fluorescence and/or sensor disappearance. Importantly, due to the absence of dual nucleophilicity, common biothiols
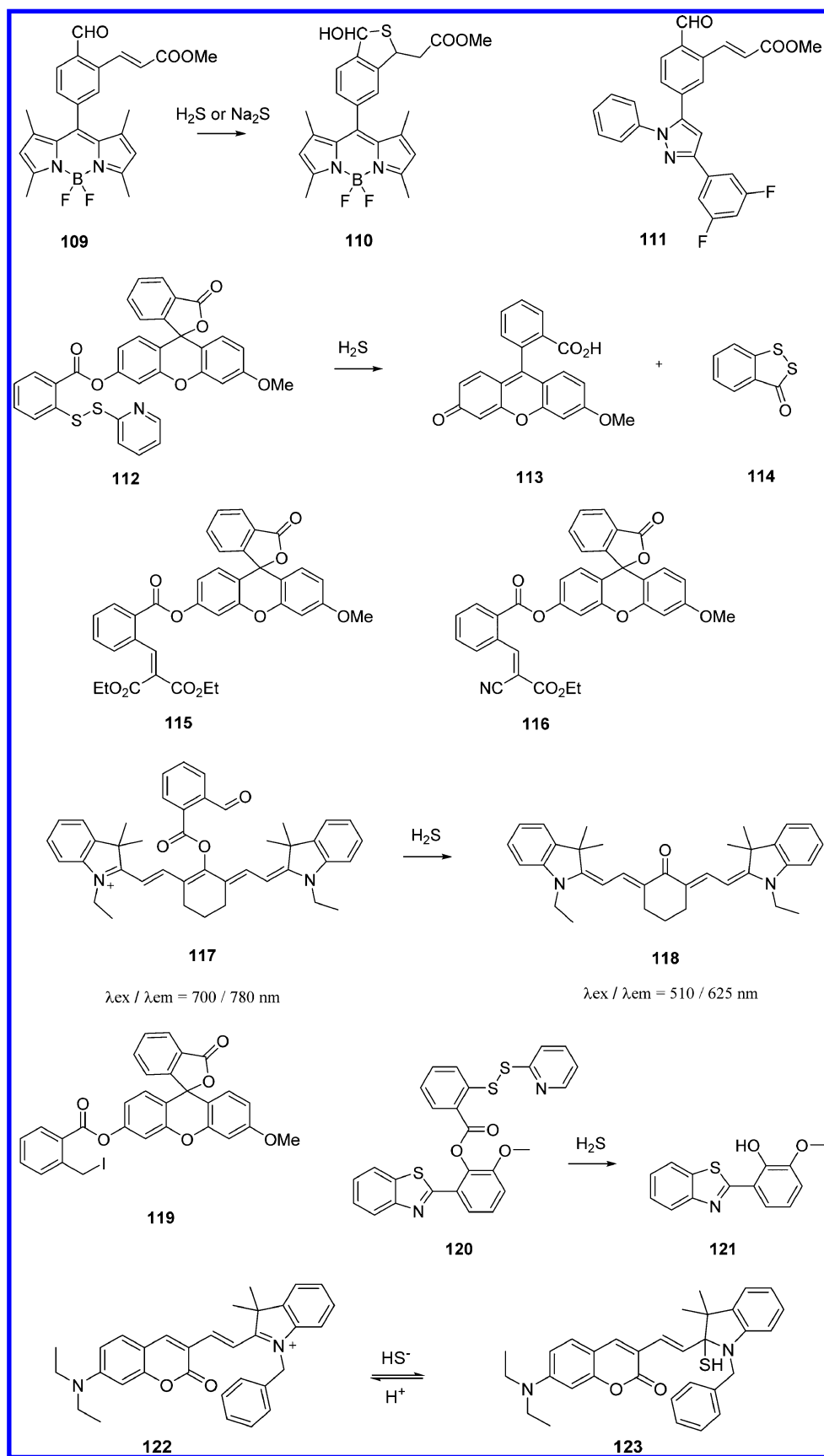
Figure 25. H$_2$S fluorescent sensors based on nucleophilic addition.

such as Cys, Hcy, and GSH cannot perform a continuous cyclization reaction, ensuring the high selectivity of these types

of sensors for H$_2$S detection. Using this general strategy, He and co-workers designed elegant sensors **109** and **111** with an

Table 2. Summary of Fluorescent H$_2$S Sensors Based on Nucleophilic Addition Reactions

	$\lambda_{ex}/\lambda_{em}$ (nm)	fluorescent enhancement	response time	detection limit	appliction in vivo
109	465/510	13-fold	60 min	5 μM	cell imaging with HeLa cells
111	300/388	10-fold	60 min		cell imaging with HeLa cells
112	465/515	70-fold	60 min	1 μM	cell imaging with COS7 cells
115	476/513	11-fold	30 min	1 μM	cell imaging with COS7 cells
116	476/513	160-fold	30 min	1 μM	cell imaging with COS7 cells
117	295/487	30-fold	2 min	0.12 μM	cell imaging with HeLa cells
119	510/625	2500-fold	35 min	0.005−0.01 μM	cell imaging with human A549 cells[a]
120	455/517	50-fold	30 min	0.1 μM	cell imaging with COS-7 cells
122	475/652	120-fold	1 min	1 μM	cell imaging with MCF-7 cells

[a]Ratio in fluorescence imaging.
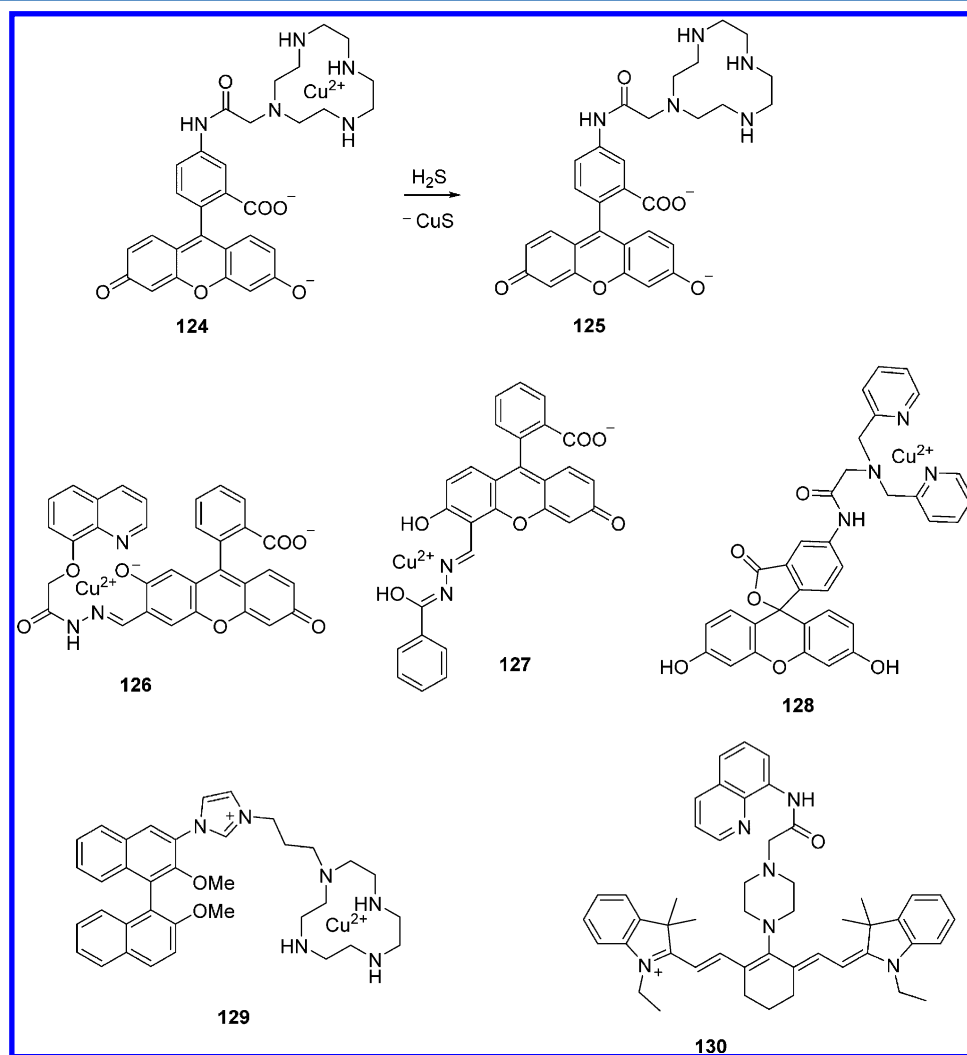
Figure 26. Fluorescent H$_2$S sensors based on CuS precipitation.

aldehyde group ortho to an α, β-unsaturated acrylate methyl ester on an aryl ring, Figure 25.[122] Nucleophilic addition of H$_2$S to the aldehyde group generates a thiol that further undergoes Michael addition with the unsaturated ester group to yield a final dihydrobenzothiophene derivative. Notably, other thiols can reversibly react with the aldehyde moiety; the resulting thioacetal product cannot participate in further nucleophilic addition. The two blue-emitting sensors, **111** and **109**, were just designed based on this Michael addition trigger strategy, Table 2. Both undergo selective reaction with H$_2$S. **109**

displayed a 13-fold fluorescent enhancement with a H$_2$S detection range from 0 to 200 μM in cells.

Another cleverly designed H$_2$S sensor **112** described by Xian and co-workers is based on a related strategy of two electrophilic sites.[123] In this case, H$_2$S displaces 2-thiopyridine to produce a persulfide in which the terminal sulfur attacks the ester moiety. This process is followed by cyclization to form a benzodithiolone with simultaneous release of methoxyfluorescein. This sensor responded to 50−500 μM H$_2$S in bovine plasma and 250 μM H$_2$S in cells. **112** also showed a high selectivity for H$_2$S over other thiols. This group developed two

additional sensors **115** and **116** bearing benzylidienemalonate and cyanoacrylate moieties as active sites for Michael addition, where the release of methoxyfluorescein took place.[124]

Tang et al. described the cyanine dye-based, near-infrared, ratiometric fluorescent sensor **117** for H_2S detection. The initial nucleophilic addition of H_2S to the aldehyde group was followed by tandem nucleophilic addition and cyclization.[125] This process induced quenching of emission at 780 nm and the appearance of a new peak at 625 nm corresponding to ketone cyanine **118**. Owing to these changes, this sensor could ratiometrically signal H_2S with a detection limit of 5.0–10 nM. The advantages of this sensor include rapid response time, high sensitivity, and mitochondria targeting ability. Endogenously generated H_2S in human A549 cells can be ratiometrically detected and imaged using **118**.

Guo et al. devised the promoted fluorescent sensor **119** that contains a 2-(iodomethyl)benzoate moiety as a new H_2S trapping group.[126] This sensor also displayed a fluorescence "'off–on'" response associated with a H_2S-induced substitution–cyclization cascade reaction involving the electrophilic CH_2–I and adjacent ester carbonyl centers. More importantly, owing to the presence of the new H_2S trapping group, **119** was more selective than 2-pyridinyl-disulfide and aldehyde-based sensors for H_2S compared to other biothiols. Finally, a sensor for live cell imaging was demonstrated. Qian designed the new ratiometric fluorescence sensor **120** for H_2S, which operates through an excited-state intramolecular proton transfer (ESIPT) mechanism.[127] This sensor showed high sensitivity and selectivity for H_2S, displaying a 30-fold fluorescence enhancement within 2 min. Moreover, the authors demonstrated that **120** could detect H_2S quantitatively with a detection limit of 0.12 μM and image H_2S in living cells.

The ratiometric fluorescent sensor **122**, which specifically senses H_2S, was developed by Guo and He. The mechanism for operation of this coumarin–hemicyanine dye involves a Michael addition reaction.[128] This sensor displayed a rapid response to H_2S and high selectivity over other biothiols. Real-time intracellular H_2S imaging using this sensor was demonstrated by employing it to preferentially target mitochondria. Moreover, visualization of the increase in the mitochondrial H_2S concentration upon NaHS addition was demonstrated by using **122** staining.

2.2.3.3. Copper Sulfide Precipitation. A strategy for detecting H_2S been successfully develop on the basis of the classic precipitation of CuS through reaction with Cu^{2+} complexes. Nagano designed the H_2S imaging sensor **124**, which consists of a cyclen macrocycle attached to a fluorescein fluorophore, Figure 26.[129] The complex showed no fluorescence initially, Table 3. In the presence of sulfide donors, CuS precipitates formed, releasing unbound **125** which induced turn-on fluorescent response with a detection limit as low as 10 μM in vitro, and its membrane-permeable diacetate derivative could detect 100 μM changes in Na_2S within cells. Zeng and Bai designed the sulfide sensor **126**, which contains fluorescein fluorophores with a pendant 8-hydroxyquinoline ligand.[130] Addition of sulfide anion at 10–100 μM concentrations leads to the precipitation of CuS and regeneration of the ligand, resulting in turn-on fluorescent response and a color change. Moreover, Zeng and Bai also prepared another **127** with a lower detection limit of 1.7 μM toward H_2S.[131] This sensor displayed a 30-fold fluorescence enhancement in the presence of H_2S.

Table 3. Summary of Fluorescent H_2S Sensors Based on CuS Precipitation

	$\lambda_{ex}/\lambda_{em}$ (nm)	fluorescent enhancement	response time	detection limit	appliction in vivo
124	491/516	50-fold		10 μM	cell imaging with HeLa cells
126	495/534	5-fold		5 μM	cell imaging with HeLa cells
127	494/523	30-fold	1 min	1.7 μM	cell imaging with HeLa cells
128	470/517	87-fold		0.42 μM	
129	331/449	4-fold		16 μM	
130	694/794	27-fold	immediately	0.28 μM	

Chang et al. reported sensor **128** for H_2S fluorescent detection, which is a Cu^{2+} complex containing a fluorescein derivative and a dipicolylamine group.[132] The sensor is nonfluorescent initially due to Cu^{2+} ions but displayed a turn-on fluorescent response in the presence of sulfide ions. The sensing mechanism is due to decomplexation of Cu^{2+} ions. Yu et al. described a fluorescent chemosensor **129** based on a cyclen-appended optically active 1,1′-bi-2-naphthol (BINOL) ligand.[133] This sensor showed reversible fluorescence responses upon addition of Cu^{2+} and S^{2-}. Thus, this sensor has the potential to be applied in physiological and environmental studies. Lin et al. reported a new NIR fluorescent sensor **130** for sulfide anion sensing.[134] This sensor showed a turn-on fluorescent response toward H_2S in aqueous media and shows excitation and emission in the NIR region. Moreover, this sensor also was highly sensitive and selective and able to operate over a wide pH range.

2.2.4. Sensors for $^1O_2$. Singlet oxygen ($^1O_2$) is an excited state of molecular oxygen, which is associated with the oxidation of cholesterol and resultant cardiovascular effects, as well as gene expression. As one of the active oxidative species, it is of high risk in biological systems due to the fact that it oxidizes various biological important molecules, such as DNA, proteins, and lipids.[5] To date, most reported fluorescent sensors for singlet oxygen were designed based on oxygen's reactivity with an anthracene moiety. 9,10-Diphenylanthracene (DPA) was first demonstrated as a recognized site for $^1O_2$ through reaction of endoperoxide. Nagano et al. designed the DPA-conjugated xanthene sensors **131**–**133** for singlet oxygen, Figure 27.[135] In the absence of $^1O_2$, these sensors are only weakly fluorescent initially due to the quenching PET effect from the DPA moiety to the xanthene moiety. After reaction with the singlet oxygen, sensors showed turn-on fluorescence responses. These responses are attributed to the formation of endoperoxide species between $^1O_2$ and the anthracene moiety, which canceled the PET process and recovered emission of the xanthene fluorophore. Nagano and co-workers also designed the 9,10-dimethylanthracene-linked xanthene sensor **137**.[136] This sensor also showed high sensitivity and selectivity toward $^1O_2$. In addition, $^1O_2$ can be detected quantitatively by using the linear relationship between fluorescence enhancement of **137** and the concentration of EP (a single source). Moreover, sensor **137** was more sensitive (53-fold) than **131**. A more sensitive and selective sensor **138** was also constructed to monitor $^1O_2$ detection in biological systems.[137] This sensor also displayed a turn-on fluorescent response toward $^1O_2$ and showed higher selectivity for $^1O_2$ than other ROS.
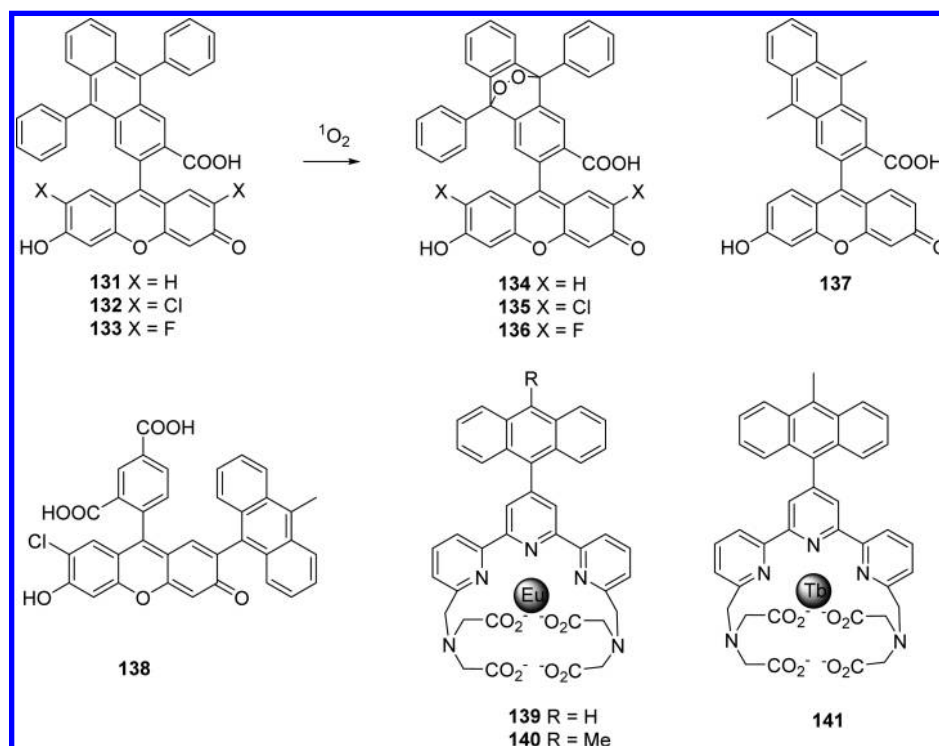
Figure 27. Fluorescent sensors for singlet oxygen.

Sensors based on lanthanide complexes have been widely developed as highly sensitive and selective time-resolved $^1O_2$ sensors, due to their ideal ability of effectively eliminating short-lived background noise arising from biological samples and optical components. On the basis of this strategy, Yuan et al. reported a series of lanthanide complex-based phosphorescent sensors **139−141**.[138,139] In the absence of $^1O_2$, the anthracene moieties of these sensors can suppress energy transfer from the excited state of terpyridine to Eu^{3+} or Tb^{3+}. Therefore, these sensors were only weakly luminescent initially. In contrast, upon addition of $^1O_2$, strong luminescence was observed due to removal of the recovery of energy transfer by formation of anthracene endoperoxides. These sensors (**139** and **140**) were shown to be highly sensitive and selective toward $^1O_2$ with detection limits of 2.8 and 3.8 nM, respectively.

2.3. Sensors for Highly Toxic Chemical-Warfare Agents

2.3.1. Sensors for Nerve Agents.
Nerve agents gained infamy as chemical-warfare agents (CWA) used in wars in undeveloped countries with hundreds of thousands of victims. They are chemically active organophosphates (OP) with a highly toxic volatile nature that irreversibly block the enzyme acetylcolinesterase (AChE) in the neuronal synapse, resulting in disrupting nerve impulse transmission and causing death. Their high toxicity is due to their strong capability of nucleophilic attack of the hydroxyl group of a serine residue at the active site of the enzyme on the electrophilic phosphorus, rendering the enzyme inoperative, and then effectively paralyzes the central nervous system.[140] Generally, a lethal dose can be as little as 0.70 mg for an average 70 kg man.

There are two main classes of nerve agents, G series and V series, including GA (Tabun), GB (Sarin), GD (Soman), and VX, as shown in Figure 28. The threat of chemical attack against civilian populations by terrorists by using nerve gas agent has been the positive motivation for extensive research in
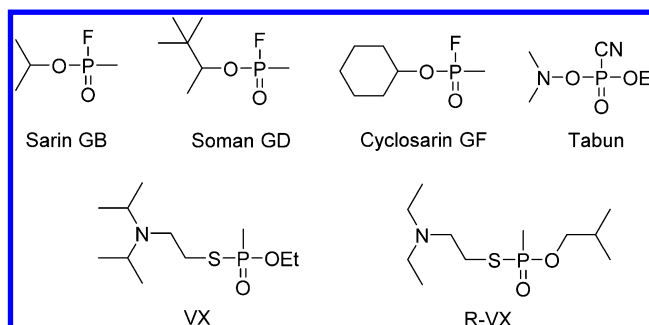
Figure 28. Structures and names of G-type and V-type nerve gas agents.

recent years. It is therefore of great interesting to develop fluorescent sensors for nerve-agent detection.

Swager et al. described a series of sensors **142−144**, as shown in Figure 30. These sensors were shown to be highly sensitive and specific fluorescent responses to diisopropyl fluorophosphate (DFP) based on intramolecular cyclization reactions.[141] Nonemissive indicator **143** reacted with DFP to produce a cyclized positively charged product, which displayed high fluorescence due to its structure becoming more planar and rigid. These sensors were demonstrated to be sensitive and selective to OP compounds with a complete response to 10 ppm DFP vapor within 5 min, Figure 29. Rebek et al. developed a series of sensors **144−148** based on pyrene compounds for fluorescent detection of organophosphorus (OP)-containing nerve-agent mimics, Figure 30.[34] The design of the chemosensors was based on suppression of the PET quenching pathway by the lone pair of electrons on the basic amine, which is known to quench the fluorescence of the nearby fluorophore. Upon binding to diethylchlorophosphate (DCP), the sensors undergo phosphorylation of the primary alcohol, and then an intramolecular substitution reaction is
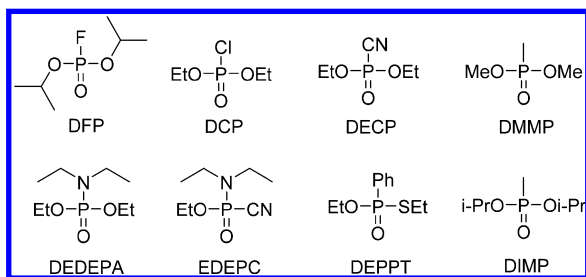
Figure 29. Structures of some relevant mimics.

undergone quickly, finally resulting in a 22-fold significant fluorescent enhancement, which could be detected by using a UV lamp. This sensor displayed an instantaneous (within 5 s) fluorescent response toward as little as 10 ppm DCP vapor. Walt et al. reported the preparation and application of polymer microbeads with fluorescein amine **149**, which showed a turn-

on fluorescent response within seconds upon exposure to diethyl chlorophosphate (DCP) vapor.[33] Aqueous solutions of sensor **149** were not fluorescent initially due to a PET effect. In the presence of DCP, its fluorescence increased. The sensing mechanism is due to the phosphorylation reaction of the aromatic amine, which cause suppression of the PET process. Moreover, fluorescent microbeads were prepared by adsorbing **149** onto carboxylate-functionalized polymer microbeads coated with poly(2-vinylpyridine). In the presence of DCP vapor, a rapid (within seconds) fluorescent response was observed. In addition, no significant response was observed in the presence of other nerve-agent simulants, a mustard gas simulant, and volatile organics in the same conditions. These wonderful characteristics of this sensor make it suitable for nerve-agent vapor detection and inclusion in microbead sensor arrays.
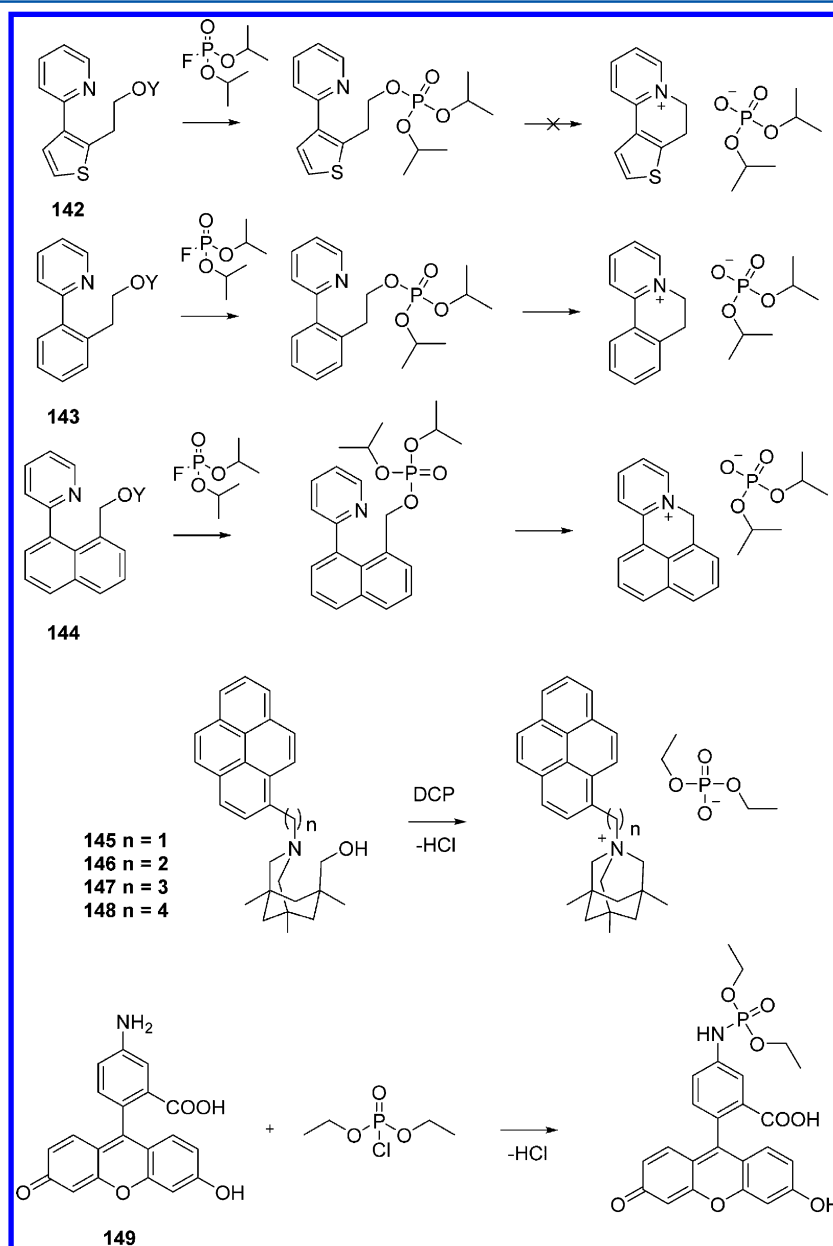
Figure 30. Structures of chemosensors based on PET mechanism.
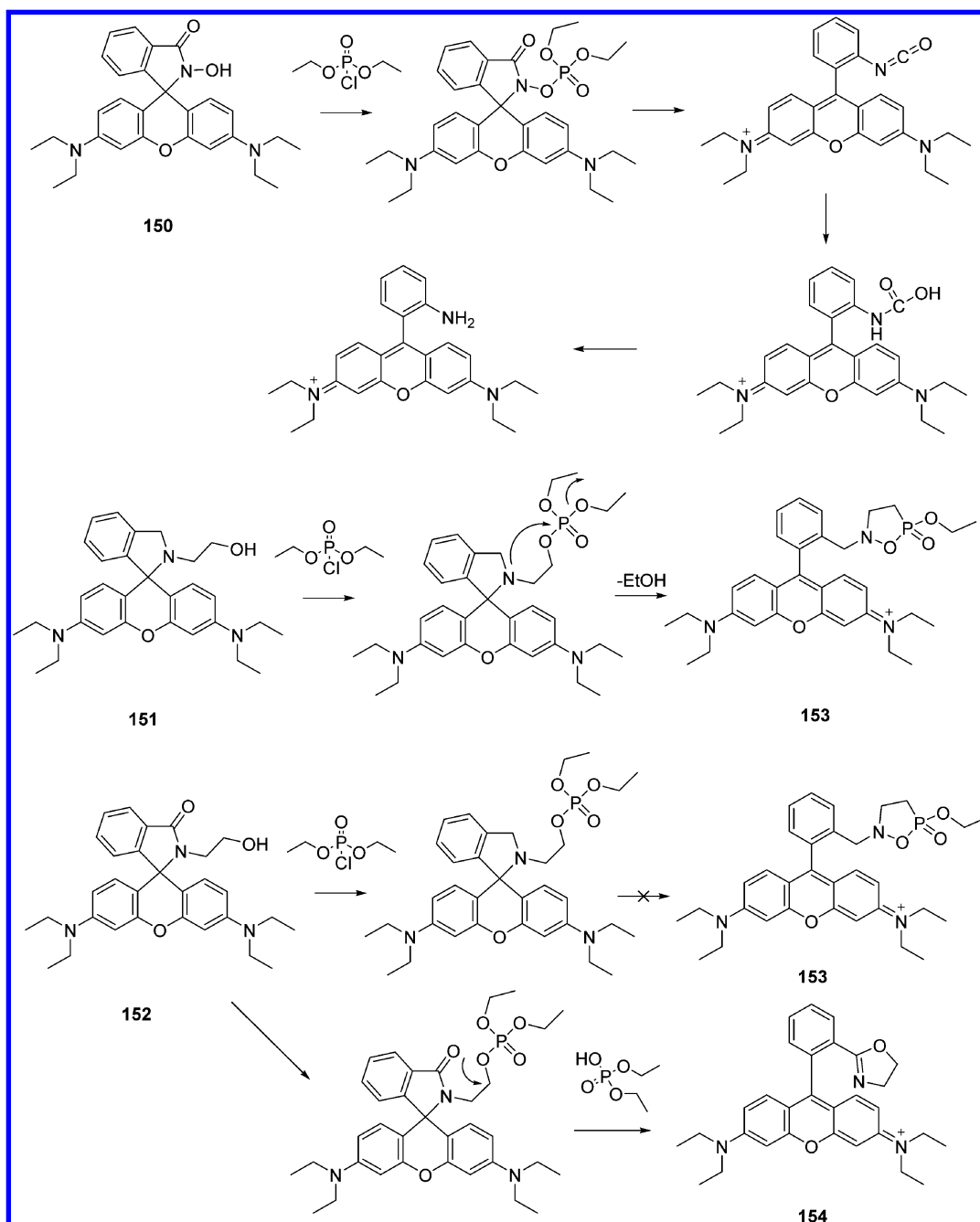
Figure 31. Structures of chemosensors based on a ring-opening mechanism.

Han et al. reported a new nerve-agent sensor **150**, which contained a hydroxamate group as a nucleophile for organophosphate.[142] Upon addition of the nerve-agent simulant (DCP) it showed a red color change and a turn-on fluorescent response. These fluorescent and colorimetic responses were achieved through a Lossen rearrangement as proved by high-resolution mass spectrometry analysis. This assay was sensitive enough to detect 25 ppm of nerve-agent mimics within 20 min. In continuing their work, this group made an improvement in the detection of a nerve-agent simulant by using *N*-(rhodamine B)-deoxylactam-2-aminoethanol **151**, Figure 31. In the presence of DCP, **151** underwent a tandem phosphorylation intramolecular cyclization to form **153**.[143] The cyclization induced highly fluorescent and colored responses. Compared to the prior sensor **150**, the assay was more sensitive and had

improved kinetics as well as highly stable fluorescence signals. Sensor **152**, the structural analog of **151**, was also tested for its detection of diethyl chlorophosphate. The results showed that nonfluorescent or colored species were produced during the reaction of **152** with DCP. These control experiments indicated that the intramolecular lactam of **152** remained closed under the assay conditions. However, by using the same sensor **152** in the same testing conditions, Wu and Dong et al. ironically reported quite different sensing responses and mechanism. In the presence of DCP, sensor **152** undergoes oxazoline formation after phosphorylation, which facilitates opening of the spirolactam ring to generate the highly fluorescent and colored species **154** with a detecting limit as low as 25 ppm.[144]

Zhou and Wang et al. reported the first FRET ratiometric fluorescent sensor **155** for the detection of OP-nerve agents.[145]
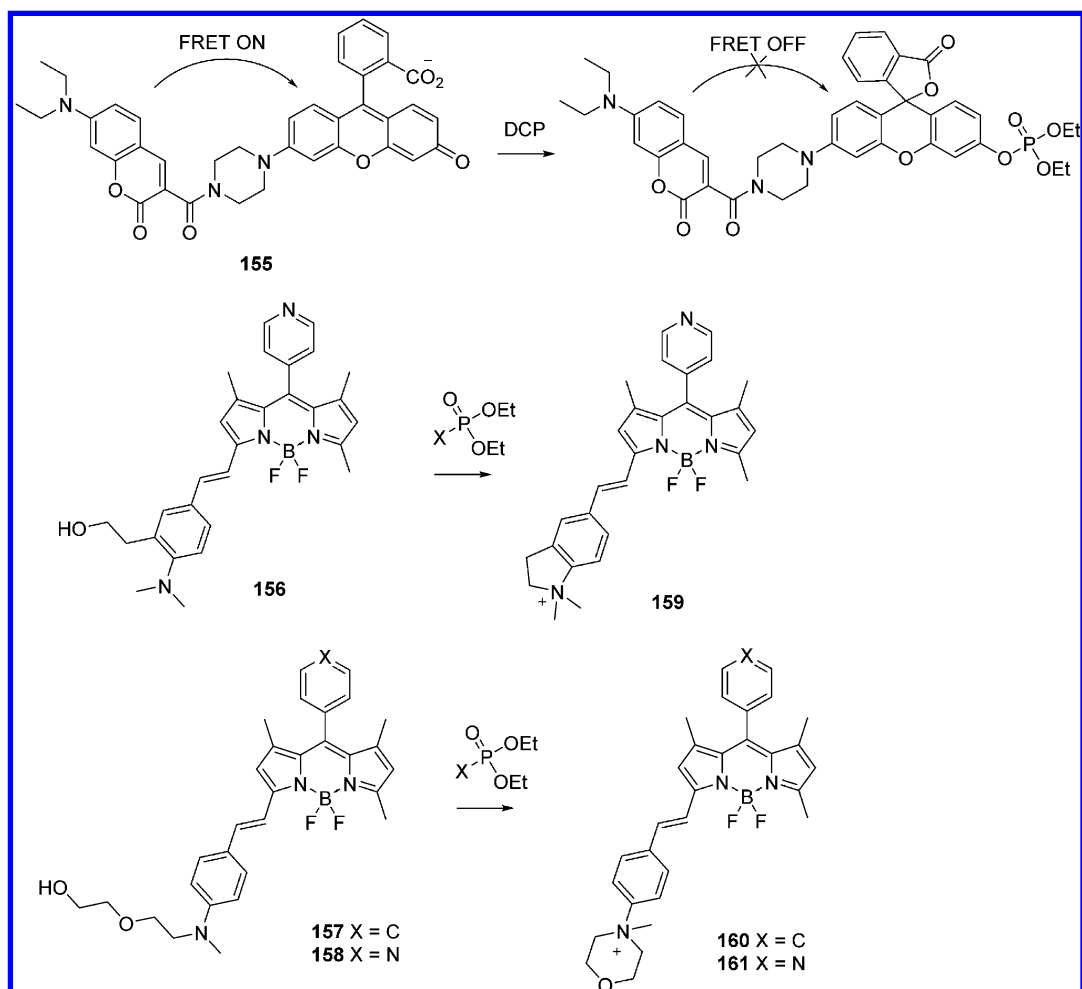
Figure 32. Structures of chemosensors for nerve gas mimics.
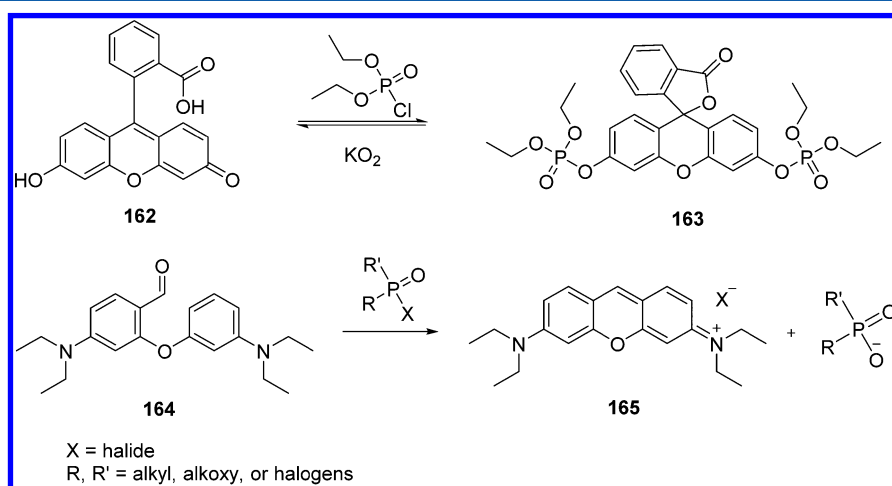
Figure 33. Structures of chemosensors for nerve gas mimics based on other mechanisms.

This sensor displayed highly sensitive ratiometric fluorescent response toward the nerve-agent mimic DCP with a 1731-fold enhancement of fluorescent intensity ratio (F_{460}/F_{536}) within 1 min along with a low detection limit of 0.17 ppm. Moreover, this sensor exhibited obvious color changes under UV light. It was also demonstrated that this sensor could detect both liquid and gaseous nerve agents. Costero and Harriman et al. reported two kinds of BODIPY derivatives **156−158** for nerve-agent

simulants detection, Figure 32.[146] The reaction of the sensors to DCNP or DFP resulted in the phosphorylation of a hydroxyl group. Next, an intramolecular N-alkylation occurred to generate a five-membered-ring quaternary ammonium salt in **159** and the corresponding morpholino cation in **160/161**. These transformations induced a significant blue shift of their absorptions, which could be easily detected by the naked eye. A more critical feature of these sensors was that they were less
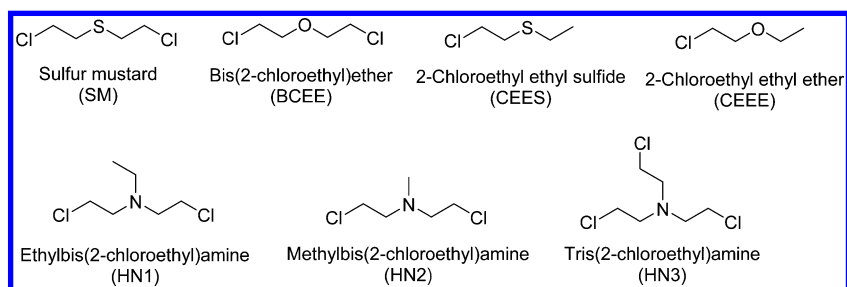
Figure 34. Structures of sulfur mustard and its mimics.
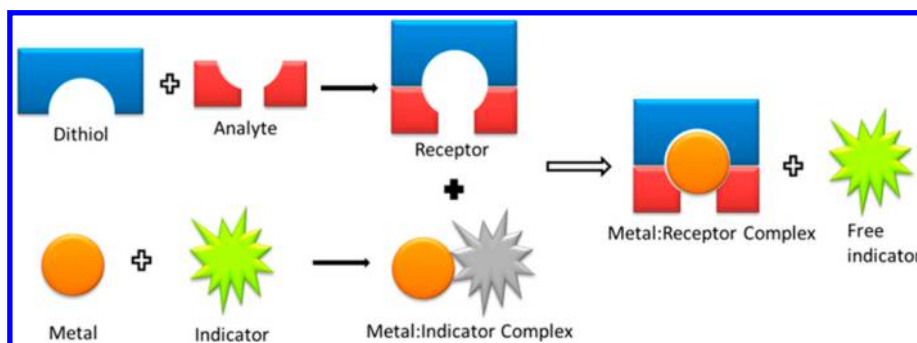
Figure 35. Presentation of an approach proposed by Anslyn et al. for the detection of mustard gas.
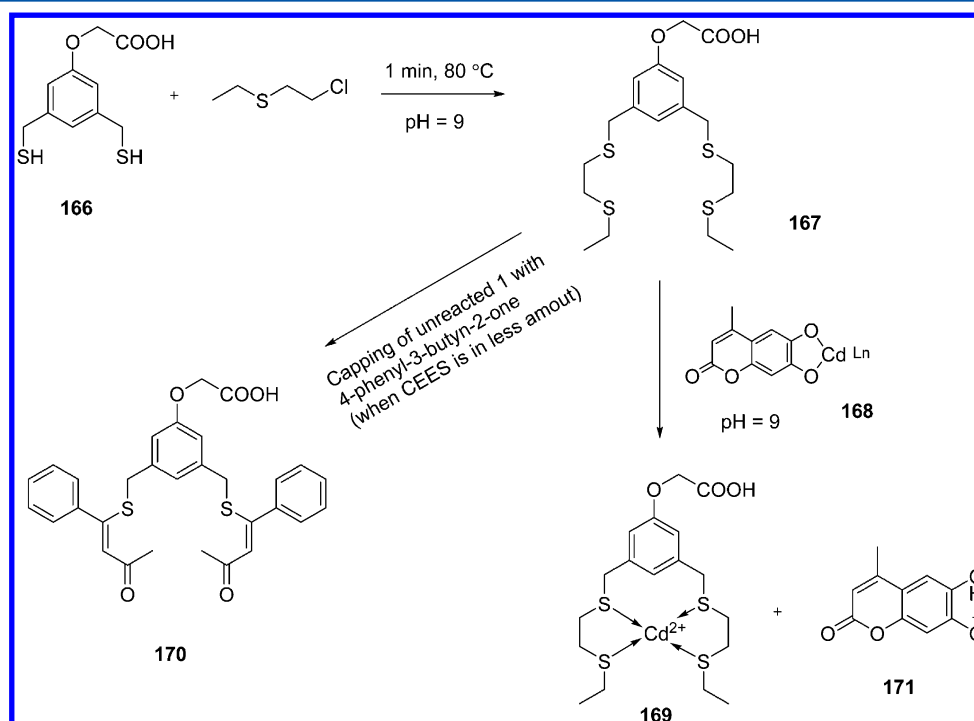
Figure 36. Presentation of a sensing mechanism for the detection of mustard gas.

prone to false readings in the presence of acids. Consequently, the sensing mechanism could work in the presence of acids, thus avoiding a false negative response.

Churchill et al. developed a reversible fluorescent sensor **162** based on fluorescein for nerve-agent simulants and superoxide, Figure 33.[147] The detection limit of fluorescein for DCP was calculated as 372.7 μM. To our own knowledge, this was the first instance where ROS and molecules related to organo-phosphonates were considered together with a single-molecular sensor. Yang et al. reported a new sensor **164** for sarin that

employed the "covalent-assembly" approach.[36] With this approach, the sensor was constructed for concise colorimetric and fluorimetric detection of sarin threats. In the absence of DCP, the **164** solution showed no absorption beyond 400 nm and exhibited no fluorescence. After 30 min, a pink color with an absorption at 563 nm and a yellow-orange fluorescence at 573 nm corresponding to pyronine B **165** was observed.

2.3.2. Sensors for Sulfur Mustard. Sulfur mustard (SM), also known as mustard gas or HD, is a powerful vesicant that has been proved as mutagenic, antimitotic, teratogenic, and

cytotoxic, Figure 34.[148−150] Sulfur mustard is considered to be a constant threat to military and humanity's security, and it may become a terrorist threat due to its simple preparation, low cost, incapacitating potential, and unavailability of an effective antidote against its toxicity.[150] Therefore, there are more motives for the development of a detection method for SM. However, unlike the developing situation for nerve agents,[151] fluorescence detection methods for SM and its mimics are nearly nonexistent due to their limited reactivity.

In 2013, Anslyn et al. developed the first fluorescent platform for SM based on a supramolecular analytical chemistry strategy (Figure 35).[152] The method proved to be a rapid, selective, and sensitive tool for SM analysis. In this method, they presented a supramolecular system containing two sections including an indicator 168 and a receptor dithiol 166. At the first stage, 166 reacted with MS to form a receptor 167, and then this new receptor 167 subsequently encapsulates Cd^{2+} and thus displaces an indicator 171 from a Cd^{2+}−indicator complex 169, Figure 36. It is notable that the unique feature of this sensing system is the tuning of reactivity and experimental conditions to avoid those potential interferents. Moreover, the detection limit was found to be 0.2 μM, which is sensitive enough to detect agent concentrations in a health risk range. However, the drawback of this method is that dithiol 166 could equally or even more strongly increase the fluorescent intensity. Thus, an intermediary step of capping any unreacted 166 prior to performing the measurement is necessary.

To overcome the drawback of above-mentioned method, Anslyn et al. reported an approach that eliminates the capping step.[153] In this approach, dithiol 166 was again employed as a reacting molecule and a thiol-susceptive organic NIR squaraine dye (172) was utilized as a new indicator. In the absence of SM, a thiol 166 reacted with 172, resulting in the bleaching of the dye, Figure 37. Nevertheless, 166 reacted with SM, resulting in retention of the chromogenic and fluorogenic properties of 172. The sensor showed a highly selective response to the SM simulant but showed no response to other electrophilic agents. The detection limit was established to be 50 μM SM simulant. The utility of such a sensing system demonstrated its usage in
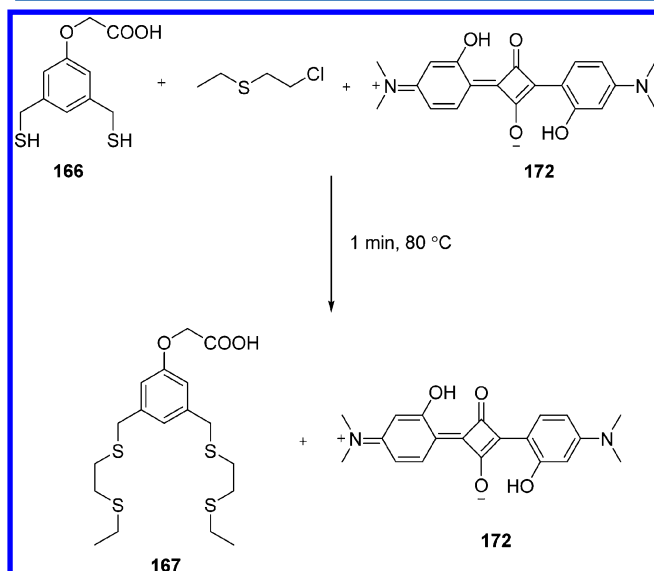
analysis of SM simulant on surfaces, in soil, and in the gaseous phase.

Pardasani et al. developed a novel turn-on fluorescence sensor 173 based on a rhodamine−thioamide derivative for selective and sensitive detection of mustard gas, Figure 38.[154] The mechanism behind the method was based on a tandem S-alkylation followed by a desulfurization reaction, which led to the spirothiolactum ring-opening reaction after reaction with SM. This process also resulted in a visual and highly fluorescent response. As shown in Figure 38, the addition of 2.5 equiv of SM caused a color change from colorless to red and exhibited intense yellow emission at 566 nm. Moreover, the control study indicated that there is no response for closely related interferences. This sensor was successfully applied to detect SM in solution and gas phase with a detection limit of 6.25 ppm.

3. SENSORS BASED ON FUNCTIONAL MATERIALS

In recent decades, nanomaterials, such as polymers, mutilporous silica materials, graphene oxide, nanotubles, and nanowires, have drawn a great deal of attention in both academic research and industrial applications due to their wonderful properties and potential values.[155−157] The development of chemosensors based on nanomaterials is a subject that continues to fascinate chemists. There has already been an explosion in the published papers on the topic of nanomaterials for gas sensing.

3.1. Sensors for Environment Gases

3.1.1. Sensors for CO₂. Recently, our group developed a sensor for CO_2 based on a polydiacetylene (PDA), 176.[37] As shown in Figure 39, the sensing mechanism is based on the primary amines that can react with CO_2 to form carbamoate anions and then neutralized the positive charge of imidazolium cations of PDA, resulting in a color and fluorescent dual response. On the basis of this strategy, naked-eye colorimetric CO_2 detection is possible both in aqueous solutions and on surfaces coated with electrospun fibers of 176. Because of its nature of the simplicity and low cost of such a PDA-based sensor, 176 may find its usage in socioeconomic environments where existing sensors would have been unthinkable.

Uemura and Kitagawa et al. reported a new luminescent sensor system for CO_2 utilizing coupled transformations of flexible porous polymers (177) and a fluorescent reporter molecule, distyrylbenzene (DSB), Figure 40.[158] In this work, the DSB molecules were introduced into the nanochannels, as shown in Figure 48. The 177−DSB composite material could selectively adsorb carbon dioxide over other atmospheric gases, such as nitrogen, oxygen, and Ar. More specifically, the adsorption of CO_2 induced a host transformation. This composite displayed a weak green fluorescence at 195 K, while a clear blue fluorescence was observed upon the absorption of CO_2 at the same temperature. Furthermore, this composite could differentiate CO_2 and acetylene, which have similar physicochemical properties, via different fluorescence responses.

Wu and co-workers utilized the pH-dependent random-coil and rodlike conformations of the halochromic polythiophene derivative, 178, to sense CO_2.[159] At high pH, 178 had a random-coiled conformation with a yellow color. On the other hand, at low pH, the color of the solution changed to pink (Figure 41). This halochromism was attributed to the conformational stretching of the polythiophene backbone and

Figure 37. Schematic illustration of the reaction between 166 and CEES in the presence of 172.
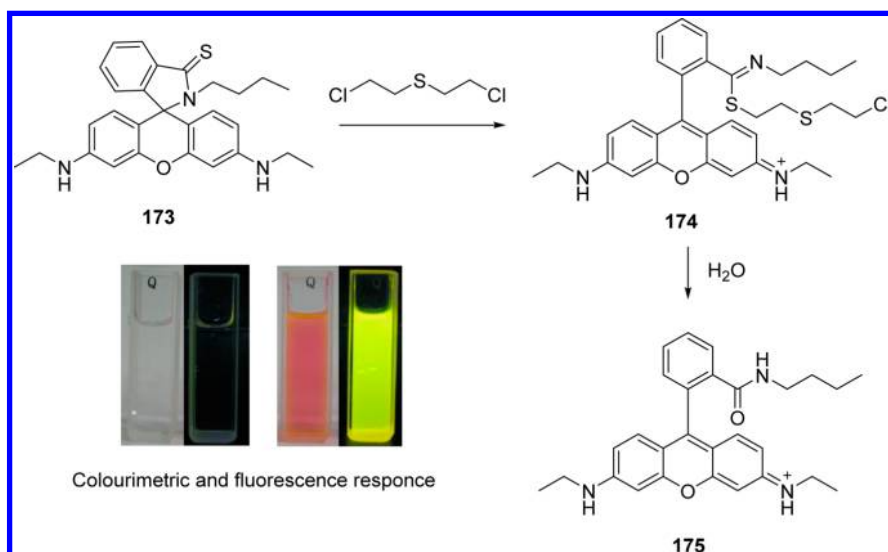
Figure 38. Schematic illustration of the reaction between **173** and mustard gas. (Inset) Color and fluorescent changes upon addition of mustard gas. Reprinted with permission from ref 154. Copyright 2014 Royal Society of Chemistry.
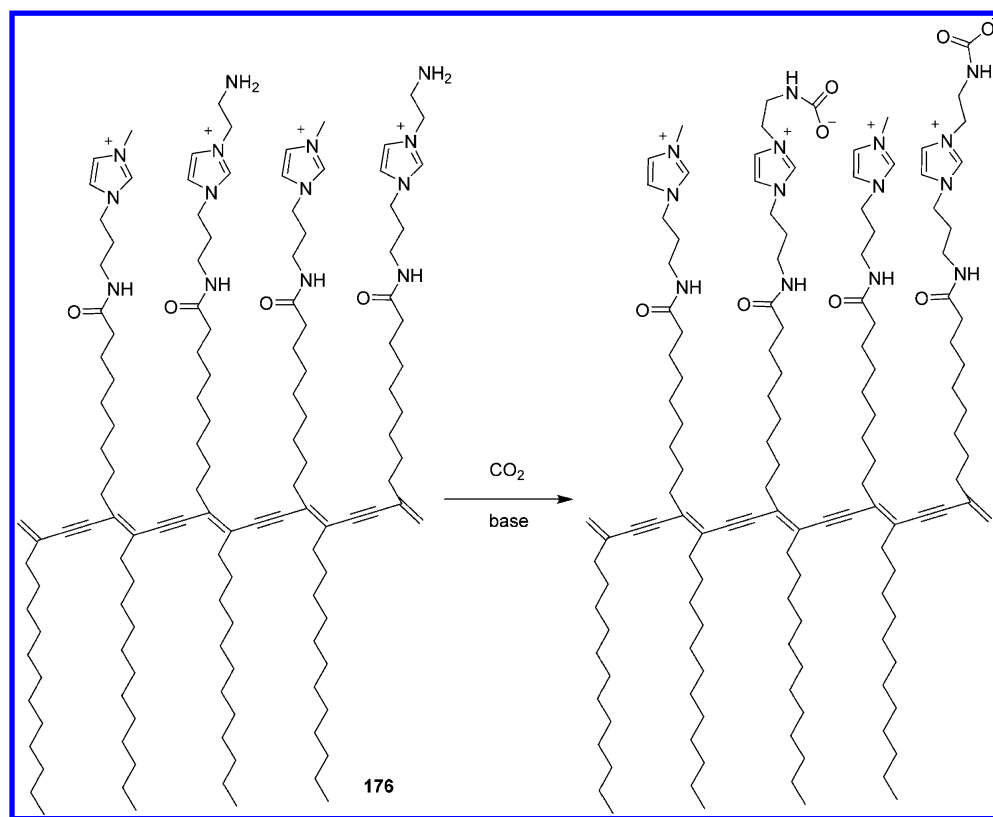
Figure 39. Structure of the PDA-based sensor **176**, and proposed mechanism of the CO_2-induced response.

formation of highly ordered aggregations, which was reversibly switched with pH oscillation between 4.0 and 10.0. The **178** solution at pH 9.8 displayed a yellow color with a maximum absorption of 408 nm, which was attributed to a random-coiled conformation. Upon bubbling with CO_2 gas for 5 min the planar conformation of **178** induced a distinct color change from yellow to red-orange. When N_2 gas was bubbled for 10 min, the solution turned back to yellow. This cycle was successfully repeated over 20 times.

Lee et al. presented a direct application of a mesoporous silica thin film as a highly sensitive sensor **179** for humidity and

CO_2 detection, Figure 42.[160] By using this mesoporous silica thin-film **179**, one of the lowest volume resolutions as well as sensitive detection of 5.1×10^{-4}% RH/Hz to water vapor in N_2 was observed, which was 70 times more sensitive than with a nonfunctionalized silica layer.

3.1.2. Sensors for O_2. Due to the use of ethylene in the food and agricultural industries, easy detection of ethylene is of great interest. The Swager group utilized the copper(I) complex **182** of fluorinated tris(pyrazolyl)borate ligand (**180** and **181**) to sense ethylene.[161] In solution, this sensory system can detect ethylene in the micromolar range. Using poly(*p*-
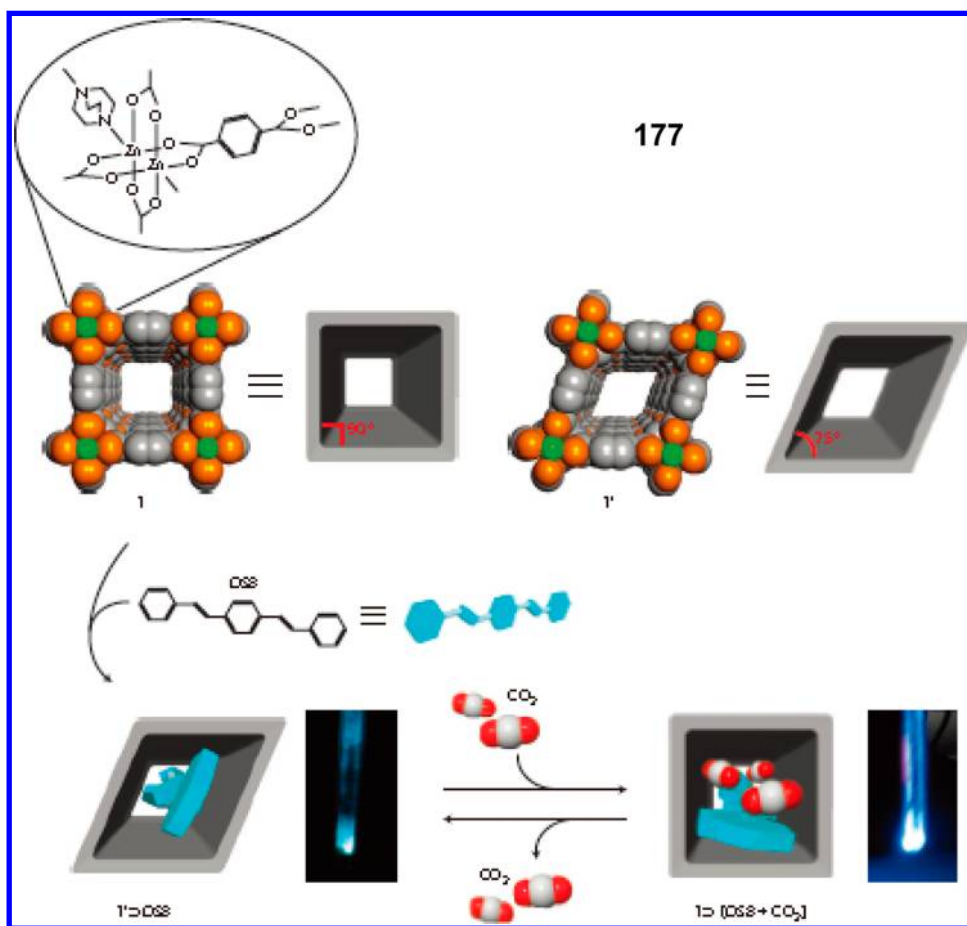
Figure 40. Scheme for the introduction of fluorescent reporter molecule DSB into flexible porous coordination polymers (**177**) and its structural and fluorescence changes upon the adsorption of CO_2. Reprinted with permission from ref 158. Copyright 2011 Nature Publishing Group.
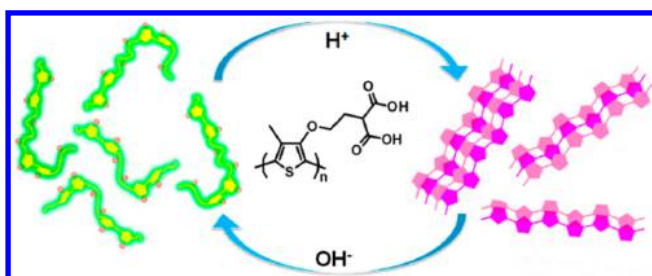
Figure 41. Structure of **178** and scheme in conformational transition due to pH changes.

Figure 42. (a) Illustration of mesoporous silica thin-film **179**. (b) Optical picture of a single die, showing an array of multiple elements. (c) Scanning electron microscope (SEM) image of the cross-section of a single CMUT resonator. (d) Optical picture of a single element with 1027 cells.

phenylene ethynylene)s (**180** and **181**)-based thin film, the sensitivity can be enhanced to as low as 1000 ppm. As shown in Figure 43, copper(I) binds to the triple bonds in the film, resulting in nearly total fluorescence quenching. Upon the addition of ethylene gas, the copper complex **182** binds to the ethylene molecules, which can revive the fluorescence, Figure 43.

Nishide et al. reported a double-layer film sensing system[162] composed of cobalt porphyrin (CoP)-linked polymer matrix and a pyrene derivative (Py) as shown in Figure 44. In this system, dual-mode oxygen sensing was possible via the formation of an oxygen adduct at the cobalt porphyrin polymer and the pyrene-induced luminescence quenching effect. More specifically, the pyrene derivative in the first layer acted as a luminesence quencher with oxygen, while the second coating of terpolymers containing CoP served to improve the oxygen

adduct formation equilibrium. As a result, the luminescence intensity of the film decreased as the oxygen partial pressure increased.

Demas et al. reported a star polymer composed of ruthenium tris(bispyridine)-linked polystyrenes (**186**) used as an oxygen sensor via measuring their sensitive luminescence lifetimes,
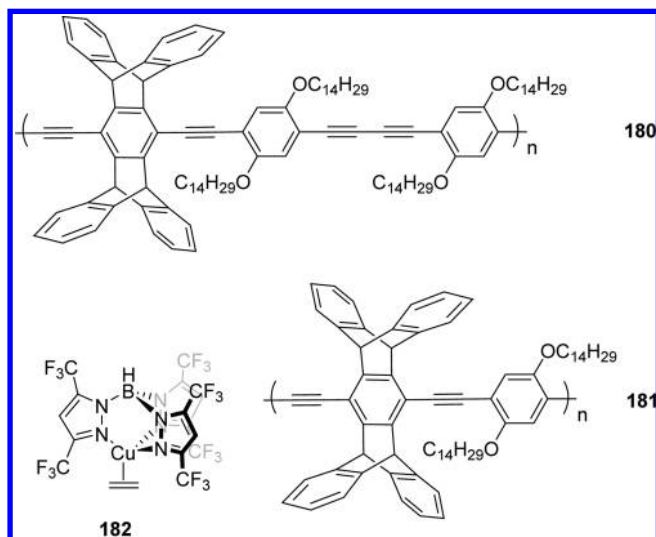
Figure 43. Structures of polymer **180** and **181** and quenching copper complex **182**.

Figure 45.[163] **186** was prepared by atom transfer radical polymerization (ATRP), one of the chain growth methods, which can provide a very narrow polydispersity (PDI). A species can be obtained by this process, solving the problem of heterogeneity, which was the main issue with the star polymer strategy.

Tian et al. chemically anchored the sensing moiety with acrylate onto a quartz surface and formed membranes by using in situ polymerization to create polymer films.[164] More specifically, they directly immobilized the quartz surface with a modified common oxygen sensor **187**. **187** is known as a phosphorescence-based oxygen sensor with a long triplet state lifetime. Hydrophilic PHEMA matrix could induce a faster response and higher sensitivity to oxygen.

3.1.3. Sensors for VOCs. Due to its excellent electrical properties, reduced graphene oxide (rGO) has been used as a platform for highly sensitive detection of gas. Meanwhile, a major issue still remained in the aspect of the poor selectivity of

rGO-based gas sensors. In this work, an array of rGO-based integrated sensors **188** was used for the performance of a single sensing element.[165] As illustrated in Figure 46, the bulk conductivity of a film was observed because of the deep penetration of water molecules into the rGO flakes. On the other hand, alcohol molecules could interact only with the top few layers of an rGO film, resulting in smaller conductivity changes. rGO-based sensor arrays could differentiate between methanol, ethanol, and isopropanol at a 100% success rate with high selectivity.

Kim and co-workers recently reported an inkjet-printed paper containing PDAs as volatile organic compound (VOC) sensor strips.[166] In the current work, a paper-based sensor strip was prepared from an inkjet-printable microemulsion system of the DA monomer (**189**), which was then photopolymerized, Figure 47. When this strip was exposed to each organic solvent vapor for 3 s at room temperature, different colorimetric changes were observed for different VOCs: a blue to purple color transition for methanol, blue to red for ethanol, acetone, toluene, EA, or ether, and blue to red or dark for THF or MC, respectively. In particular, chloroform vapor induced a color transition from blue to red to yellow, which was attributed to the exceptional solubility of the poly-4BCMU in chloroform. A reversible yellow-to-red colorimetric transition was observed for chloroform vapor. In addition, the blue-to-red transition of the PDAs was accompanied by the generation of fluorescence.

Mulchandani and co-workers fabricated a SWNTs-poly hybrid **190** through an electrochemical method and utilized it as a sensor for acetone vapor detection.[167] The optimum sensing response for hybrids fabricated at varying charge densities was found to be 19.65 mC/cm². Figure 48 explains the SEM images of SWNT and SWNT-TPP hybrid **190**. Raman spectra as well as real-time responses are illustrated in Figure 48. This chemiresistor sensor showed a dynamic range for acetone sensing from 50 to ~230 000 ppm with a detection limit of 9 ppm. It was also reported that the device showed good stability over a period of 180 days.

Duan and Xu reported functionalized SBA-15 sensors (**191**) with various loading amounts of 4,4′-diaminodiphenyl sulfone
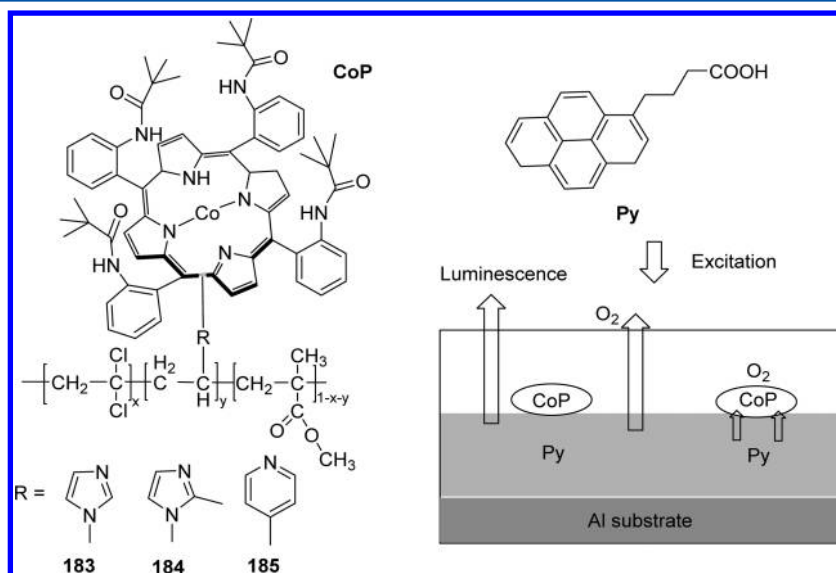
Figure 44. Structures of **183**, **184**, and **185** and a double-layer film sensing system for sensing oxygen. Reprinted with permission from ref 162. Copyright 2008 Royal Society of Chemistry.
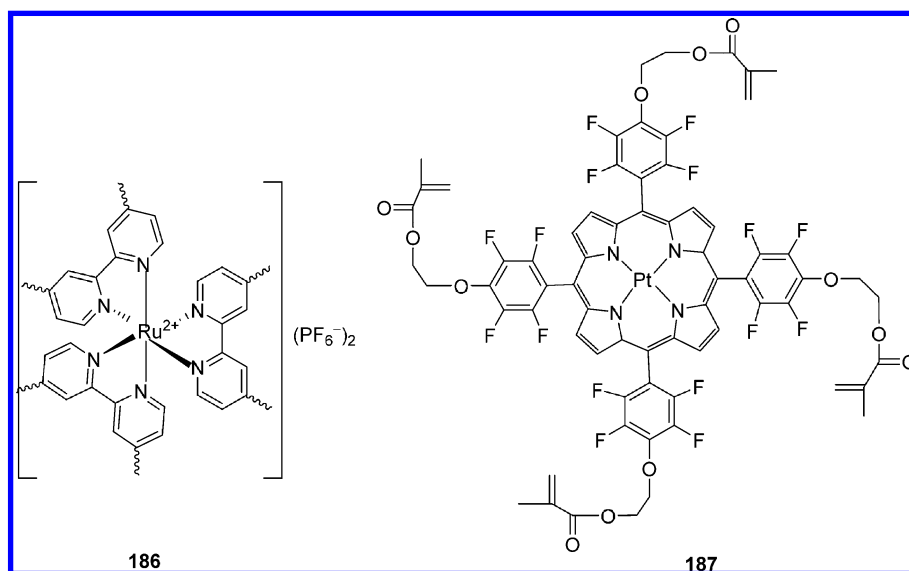
Figure 45. Structures of polymer **186** and **187**.
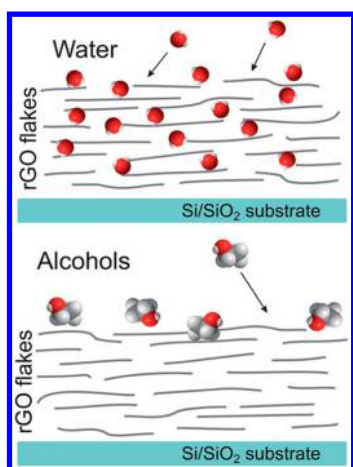
Figure 46. Proposed mechanism of analyte discrimination by gas sensors rGO films **188**. Reprinted with permission from ref 165. Copyright 2013 Royal Society of Chemistry.

(DDS) that employed a postsynthesis grafting method, Figure 49.[168] **191**-based quartz crystal microbalance (QCM) sensor showed good selectivity and sensitivity toward toluene vapor with a detection limit as low as 20 ppb. The hybrid experiments demonstrated that the highest value of 2.26×10^{-4} S cm^{-1} was observed when the DDS loading amount was 0.37 mmol g^{-1}, indicating improved proton conductivities compared to pristine SBA-15.

3.1.4. Sensors for HCl. Yoon and Kim et al. reported PDA **192**-based electrospun fibers for the detection of HCl gas via a simple color change and a fluorescence change, Figure 50.[169] For the electrospun fibers, PDA monomers containing the trimethyl amine moiety (PCDA-DMEDA) was incorporated with a poly(ethylene oxide) (PEO) matrix. As little as 2 ppm of HCl gas induced a clear color change from blue to red, which could be observed by the naked eye. On the basis of time-dependent experiments, HCl gas could be detected within 1 s. In addition, HCl gas induced large red fluorescence enhancement.

As shown in Figure 51, Wu and co-workers reported a sensor system for selective detection of HCl gas, which was fabricated

from the nanofibrous membrane of porphyrinated polyimide (**193**).[170] Along with absorption change with HCl gas, the nanofiber membrane also displayed its emission maximum at 656 nm upon excitation at 420 nm. The colorimetric and fluorescence changes of the **193** nanofiber membrane upon exposure to HCl gas were attributed to the out-of-plane distortion of porphyrins. On the basis of a surface plasmon resonance (SPR) analysis, the association constant was calculated as $(1.05 \pm 0.23) \times 10^4$ M^{-1}.

3.1.5. Sensors for NH₃. Suslick and co-workers utilized simple pH indicators to detect the change in basicity based on the reaction of a primary amine with aldehyde as a simple colorimetric system for gaseous formaldehyde (Figure 52).[171] Six different pH indicators, such as methyl red, bromocresol purple, 4-nitrophenol, alizarin, nitrazine yellow, and bromoxylenol blue, were introduced into a poly(ethylene glycol) (PEG) polymer containing five different amounts (0.24, 0.48, 0.58, 0.82, and 1.03 wt %) of PEG with amine termination. This polymer film **194** displayed distinct colorimetric changes with different concentrations of formaldehyde. It takes about 1 min to respond with 250 ppb of formaldehyde, IDLH limit (immediately dangerous to life or health limit), while 50 ppb detection, the PEL limit (permissible exposure limit), requires 10 min.

Immobilized PDAs **195** on the surface of Sc₂O₃/GaN/Sapphire substrate was utilized as NH₃-selective gas sensor by Kim et al., Figure 53.[172] For the preparation of immobilized **195** on Sc₂O₃/GaN/Sapphire, the amine group-modified Sc₂O₃/GaN/Sapphire substrate was reacted with self-assembled monomers containing PCDA-ABA and PCDA-EDEA-SA-NHS via the reaction between NHS and the amine group. Exposure of UV light induced polymerization to give the blue PDAs. Among the five different gases tested (CH₄, NO, air, N₂, and NH₃), only NH₃ induced a distinct color transition as well as fluorescence enhancement. The optical changes were attributed to the strong ionic interaction between the carboxylate of PDA and ammonium, which can disrupt the conjugation in the backbone of PDA.

Huang et al. reported the polyaniline **196**-deposited filter paper as a reversible colorimetric sensor of gaseous ammonia.[173] Although widely used, ammonia is known to be
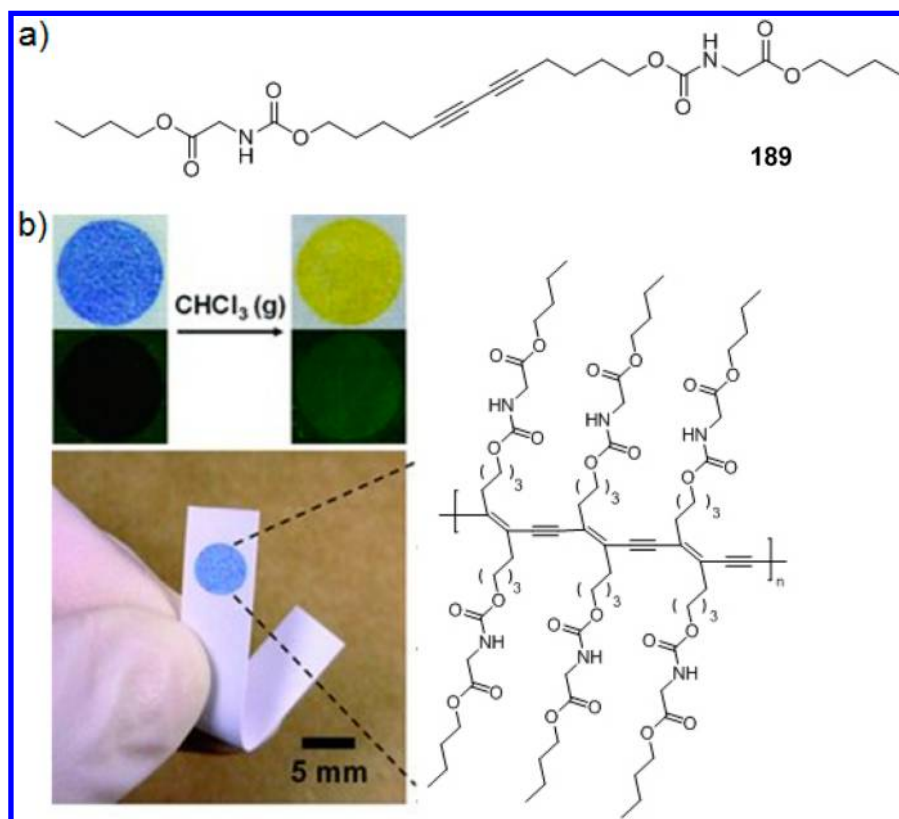
Figure 47. (a) Chemical structure of **189**. (b) Colorimetric and fluorometric changes of inkjet-printed microemulsion with chloroform (top), an image of the paper-based sensor strip for the detection of VOCs (bottom, left), and the structure of polymer **189** (bottom, right). Reprinted with permission from ref 166. Copyright 2013 WILEY-VCH Verlag GmbH & Co. KGaA, Weinheim.
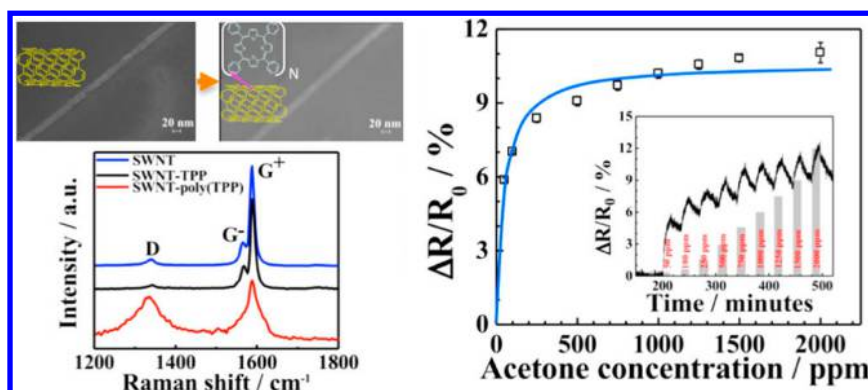
Figure 48. (Left top) SEM image of the same SWNT before and after TPP polymer deposition of **190**. (Left bottom) Raman spectra (λ_{ex} = 532 nm) of SWNTs. (Right) Real-time responses ($\Delta R/R_0$) of SWNT-TPP hybrid **190** to acetone vapors (50−2000 ppm) (inset) and corresponding calibration curve.

toxic and hazardous. In this research, they utilized conducting polymer **196**, which has various advantages, such as tunable conductivity, a reversible doping/dedoping mechanism, and a high affinity for ammonia. Nanometer-thick films were uniformly coated on cellulose nanofiber via in situ polymerization of anilines (Figure 54b). Upon protonation by hydrochloride, the emeraldine salt type of **196** displayed a green color, while the emeraldine base underwent deprotonation upon the addition of ammonia, resulting in color changes into blue (Figure 54a). The detection limits of this film by the naked eye were 100 ppm for the gaseous state ammonia in nitrogen and 10 ppm for the evaporated ammonia aqueous

solution, respectively. Furthermore, these color transitions were fully reversible.

Recently, artificial arrays of cross-reactive receptors have been used extensively for chemical and biological hazards. Since Ansyln et al. nicely covered this topic recently,[23] we will describe only a few examples related to supramolecular systems in this section. Citterio and co-workers reported a colorimetric sensor array **197**,[174] which can discriminate seven volatile amines. In this case, two different approaches were combined to discriminate these alkylamines; a general selectivity of chromogenic azo dye toward amines was combined with specific selectivities of polymer nanoparticles among these amines via introduction of different polarities. Different
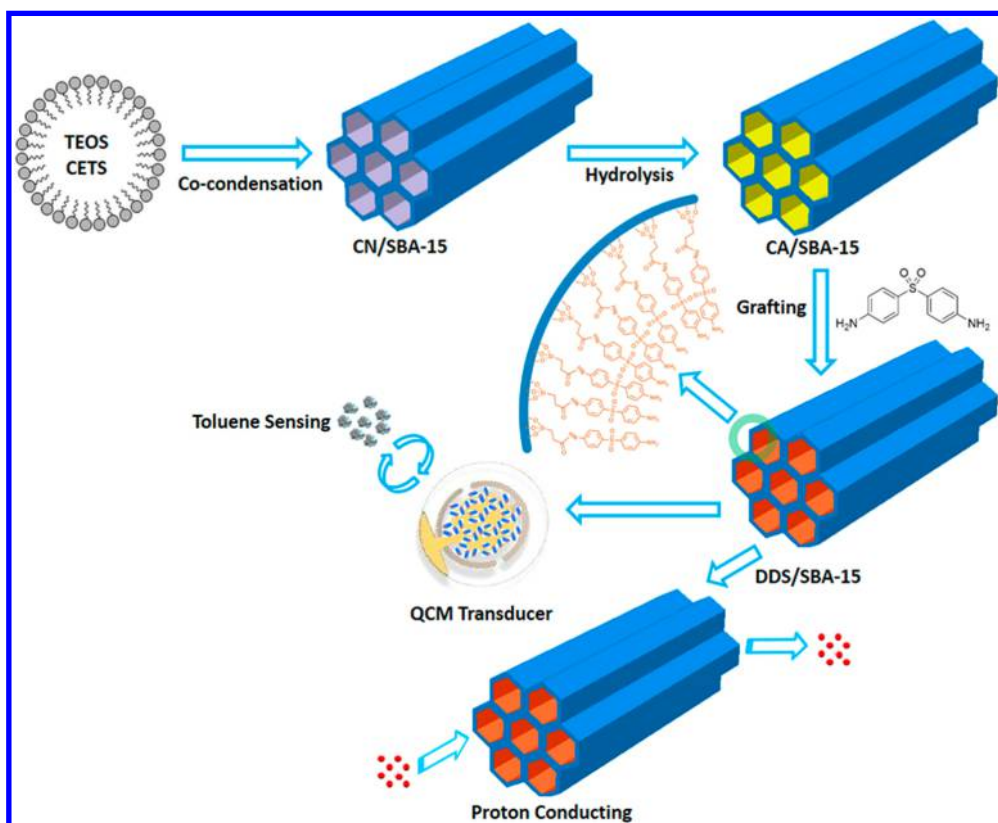
Figure 49. Synthesis of DDS functionalized mesoporous silica **191**.

polarities of polymer nanoparticles were induced by changing the ratios of dye-encapsulating hydrophobic (pBzMA) and hydrophilic [p(DEGMMA-*co*-MMA)] polymers. The red−green−blue (RGB) color-coordinate system was adopted for transforming the scanned images (JPEG) of the sensor array into numerical color values before and after addition of amine. By using these unique systems, up to 50 ppm of different amines could be detected, Figure 55.

Single-walled carbon nanotube/polyaniline composite nanofibers **198** were reported as high-performance chemosensors for HCl and NH_3.[175] The composite nanofibers displayed widely tunable conductivities (10^{-4}−10^2 S/cm) when up to 5.0 wt % single-walled carbon nanotube (SWCNT) was loaded. Chemosensors fabricated from the composite nanofibers containing 1.0 wt % SWCNT responded within 120 s to low concentrations (100 ppb) of HCl and NH_3, whereas the response time of polyaniline nanofibers was reported as 1000 s. Following the alternative introduction of HCl and NH_3, typical current−voltage (I−V) curves of the fully dedoped composite nanofiber monolayer films are displayed in Figure 56. A typical device system is also illustrated in the insets of Figure 56.

3.1.6. Sensors for Other Gases. *3.1.6.1. Sensor for H_2O_2.* Triacetone triperoxide (**199**) is known as one of the most dangerous explosives in existence. In this study, **203** was pretreated with a solid acid catalyst and the resulting decomposed products, such as H_2O_2, were detected, Figure 57.[176] For quantification, digital images of the colorimetric array were obtained using a flatbed scanner in which the red, green, and blue values in each spot were determined upon exposure to analytes at different concentrations. The colorimetric array sensor composed of redox-sensitive dyes could detect H_2O_2 with a detection limit of 2 ppb. Other common interferences, such as humidity, perfume, laundry

supplies, volatile organic compounds, etc., did not elicit any significant array response.

3.1.6.2. Sensor for CO. A hybrid sensor **200** was reported by Ho and Liao et al. in which the "key" and "lock" represented different sensing elements and specific target gases, respectively. In this case, E-mode Mg-doped In_2O_3 nanowire FET arrays were employed as the gas sensing platform and decorated with Au, Ag, and Pt nanoparticles to provide specific selectivity for reducing gases such as CO, C_2H_5OH, and H_2.[177] Figure 58 illustrates an example of a "one lock to one key" sensor system. On the other hand, the metal nanowire channel in the deep E-mode FETs decorated with nanoparticles could exhibit unique single-target gas-specific responses. In particular, the sensor arrays decorated with Au showed a selective response to CO (100 ppm) among a mixture of gases with a response time of ∼4 s and a detection limit as low as ∼500 ppb.

3.1.6.3. Sensor for NO_2. Nanowire-based devices are actively studied as bio and chemical sensors. Offermans and co-workers recently reported gold-free grown vertical InAs nanowire arrays as a nanoscale gas sensing device **201**.[178] As shown in Figure 59, the nanowires in **201** are contacted in their as-grown locations via an air bridge construction and the nanowire surface was saved for gas adsorption. These devices could detect NO_2 as low as 100 ppb. NO_2 exposure could induce both a reduction in carrier density and electron mobility. More specifically, the expected role of NO_2 is as an electron acceptor, which can reduce the electron density in the surface electron accumulation layer.

3.1.6.4. Sensor for H_2. Collins and co-workers reported that Pd-decorated defects can amplify the chemoresistive response of SWCNT devices **202** for H_2 gas.[179] Deposition of a Pd cluster onto a SWCNT sidewall defect site could induce as much as 1000-fold increases in resistance. The responses of the
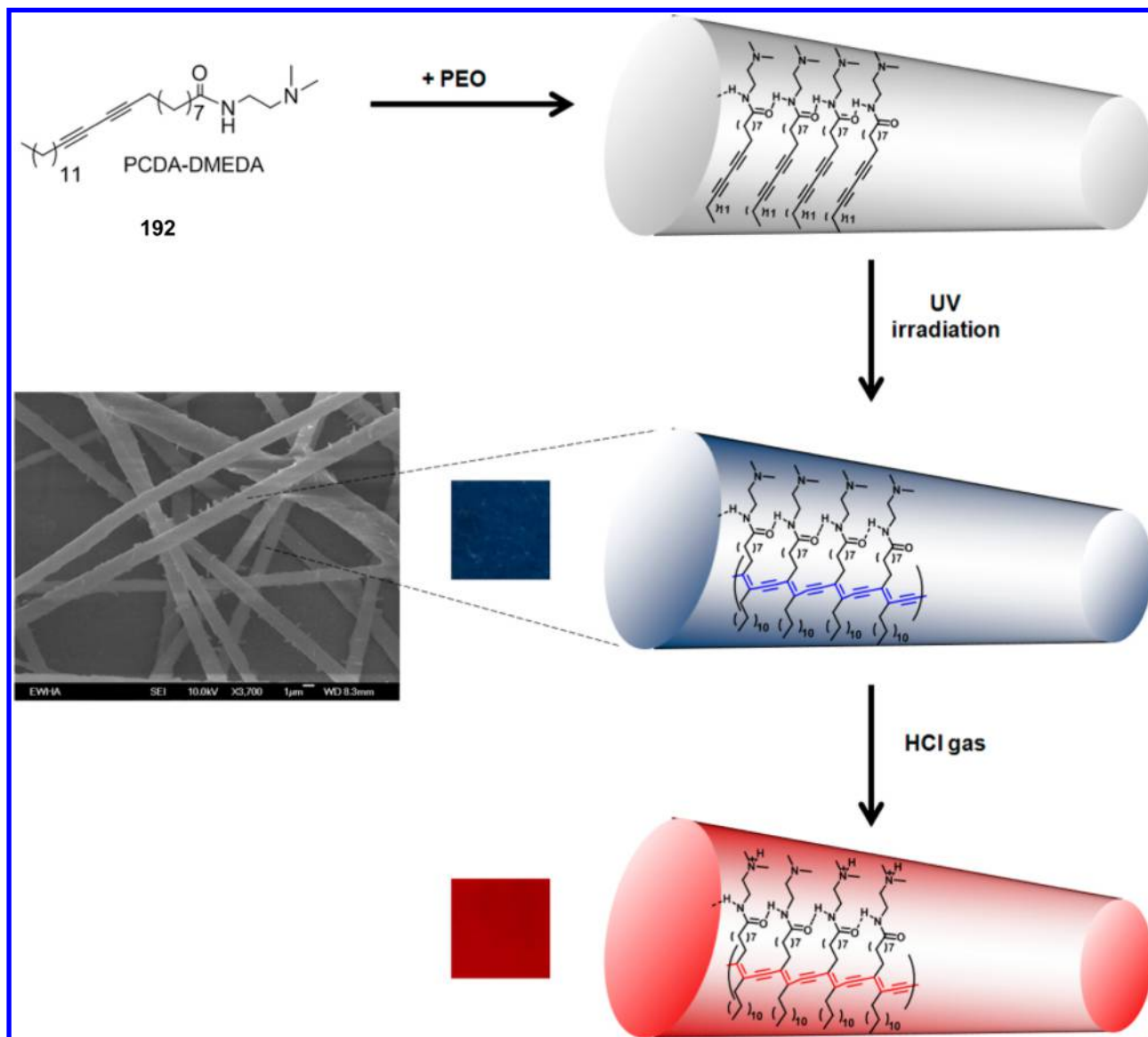
Figure 50. Schematic representation of the preparation of PDA **192**-embedded electrospun microfibers.

Figure 51. Structure of porphyrinated polyimide **193**.

Figure 52. Schemetic presenceion of sensor **194** for formaldehyde.

device to pulses of H_2 in the air before (blue) and after (red) Pd deposition are displayed in Figure 60 (top). Responses of the defective device before (blue) and after (red) Pd deposition show nearly 1000-fold increases as illustrated in Figure 60 (bottom).

3.2. Sensors for High Dangerous Gases

3.2.1. Sensors for Nerve Agents. Kim et al. reported a new colorimetric azo-pyridine-based sensor **203** and its mesoporous silica-immobilized nanoparticles **205** for nerve-agent detection, Figure 61.[180] This sensor **203** showed ratiometric changes in absorption in the presence of DCP. This change corresponded with the color change of **203** from yellow to red that can be detected by the naked eye with concentrations around 1.0 μM of the DCP nerve-agent mimic. In addition, mesoporous silica nanoparticles **205** were also used for DCP detection. **205** also showed a color change from red to yellow in an aqueous DCP solution and recovered to red again after being treated with NaOH solution.

Recently, a chromogenic array was reported to discriminate between different organophosphorus-containing derivatives.[181] DFP, DCP, and DCNP were used as simulants for nerve gases, such as Tabun, Sarin, and Soman. As shown in Figure 62, 16 different colorimetric probes were embedded in a silica gel plate to form a colorimetric array **206**. These push–pull colorimetric probes contain reactive sites, such as alcohol, amine, and pyridine moieties, which can react with nerve agents resulting in distinct color changes. In this work, optical outputs were

analyzed by a linear pattern recognition procedure, PCA, which can project data onto a two-dimensional plane.

Roukes and co-workers demonstrated that polymer-functionalized high-frequency nanoelectromechanical system (**207**) resonators coupled with micro-GC systems can provide fast and sensitive analysis of chemical vapors.[182] As shown in Figure 63, an array **207** resonators encapsulated in a micromachined flow channel were connected to a GC column. Chromatograms of 13 mixed chemical compounds from a resonator (top, blue) and a downstream FID detector (bottom, magenta) are displayed in Figure 63. These NEMS resonators displayed particular selectivity for organophosphate derivatives such as DMMP, DEMP, and DIMP. These sensors could detect subparts per billion (ppb) concentrations of a phosphonate analyte. Using the combination of these two NEMS detection channels, chromatographic analysis of 13 chemical vapors could be obtained within 5 s.

Yoon and Jang et al. reported fabricated flexible sensors based on the use of multidimensionally structured conducting polymer nanotubes as sensors for chemical nerve gas.[183] Specifically, in this work, hydroxylated poly(3,4-ethylenedioxythiophene) (PEDOT) nanotubes (**208**) were fabricated and decorated with substructures such as nanonodules (NNs) and nanorods (NRs), Figure 64. It was reported that hydroxyl groups play a key role in the interaction with the nerve agents. Among the nerve gas stimulants tested, DMMP, a simulant for sarin, displayed high sensitivity with the detection limit of 10 ppt.

3.2.2. Sensors for Explosives. Bayindir et al. reported that highly porous and transparent organically modified silica (ORMOSIL) aerogel films could sense TNT and DNT gases via fluorescence changes.[184] Mesoporous ORMOSIL materials were first prepared as thin films with hybrid aerogel (super critically dried) and aerogel-like xerogel (ambient dried) (Figure 65). The thin films could encapsulate *meso*-tetrakis-*p*-
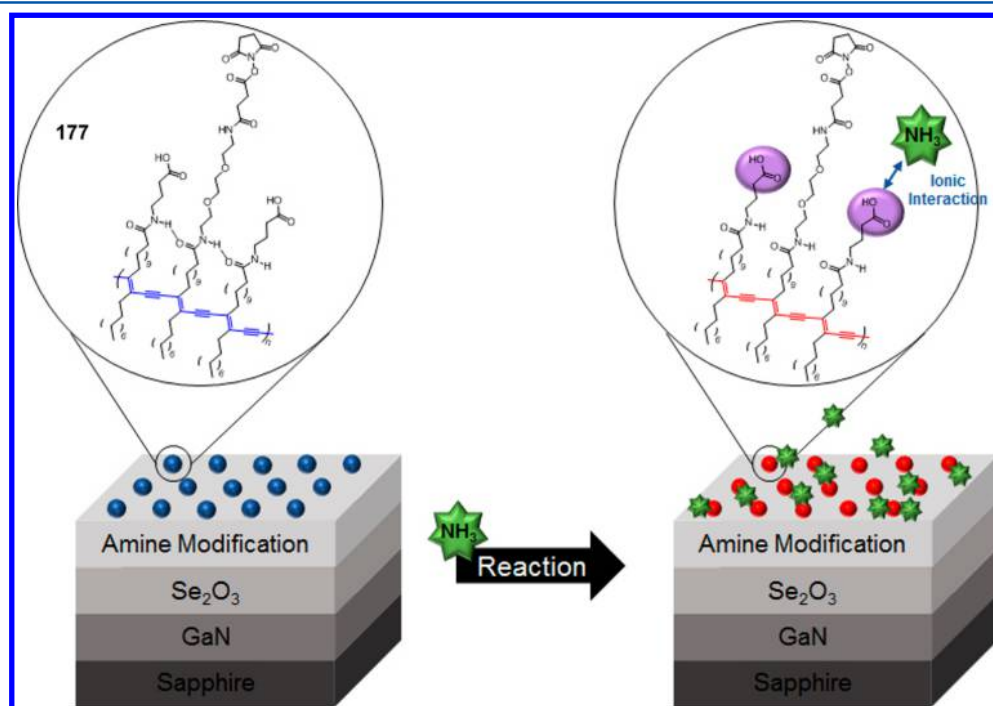
Figure 53. Schematic diagram and detection mechanism of PDA-based NH_3 sensor **195**. Reprinted with permission from ref 172. Copyright 2007 WILEY-VCH Verlag GmbH & Co. KGaA, Weinheim.
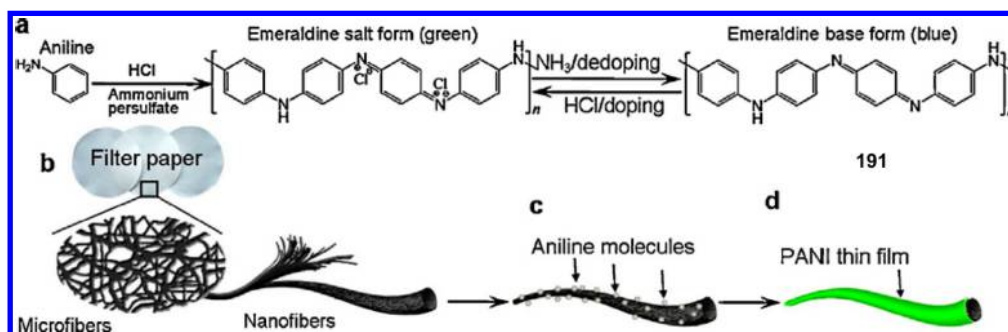
Figure 54. Scheme for the color transition of **196** (a) and the fabrication process of the **196**-deposited filter paper (b−d). Reprinted with permission from ref 173. Copyright 2013 Elsevier B.V. All rights reserved.
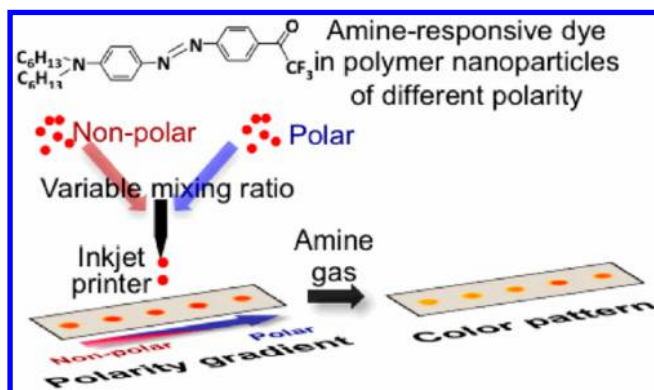
Figure 55. Inkjet-printed paper-based sensor array **197** for the discrimination of volatile primary amines.

Figure 57. (a) Mechanism for acid-catalyzed decomposition of **199**. (b) Color difference maps of **199** vapor with different concentrations after 5 min exposure.

carboxy-phenylporphyrin (TCPPH$_2$) in their silica network. TNT and DNT gases induced fluorescence quenching of these films. Even though both TNT and DNT showed similar quenching efficiencies at the beginning, TNT quenching efficiency sharply increased compared to that of DNT gas after the first minute. These results were attributed to the higher binding affinity of TNT with electron-rich porphyrin rings.

Li et al. reported the synthesis of functionalized mesoporous silica SBA-15 as a new kind of high-performance chemical sensor **210** for highly specific chemical-vapor detection at trace levels, Figure 66.[185] In this case, two sensing materials for trinitrotoluene (TNT) and ammonia/amine were prepared, respectively. Experimental results indicated that the sensors

showed highly specific and rapid detection of TNT vapor with a detection limit at the parts per trillion level. Moreover, the mesoporous silica was loaded onto the cantilever resonating sensor after functionalization with a carboxyl group that exhibited an ultrafine detection limit of tens of parts per billion to ammonia/amine gases.

Knapp and co-workers utilized Zn (salicylaldimine) (ZnL) complexes as fluorescent chemosensors for the detection of
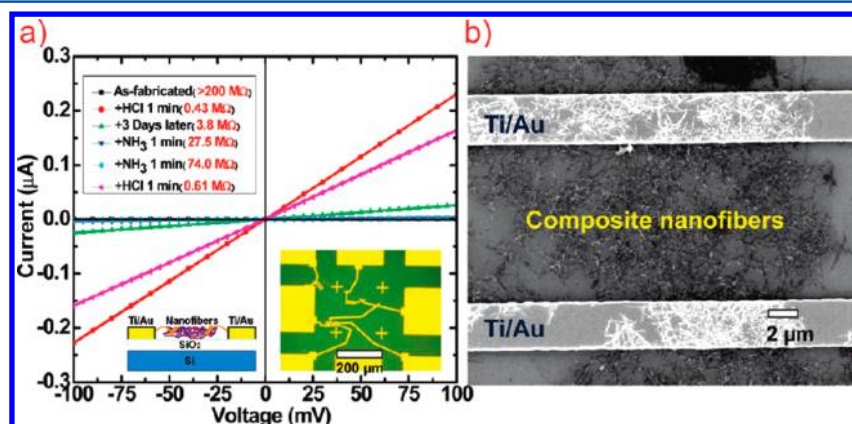
Figure 56. (a) Typical $I-V$ curves of nanofibrillar 1.0 wt % SWCNT/polyaniline composite films **198** upon exposure to alternating vapors of HCl and NH$_3$. (Insets) The geometry of the device: (left) front view and (right) top view. (b) SEM image of the device.
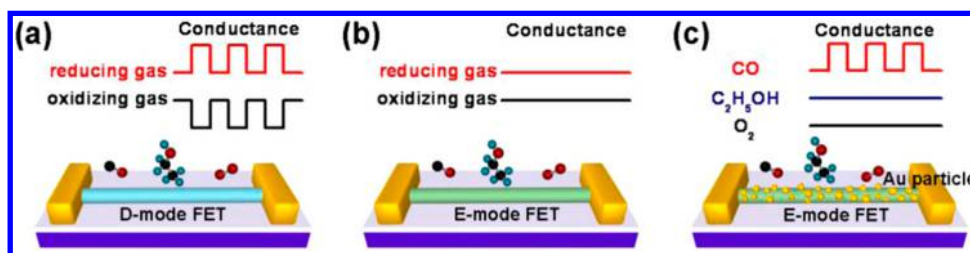
Figure 58. Example of "one lock to one key" sensor system **200**.
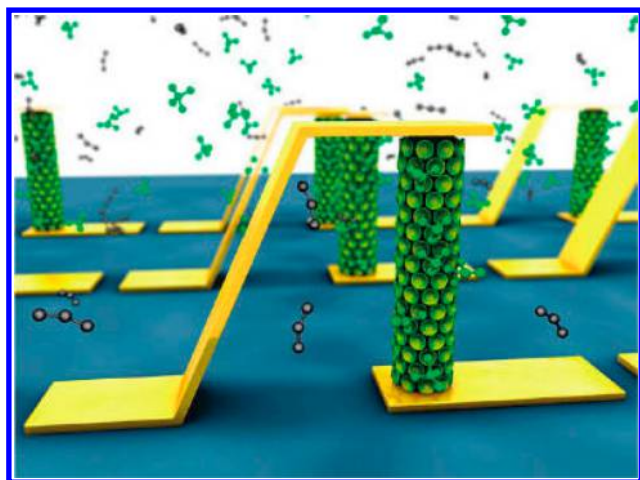
Figure 59. Illustration of selective adsorption of gas molecules on a contacted vertical nanowire surface of **201**.
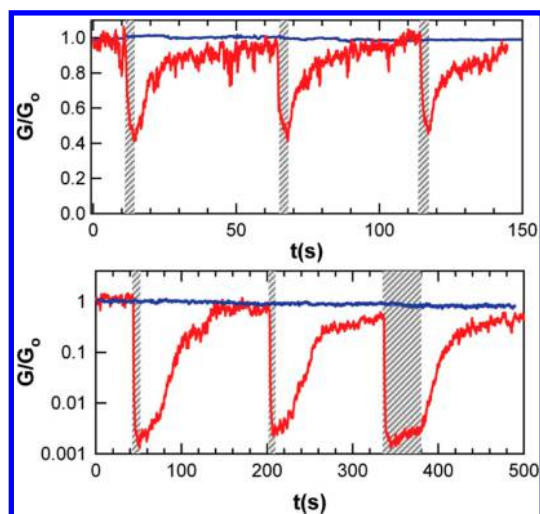
Figure 60. Response of the device to pulses of H_2 in air: before (blue) and after (red) Pd deposition (top). Response of the defective device **202** before (blue) and after (red) Pd deposition.

explosives, Figure 67.[186] Nitroalkanes and nitroaromatics induced fluorescence quenching effects by photoinduced electron transfers. On the basis of these different fluorescence quenching effects, an array **211** containing seven ZnL derivatives (a-g) and a fingerprint for each of nine different nitroalkanes and nitroaromatics was generated. Even though some overlaps were observed between analyte classes, the unknown samples tested could be identified 100% correctly.

4. CHEMOSENSORS BASED ON METAL OXIDE SEMICONDUCTOR

Following the first attempt to use ZnO thin films as a gas chromatographic detector by Seiyama et al. in 1962,[187] metal oxide semiconductors (MOS) material-based gas sensors have attracted extensive attention due to their low cost, compact size, high sensitivity, fast response/recovery time, simplicity of fabrication, large number of detectable gases, and low detection limits (<ppm levels).[188] The reactions between the surface complexes such as O^-, O_2^-, H^+, and OH^- reactive chemical species and the gas molecules induce MOS's resistance changes which signal the target gas.[189] On the basis of their sensing mechanism, there are two main types of MOS gas sensors including n-type semiconductor in which electrons are the majority carriers (such as SnO_2, Fe_2O_3, ZnO, In_2O_3, TiO_2, WO_3, MoO_3, Nb_2O_5, V_2O_5, etc.) and p-type semiconductor (such as NiO, CuO, CoO, etc.).[190,191] The MOS gas sensors have developed to be one of the mostly applied gas sensors in various fields including environment, transportation, medicine, and agriculture.[192,193]

In recent years, efforts on MOS gas sensors have been focused on improving sensitivity, selectivity, stability, and reproducibility.[194] These MOS gas sensors are closely related to their morphologies and compositions. The sensitivity can be improved by decreasing grain sizes to the nanoscale comparable to twice their Debye length by the addition of appropriate dopants. A number of nanostructured MOS sensors such as nanowires, nanobelts, nanoparticles, nanorods, and nanotubes, etc., have been demonstrated to be excellent candidates with ultrahigh sensitivity due to their high surface-to-volume ratio.[195,196] These progresses on MOS materials have been reviewed from different aspects, such as nanoscale materials,[196−198] synthesis methods,[47] and sensing mechanism.[189,199] However, the realm of MOS gas sensors is too wide to have a comprehensive understanding of the entire field.[200] In this review, the ongoing research of MOS gas sensors is summarized according to the classification of gas species, which would be an accessible way to help those new to the field to get a full picture of the field. Most of the representative MOS sensors in the past 10 years were reviewed, and their sensing properties were listed in tables. Important progress with respects to the sensitivity, selectivity, and operation temperature was, discussed and readers can refer to the literature for more details.

4.1. Sensors for Environmental Gases

4.1.1. Sensors for VOCs. Volatile organic compounds (VOCs) are chemical byproducts emitted from industries and accumulated little by little in our living atmosphere. These VOCs not only cause environmental pollution but also directly affect human health. For example, alcohols and aromatic hydrocarbons are potentially hazardous to human health due to
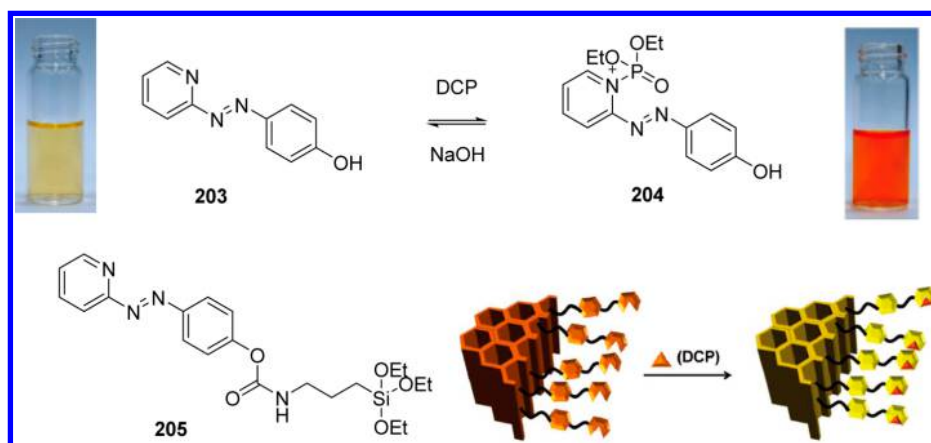
Figure 61. Proposed mechanism and color response of silica-based sensor **205** in DCP sensing. Reprinted with permission from ref 180. Copyright 2011 WILEY-VCH Verlag GmbH & Co. KGaA, Weinheim.

their capabilities to stimulate the mucous membranes and upper respiratory tracts. Formaldehyde (HCHO) is highly toxic even at low concentration. Despite their toxicity and hazard, VOCs are still used in industries as intermediates to produce other chemicals and as solvents in research laboratories. Therefore, the development of gas sensors for early detection of VOCs is necessary.

MOS-based chemoresistive sensors are popular for detecting toxic and inflammable VOCs in these years. In this context, binary metal oxide sensors (e.g., SnO_2, ZnO, WO_3, TiO_2, etc.) and their cation-modified counterparts have extensively been studied by various research groups. In this part of the review, we place special focus on the detection of various VOCs including ethanol, formaldehyde, BTX (benzene, toluene, and xylene), and acetone using all kinds of MOS sensors.

4.1.1.1. Ethanol. Ethanol (C_2H_5OH), which is a volatile, flammable, colorless liquid, is most commonly used as a solvent and in alcoholic beverages.[201] A variety of metal oxides have been investigated for ethanol sensing as shown in Table 4. Among these, the most representative sensor materials are SnO_2 and ZnO. For instance, a SnO_2 sensing thin film was produced via a combustion chemical vapor deposition process, and 500 ppm ethanol was investigated at an operating temperature of 300 °C.[202] In order to improve the sensitivity for ethanol, Li et al. prepared a SnO_2 nanoplate. The SnO_2 nanoplates can respond to a low concentration of 1.5 ppm ethanol. Meanwhile, the sensitivities of multilayer SnO_2 nanoplates were measured to be twice as high as that of the single-layer SnO_2 nanoplates for 50 ppm ethanol attributing to the larger surface area of multilayer nanoplates.[203] Furthermore, a nanopillar ZnO array sensor was formed by means of a chemical two-step route, with a response to ethanol at a concentration of 10−2500 ppm diluted in dry air at an operating temperature of 350 °C.[204] In addition, the unloaded ZnO semiconducting oxide sensor was also reported by Hsueh et al.[205] and Chu et al.,[206] which were able to detect parts per million level of ethanol at a relatively lower operating temperature.

Later, in order to enhance the ethanol gas selectivity, sensitivity, and response/recovery speed, noble metal catalysts, such as Pd,[207] Pt,[208] and Sb[209] have been loaded onto SnO_2 and ZnO. Wan et al. reported the synthesis of Sb-doped SnO_2 nanowires by the thermal evaporation process. They find that Sb−SnO_2 nanowires showed a very short recovery time of about 5 s to 10 ppm ethanol gas at 300 °C.[209] Furthermore, the

SnO_2 nanowires decorated by isolated Ag were presented by Hwang et al. (Figure 68a and 68b), which displayed a 3.7-fold enhancement in gas response to 100 ppm of C_2H_5OH at 450 °C compared to pristine SnO_2 nanowires.[210] Figure 68c and 68d shows the response of the pure SnO_2 nanowires and 5Ag−SnO_2 sensor to 100 ppm of C_2H_5OH, NH_3, H_2, and CO at 450 °C and indicated that the decoration of Ag nanoparticles is very effective for enhancing not only gas response but also selectivity for C_2H_5OH. Another semiconducting oxide with high selectivity to C_2H_5OH was In-doped ZnO nanowires. It can detect at a low concentration of 1 ppm of C_2H_5OH and exhibited very fast response and recovery times (2 s, respectively).[211]

In addition, oxide additives, such as SiO_2,[212] Mn_3O_4,[213] and WO_3,[214] can also be loaded to SnO_2 and ZnO semiconducting oxide as ethanol sensors as shown in Table 4. Tricoli et al. reported the SiO_2-doped SnO_2 particles produced in one step by flame spray pyrolysis (FSP). The sinter neck size can be controlled by addition of 0−4 wt % of silica, thus enhancing the sensitivity and detecting even at a low concentration of ethanol (100 ppb).[212] The SnO_2 nanowires coated with a La_2O_3 layer were prepared by deposition of $La(NO_3)_3$ aqueous solutions for accomplishing both high sensitivity and high selectivity to C_2H_5OH.[215] Mn_3O_4-decorated ZnO also exhibited high selectivity to ethanol as shown in Figure 69.[213] The responses of both sensors to 100 ppm of C_2H_5OH were higher than that to 100 ppm of NH_3, CO, C_3H_8, and H_2 in the range of 300−450 °C. However, compared to pure ZnO nanobelts, the C_2H_5OH responses of Mn_3O_4-decorated ZnO nanobelts are significantly higher especially at 400 °C. It is noteworthy to mention that in all these studies the selectivity of the oxide semiconductor sensors to C_2H_5OH was enhanced, indicating chemical sensitization of noble metals or noble metal oxides.

Apart from SnO_2 and ZnO, which exhibit classical n-type oxide semiconductivity, various semiconducting metal oxides have been extensively studied by researchers, including other n-type oxide semiconductors such as WO_3,[216] In_2O_3,[217] and Fe_2O_3,[218] and various p-type oxide semiconductors such as NiO,[219,220] CuO,[221] Co_3O_4,[222] and Cr_2O_3.[223] For instance, Vallejos et al. reported the codeposition of WO_3 nanoneedles and Au nanoparticles via aerosol-assisted chemical vapor deposition (AACVD) to construct Au−WO_3 samples, which have high sensitivities to low concentrations (1.5 ppm) of ethanol at a relatively low temperature of 250 °C.[216] In addition, the porous NiO nanotubes with controllable interior
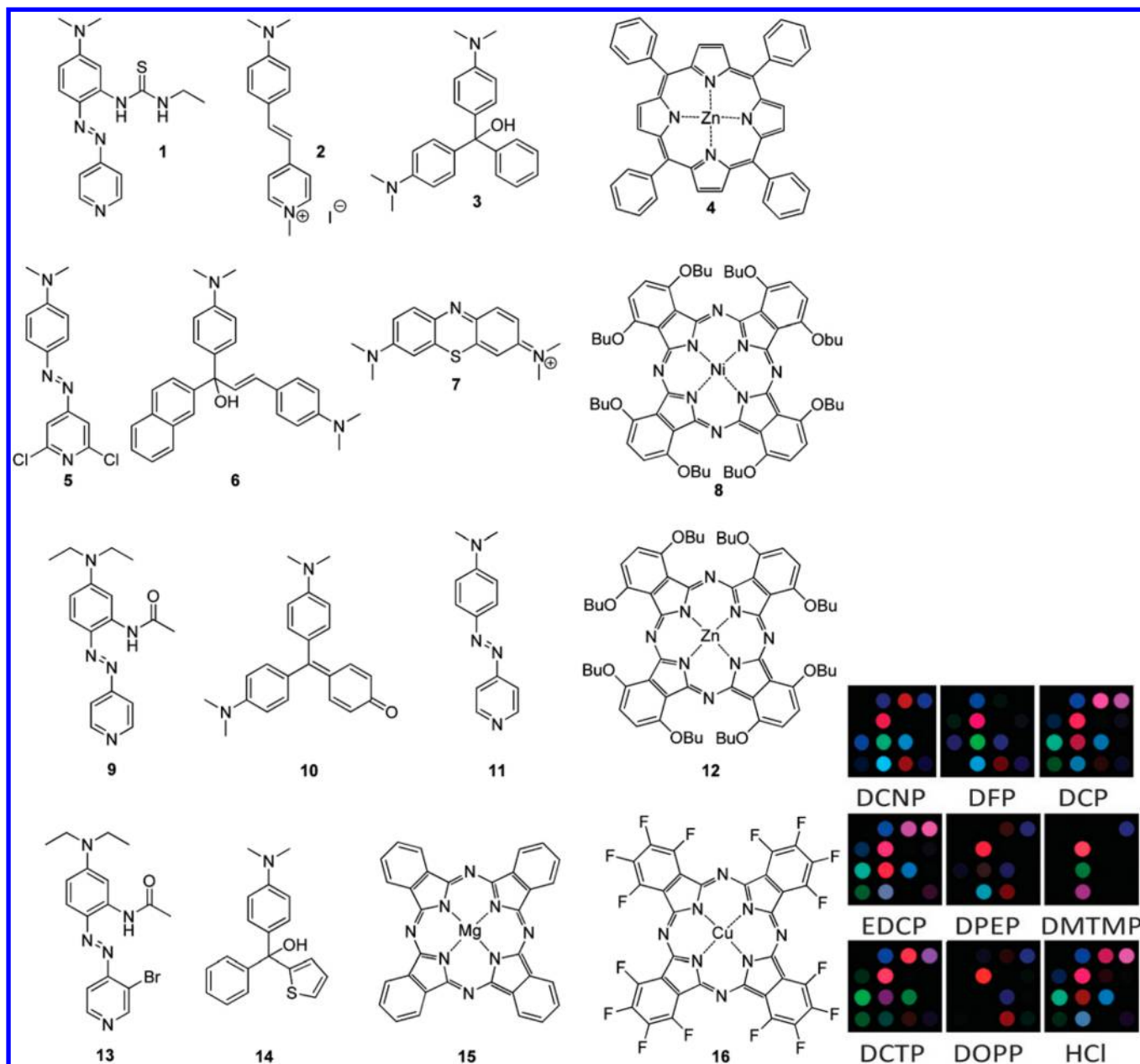
Figure 62. Structures of dyes used for the colorimetric array **206** (left). Images of maps generated from the differences between the red, green, and blue values for each dye upon the addition of analytes (right). Reprinted with permission from ref 181. Copyright 2012 Royal Society of Chemistry.
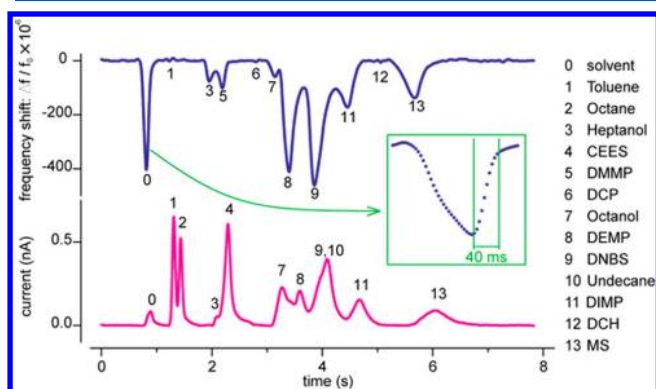
Figure 63. Experimental setup: **207** resonator gas sensing performance (left) and rapid chromatographic separation and nanomechanical detection of 13 mixed chemical compounds (right).
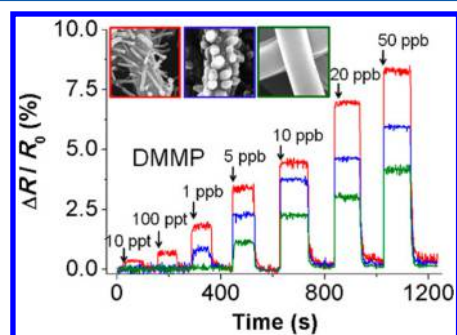
Figure 64. Real-time responses of **208** upon cyclic exposure to DMMP (10 ppt to 50 ppb) and N_2 streams.

volume were prepared by Song's group. The porous core−shell nanotubes can efficiently adsorb ethanol and then disperse it
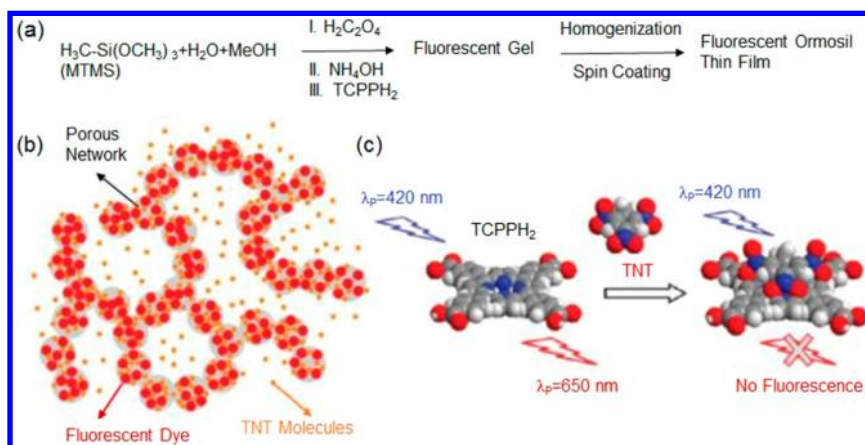
Figure 65. (a) Preparation of fluorescent mesoporous thin films **209**. (b) Schematic illustration of the porous network upon TNT exposure. (c) Schematic illustration of TNT sensing with TCPPH$_2$ dye.
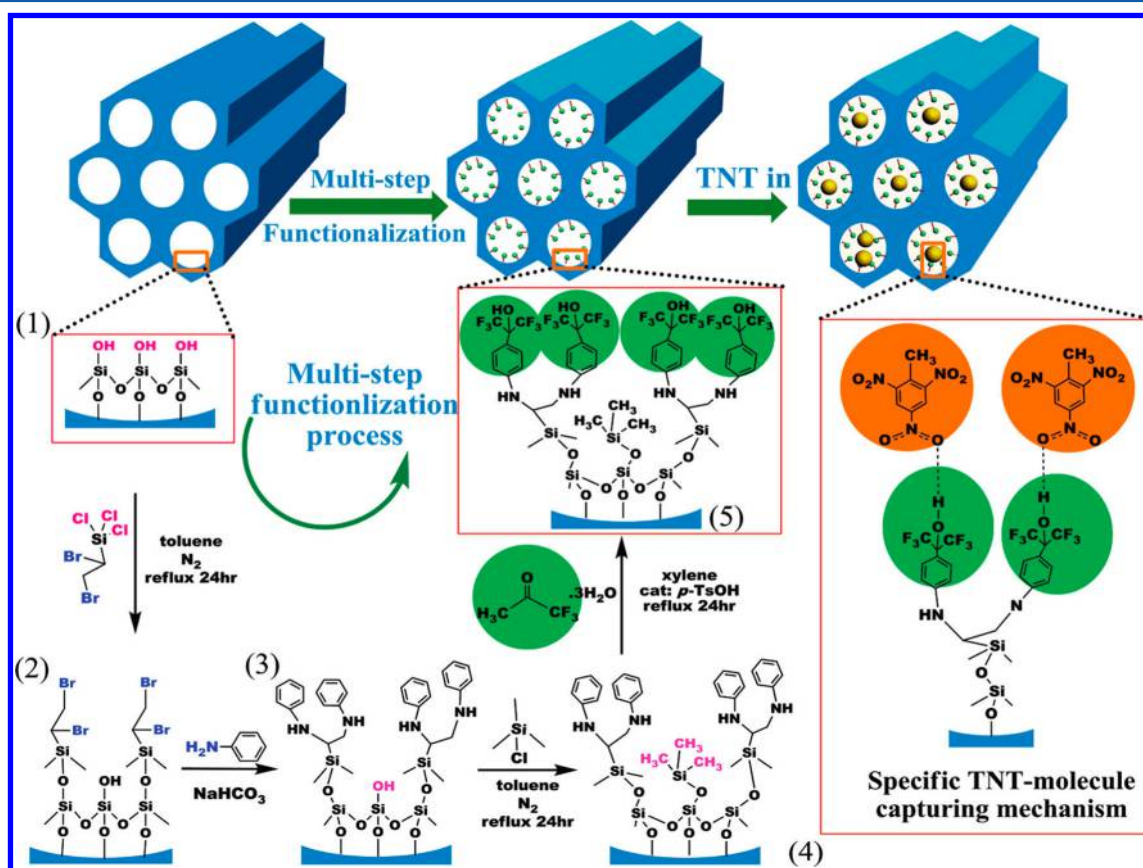
Figure 66. Schematic of HFIP sensing group modification on the inner wall of SBA-15 mesoporous silica **210** and the specific capturing mechanism for TNT molecules.
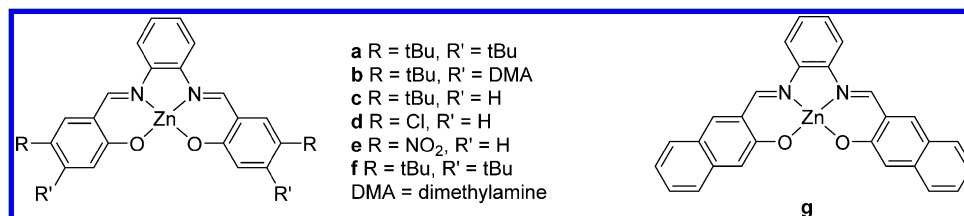
Figure 67. Structures of Zn (salicylaldimine) (ZnL) complexes.

rapidly owing to the porous structure.[220] Furthermore, Kim et al. demonstrated that loading Pt nanoparticles onto both the inner and the outer walls of thin NiO tubes can efficiently enhance the sensitivity and selectivity to C_2H_5OH.[224] However,

Table 4. Gas Sensing Properties of MOS Sensors for Ethanol

material	structures	particle size (nm)	gas concentration (ppm)	operating temperature	response time (s)	recovery time (s)	ref
SnO_2	thin film	1000	500	300	31	8	202
SnO_2	nanowires	50–150	10–100	400	4	30	225
SnO_2	nanoplates	35–85	1.5–50	350			203
$Pt–SnO_2$	nanowires	8.3	100–500	200	48	2	208
$Sb–SnO_2$	nanowires	40–100	10–1000	300	1	5	209
$Ag–SnO_2$	nanowires	5–50	5–100	450	0.4–0.8	40–80	210
WO_3/SnO_2	nanoplates	100	5–60	300–450			214
$SiO_2–SnO_2$	films	5–10	0.1–50	320			212
$La_2O_3–SnO_2$	nanowires	50–100	100	400	1	110	215
$ZnSnO_3$	nanowires	20–90	1–500	300	1	1	226
Zn_2SnO_4	nanofibers	380–718	1–100	450			227
ZnO	circular platelets	300–500	5–80	350–500			228
ZnO	nanopillars	10–30	10–2500	350	10	20	204
ZnO	nanowires	80	50–1500	300			205
ZnO	nanotetrapods	20–100	50–1000	300	~20	~20	206
In–ZnO	nanowires	60–150	1–1500	32	2	2	211
Pd–ZnO	nanowires	50	5–500	230			207
$Mn_3O_4–ZnO$	nanobelts	50–80	2.5–100	300–450			213
$Au–WO_3$	nanoneedles	~100	1.5	250			216
$Rh–In_2O_3$	hollow spheres	171–180	2–100	371			217
Fe_2O_3	nanowires	120	5–1000	150	1–3	1–3	218
NiO	hemispheres	800	5–200	300	49–58	40–66	219
NiO	nanotubes	350	50–200	250			220
Pt–NiO	nanotubes	50	1–100	400			224
CuO	microspindles	10–110	2–800	140–300			229
CuO	nanorods	15–20, 60–80	5–1000	160–300	13–42	17–51	221
Co_3O_4	microspheres	50	100–500	135			222
Cr_2O_3	mesoporous	20	10–1000	RT			223
V_2O_5	mesh of nanobelts	60–100, 10–20	10–1000	150–400			230
$CdIn_2O_4$	nanocrystals	10	100–1000	175–400	6	30	231
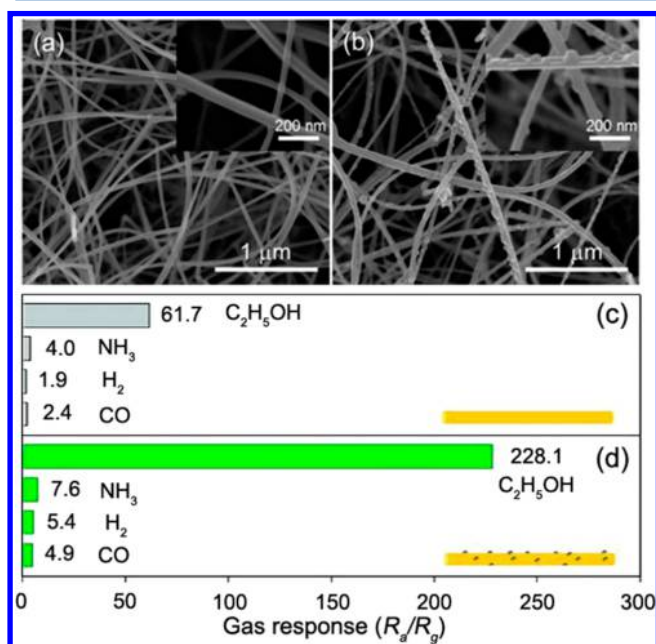
Figure 68. Scanning electron micrographs of (a) pure SnO_2 nanowire networks and (b) $5Ag–SnO_2$ nanowire networks. Gas responses to (c) 100 ppm of C_2H_5OH, NH_3, H_2, and CO at 450 °C of pure SnO_2 sensor and (d) $5Ag–SnO_2$ sensor.
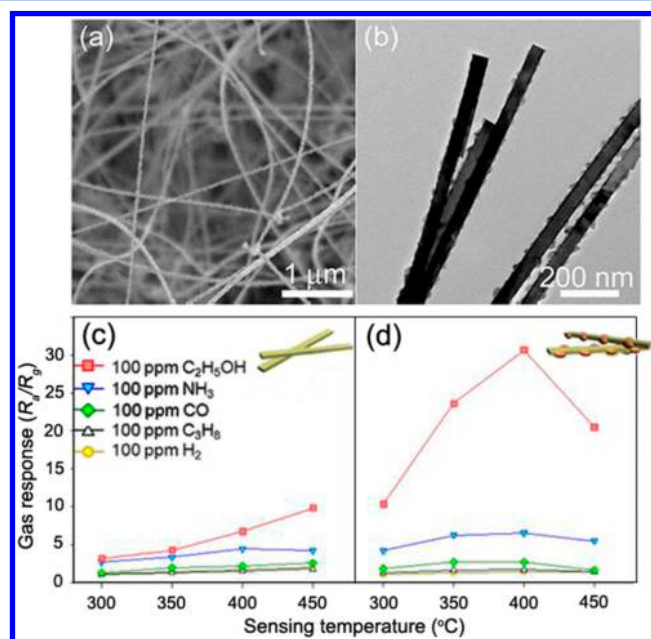
Figure 69. (a) SEM image and (b) TEM image of Mn_3O_4-decorated ZnO nanobelts grown on Si substrates. Gas responses (R_a/R_g; R_a resistance in air and R_g resistance in gas) to 100 ppm of C_2H_5OH, NH_3, CO, C_3H_8, and H_2 gases measured in the range of 300–450 °C for sensors produced with (c) ZnO nanobelts and (d) Mn_3O_4-decorated ZnO nanobelts.

only a limited number of studies have reported the effects of noble metal catalysts on the ethanol detection characteristics of

Table 5. Gas Sensing Properties of Unloaded/Loaded MOS Sensors for Formaldehyde

materials	structures	particle size	gas concentration	working temperature	response time (s)	recovery time (s)	ref
Pd–SnO$_2$	fibers	3–5	0.05–0.5	190	53	103	232
Pd–SnO$_2$	film	15	0.03–10	250	50	50	233
NiO–SnO$_2$	nanofibers	80–100	0.08–100	200	50	80	234
Pt–SnO$_2$	nanopowder	20	0.45–4.2	400	20		235
SnO$_2$	nanospheres	90–150	0.5–100	260	13	14	236
ZnO	thick film	10–50	0.001–1000	210	10	20	237
NiO	thin films	150/300	5	50–350			238
NiO	nanosheets	1–15	1–1000	150–400	<60	<60	239
Co$_3$O$_4$	nanocrystals	430–560	5–1000	200			240
In$_2$O$_3$	octahedron strings	1 um	5–100	340–440	48	58	241

Table 6. Summary on the Gas Sensing Properties of MOS Sensors for BTX Gases

gas	materials	structures	gas concentration	working temperature	response time (s)	recovery time (s)	ref
toluene	NiO	nanowires	11–1100	350	25–43	35–50	242
toluene	α-Fe$_2$O$_3$/NiO	hollow structure	5–100	300	1	12	243
toluene	ZnO	microspheres	1–1000	300	0.3	3	247
toluene	Cr$_2$O$_3$	microspheres	1–200	170	83	418	248
toluene	Co$_3$O$_4$	hollow nanospheres	10–1000	100	1–3	4–8	249
toluene	Pd–SnO$_2$	nanoparticles	50	300			250
xylene	Cr–NiO	micro/nanospheres	1–10	220			251
xylene	Cr–NiO	hierarchical spheres	0.25–5	400			244
toluene			0.1–5				
xylene	Pd–SnO$_2$	yolk–shell spheres	1–5	350			245
toluene			5				
xylene	Co$_3$O$_4$	nanocubes	10–500	200			252
benzene	Au–SnO$_2$	thin film	0.005–0.1				246
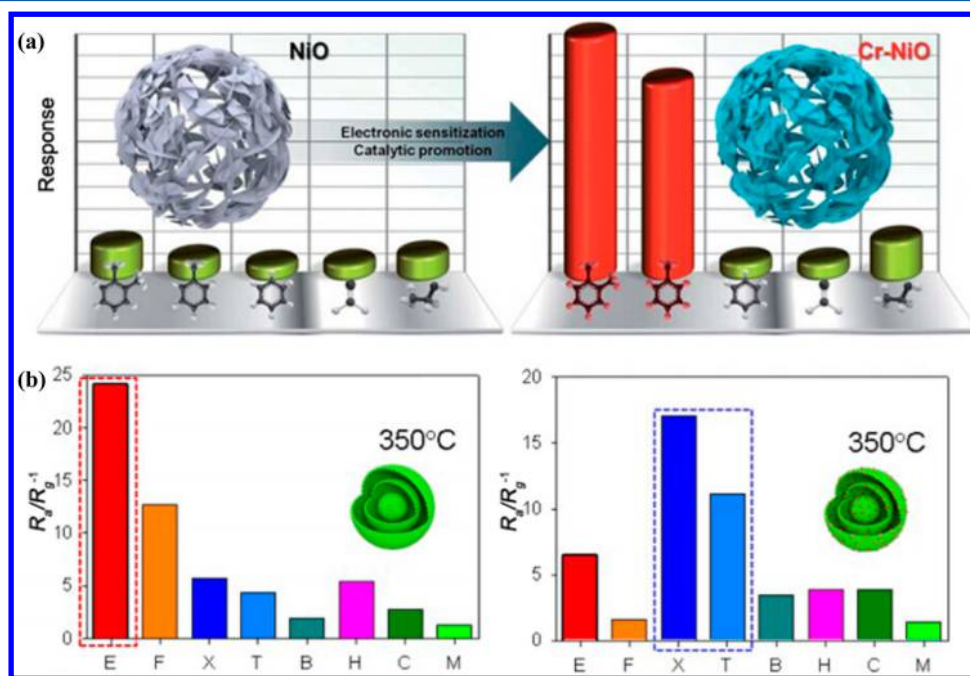
Figure 70. (a) Selective toluene and xylene sensors for indoor air monitoring using Cr-doped NiO hierarchical nanostructures. Reprinted with permission from ref 244. Copyright 2013 Royal Society of Chemistry. (b) Gas responses to 5 ppm of C$_2$H$_5$OH, HCHO, o-xylene, toluene, benzene, H$_2$, and CO and 50 ppm of CH$_4$ of SnO$_2$ and Pd-loaded SnO$_2$ yolk–shell spheres at 350 °C. Reprinted with permission from ref 245. Copyright 2014 WILEY-VCH Verlag GmbH & Co. KGaA, Weinheim.

p-type oxide semiconductors. Therefore, more investigations are needed in order to elucidate the effects.

4.1.1.2. Formaldehyde. Formaldehyde (HCHO), which can be released from building materials, decorating materials, wood furniture, and carpet, is one of the most important pollutants

among VOCs in the indoor environment. As we all know, formaldehyde is a human carcinogen and associated with asthma, nasopharyngeal cancer, and multiple subjective health complaints. OSHA (Occupational Safety and Health Administration, USA) sets the immediate danger level of form-

aldehyde to life or health (IDLH) at 20 ppm and the exposure limit at 0.75 ppm in the workplace.

Various MOS have been investigated for formaldehyde detection as shown in Table 5. Among these metal oxides, unloaded/loaded SnO_2 are the most effective materials for detection of formaldehyde. For instance, Tian et al. reported a formaldehyde sensor based on SnO_2 fibers loaded with Pd nanodots.[232] The Pd-loaded SnO_2 fibers showed an ultralow detection limit of 50 ppb and excellent sensor selectivity to HCHO at a low working temperature of 190 °C. Meanwhile, other SnO_2-based sensors such as 1 mol % Pd–SnO_2 film,[233] NiO–SnO_2 nanofibers,[234] Pt-decorated SnO_2,[235] and unloaded SnO_2 nanospheres[236] have been prepared to respond to a low detecting concentration of 30, 80, 450, and 500 ppb, respectively.

Among them, ZnO nanopowder synthesized by Chu et al. was found to exhibit appreciable HCHO-sensing characteristics.[237] The ZnO sample obtained with low power and 10 × 10 min showed high response to 0.001 ppm formaldehyde when operating at 210 °C. Meanwhile, it exhibited better selectivity to HCHO than to benzene and toluene at 210 °C. Furthermore, other sensors with lower responses are listed in Table 5.

4.1.1.3. Benzene, Toluene, and Xylene. Besides formaldehyde, benzene, toluene, and xylene (BTX gases) are representative indoor pollutants that pose direct threats to human beings. Thus, it is important to develop BTX gas sensors with high selectivity and enhanced sensitivity.

Sensors for toluene detection have been widely studied compared to xylene and benzene. Liu et al. reported NiO crystallites-based nanowires to detect toluene at a low concentration of 11 ppm at 350 °C.[242] However, the selectivity of this metal oxide sensor was poor. It can respond to ethanol, acetone, triethylamine, and methanol at the same time. In order to improve the selectivity, Wang et al. prepared a hollow hierarchical α-Fe_2O_3/NiO nanostructure.[243] With α-Fe_2O_3/NiO, pure α-Fe_2O_3 and pure NiO were exposed to various VOC gases. Some other metal oxide sensors and the parameter are shown in Table 6.

It is extremely challenging to discriminate xylene and toluene, because they can induce similar symptoms such as irritation of eyes, nose, and skin, headaches, fatigue, etc. The 1.15 atom % Cr-doped NiO hierarchical nanostructures were prepared for the detection of various gases.[244] Kim et al. found that it shows high responses to 5 ppm of o-xylene and toluene and negligible cross-responses to 5 ppm of benzene, formaldehyde, ethanol, hydrogen, and carbon monoxide as shown in Figure 70a. Furthermore, the detection of xylene and toluene using a special yolk–shell nanostructure synthesized with Pd-loaded SnO_2 was reported by Hong et al.[245] Figure 70b demonstrates that the Pd-loaded SnO_2 yolk–shell spheres exhibited excellent selectivity to methylbenzenes compared to all other indoor pollutants.

Benzene sensors have not yet been extensively studied. It generally provides lower signals than toluene and xylene on MOS sensors, as shown in ref 244. In a recent study, Elmi et al. prepared 5–10 wt % Au-loaded SnO_2 thin film with enhanced sensitivity and selectivity for benzene.[246] This small quantity of gold nanoclusters on the SnO_2 thin film acted as a catalyst for reaction of the VOCs on the sensing layer surface, thus enhancing sensitivity toward those compounds and improving the sensor selectivity.

4.1.1.4. Acetone. Unlike BTX and formaldehyde gases, acetone is believed to exhibit only a slight toxicity with normal use, but its hazard lies in its extreme flammability. Vomiero et al. reported the preparation of In_2O_3 nanowires on alumina substrates by thermal evaporation at 1500 °C.[253] The prepared material showed a broad distribution on the diameter of the wires from 100 to 500 nm. The response to acetone increases with operating temperature up to a maximum located at about 400 °C. However, this In_2O_3 nanowire can detect NO_2 at the same time. Actually, high selectivity is one of the important challenges for researchers for preparing various semiconductor sensors. For example, macroporous Co_3O_4 nanorods prepared by Nguyen et al. were found to simultaneously detect acetone, benzene, and ethanol effectively.[254] In order to improve the selectivity of the gas sensor, Song's group presented the Ce-doped SnO_2 hollow spheres as shown in Figure 71a.[255] The gas
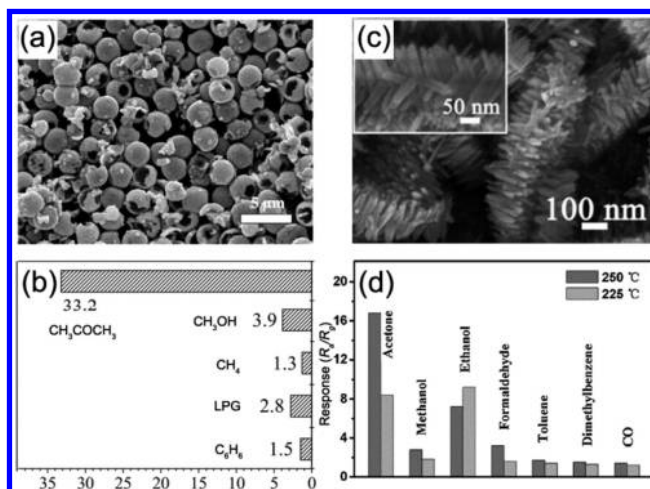
Figure 71. (a) FESEM image of the Ce-doped SnO_2 hollow spheres. Reprinted with permission from ref 255. Copyright 2012 Elsevier B.V. All rights reserved. (b) Gas response of Ce-doped SnO_2 hollow spheres to 500 ppm acetone, methanol, benzene, CH_4, and LPG at 250 °C. (c) FESEM image of hierarchical α-Fe_2O_3/SnO_2 composites. (d) Response of α-Fe_2O_3/SnO_2 sensor to 100 ppm various gases at 225 and 250 °C. Reprinted with permission from ref 256. Copyright 2013 Elsevier B.V. All rights reserved.

responses (R_g/R_a) of the sensor based on Ce-doped SnO_2 hollow spheres to 500 ppm acetone, methanol, benzene, CH_4, and LPG were measured at 250 °C, Table 7. It can be found that the response to acetone was significantly higher than the responses to others regardless of the sensor used (Figure 71b). Figure 71c shows field emission scanning electron microscopy (FESEM) images of the hierarchical α-Fe_2O_3/SnO_2 composites reported by Sun et al.[256] The selectivity of the sensor was evaluated on exposure to different VOC gases (100 ppm). The results indicated that the sensor showed an obvious response to acetone over the other gases at 250 °C (Figure 71d).

In recent years, sensors for acetone detection have been widely studied because acetone not only pollutes the environment but also is an important product in exhaled breath of diabetics. A key technique for noninvasive diagnosis of diabetes was developed largely based on an acetone breath test.[257] The exhaled acetone level of diabetes patients is found to exceed 1.8 ppm, which is 2–6-fold higher than that (0.3–0.9 ppm) of healthy people.[258] Thus, superior detection sensitivity to acetone below 1 ppm is necessary for accurate diagnosis of

Table 7. Summary on the Gas Sensing Properties of MOS for Acetone

material	structures	particle size (nm)	gas concentration	working temp. (°C)	response time (s)	recovery time (s)	ref
In_2O_3	mesh of nanowires	100−500	25−100	400			253
Co_3O_4	nanorods	200	200−1000	300	0.4 min	3 min	254
$Ce−SnO_2$	hollow spheres	10−15	100	250	∼18	∼7	255
Fe_2O_3/SnO_2	composites		100	250	∼3	∼90	256
$BaO·6Fe_2O_3$	particles	70	20	325	26	80	261
WO_3	nanoplates/nanoparticles	200−300/30−60	2−1000	300	∼8	∼13	262
$Pt−SnO_2$	fibers	230	0.12−3	200−400	11	6	259
$Cu−WO_3$	hollow fibers	300−500	0.25−20	300	15	40	260
WO_3/SnO_2	nanoplates	100	0.5−6	300−450			214
ZnO	circular platelets	300−500	0.5−8	350−500			228
$Au−Fe_2O_3$	thick films	6−10 190−200	1−100	270	0.5	20	263

Table 8. Summary on the Gas Sensing Properties of MOS for CO_2

material	structures	particle size (nm)	gas concentration (ppm)	operating temp. (°C)	response time	recovery time	ref
$LaOCl−SnO_2$	nanowire	22−35	250−4000	500−700	3−20s	4−19s	264
$Ag−BaTiO_3−CuO$	thin film	400	500−10000	200−300	15 min	10 min	265
$CuO−Cu_xFw_3−xO_4$	film	50	1000−5000	250	9.5 h		270
$BaTiO_3−CuO$	film	125	500−5000	300	2 min	3 min	266
$La_{1−x}Sr_xFeO_3$	nanocrystalline powder	26−43	2000−4000	380	11 min	15 min	271
Gd_2O_3	hollow microspheres	0.7−2.5 μm	1% in the air	470			267
La_2O_3	film	15	200	RT	10 min	7000 s	272
Nd_2O_3	microspheres	0.5−1.4 μm	100−250	400	3.6 s	2.5 min	268
$ZnSb_2O_6$	nanowire	<1 μM	100−400	400	19 s		273

diabetes. Shin et al. prepared hierarchical SnO_2 fibers with a uniform coating of catalytic Pt nanoparticles onto the inner SnO_2 layers, and a superior detecting capacity with appreciable response (R_{air}/R_{gas}—1 = 0.72) was achieved at low acetone concentration (120 ppb). Meanwhile, catalytic Pt-decorated thin-wall-assembled SnO_2 fibers demonstrated enhanced acetone response (<11 s) and recovery times (<6 s) at a very low concentration range (0.2−1 ppm) that satisfies the minimum requirement of a real-time diabetes breath diagnosis sensor.[259] Furthermore, the high response to a low acetone concentration was also reported by Bai et al.[260] and Hernandez et al.[214] using Cu-doped WO_3 and WO_3-decorated SnO_2 sensors.

However, to date, enhancing the sensitivity and selectivity for various VOC gases is still a great challenge for researchers. Because most of the MOS sensors reported can respond to multiple VOC gases, their rare production can be an application in life. Therefore, more efficient VOC gas sensors are needed to increase the quality of our life.

4.1.2. Sensors for CO_2. Carbon dioxide detection is necessary in monitoring indoor air quality, controlling greenhouse gases, packaging atmospheres, and refrigerant systems. Many different kinds of metal oxide semiconductor materials have been investigated to detect carbon dioxide including SnO_2, $BaTiO_3$, Gd_2O_3, and LaOCl. MOS sensors for CO_2 are summarized in Table 8.

Trung et al.[264] fabricated a LaOCl-functionalized SnO_2 nanowires sensor as a recognized carbon dioxide as shown in Figure 72. Compared to bare SnO_2 nanowires sensor, p−n junction formation of LaOCl (p-type) and SnO_2 nanowires (n-type) led to the extension of electron depletion. LaOCl is also a favorable catalyst, which makes CO_2 chemically react with these adsorbed species to form polydentate carbonates and hydroxyl carbonates resulting in decreased resistance of the LaOCl−SnO_2 nanowires sensor. Sensing performance reveals that

LaOCl−SnO_2 nanowires sensors exhibit much higher response, shorter response−recovery, and better selectivity in detecting CO_2 gas at 400 °C operating temperature than the bare SnO_2 nanowires sensors.

Herrán et al.[265] used $BaTiO_3$−CuO semiconductor thin films as a sensitive material. The response, both resistance and capacitance, was tested without additives and with Ag at several CO_2 concentrations. The best response and recovery times, taking place at 300 °C, are 15 and 10 min, respectively. Herrán et al.[266] corrected their theoretical foundations and technology to improve the properties of $BaTiO_3$−CuO thin film. Because the sensing reaction takes place on the material surface, the thicker film can get shorter response and recovery times. Michel et al.[267] prepared Gd_2O_3 hollow microspheres in aqueous media with the coprecipitation method. The use of formic acid played a key role in the formation of microspheres, because the synthesis in acetic acid and pectin produced a different morphology. The diameter of hollow microspheres is between 0.7 and 2.5 μm. The films using the as-prepared microspheres simply deposed can detect 1% CO_2 in air repeatedly and reproducibly at 470 °C. Under a similar strategy, Michel et al.[268] reported a Nd_2O_3 microspheres material. The best operating condition was registered at 400 °C using an applied frequency of 100 kHz. The response time at this condition can decrease to 3.6 s. Jinesh et al.[269] used capacitance measurements with MIS devices, comprising atomic-layer-deposited ultrathin La_2O_3, to detect CO_2 down to 200 ppm at room temperature.

4.1.3. Sensors for NO_2. Nitrogen gas and oxygen gas combine in combustion engines with the aid of combustion reaction energy. The main harm of nitrous oxides is forming photochemical smog, which is irritating to the eyes, causing lungs damage, and effecting plant life. Monitoring nitrous oxides in the environment, particularly at a high-risk area, is desirable for environment protection and public health. The
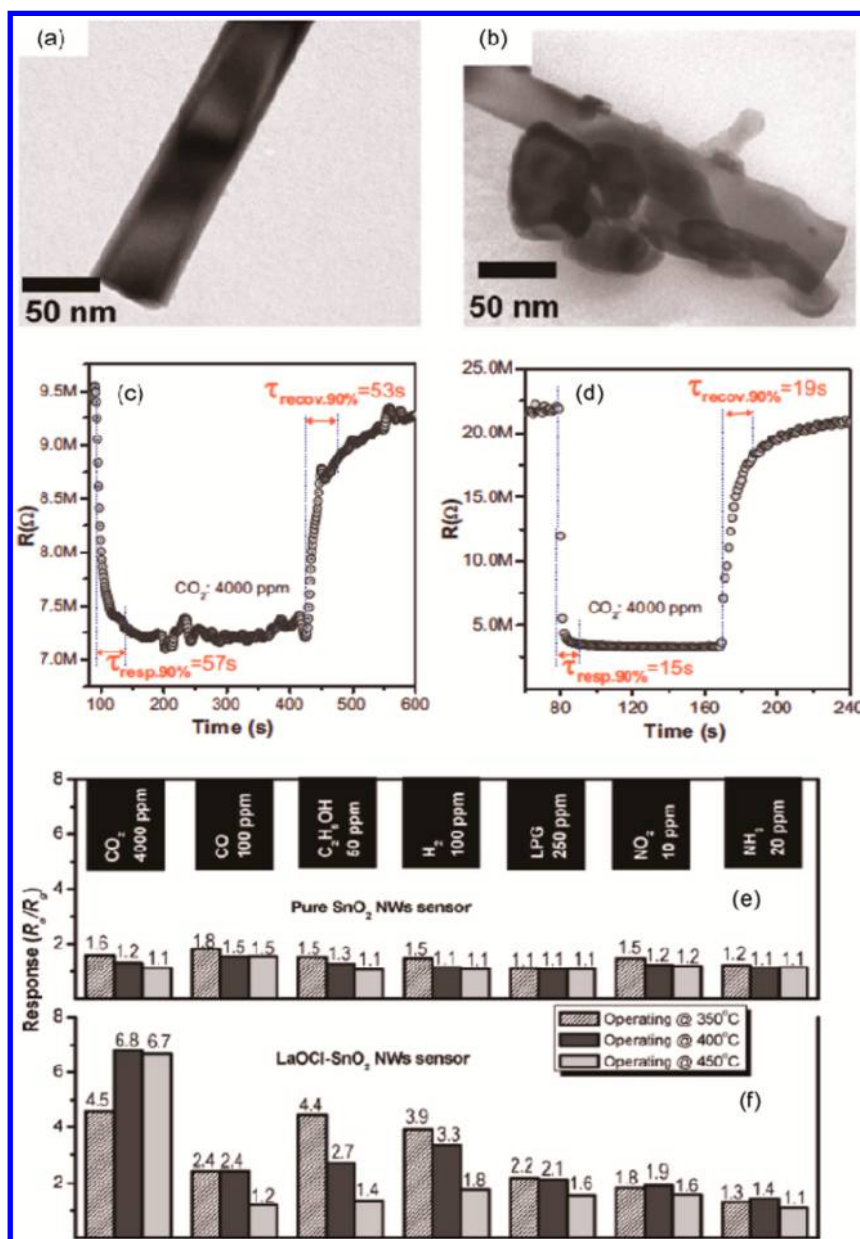
Figure 72. TEM images, response−recovery times, and gas selectivity of the bare SnO_2 nanowires (a, c, e) and LaOCl−SnO_2 nanowires samples (b, d, f). Reprinted with permission from ref 264. Copyright 2012 Elsevier B.V. All rights reserved.

most common nitrous oxide semiconducting metal oxide sensors are based on materials such as SnO_2, tungsten oxide WO_3, and ZnO. MOS sensors for NO_2 are summarized in Table 9.

Polleux et al.[274] fabricated a kind of WO_3 nanowire with a diameter of 1 ± 0.1 nm and length of 300−1000 nm. It showed an extraordinarily high sensitivity to low NO_2 concentrations (50 ppb) at relatively low temperature (150 °C).

Andringa et al.[275] investigated the detection mechanism of ZnO film field-effect transistors. The current decrease originates from the trapping of electrons, yielding a shift of the threshold voltage toward the applied gate bias. The shift is observed for extremely low NO_2 concentrations down to 10 ppb at room temperature and can phenomenologically be described by a stretched-exponential time relaxation. Na et al.[276] reported a nanowire network sensor, which achieved selective detection of two gases, NO_2 and ethanol. The sensor

used a p-type Co_3O_4-decorated n-type ZnO nanowire. The gas selectivity was explained by the catalytic effect of nanocrystalline Co_3O_4 and the extension of the electron depletion layer via the formation of p−n junctions. In SEM imaging, the lenticular Co_3O_4 islands were uniformly formed on the ZnO, whose lengths ranged from 80 to 110 nm. This unique structure made the sensor highly sensitive to 5 ppm of NO_2 at 200 °C. Reduced graphene oxide is usually used to enhance the performance of semiconductor gas sensor.[277,278] Deng et et al.[278] prepared reduced graphene oxide-conjugated Cu_2O nanowire mesocrystals, which formed by nonclassical crystallization in the presence of GO and o-anisidine under hydrothermal conditions (Figure 73).

Park et al.[279] fabricated nanograined ZnO nanowires by thermal oxidation of ZnSe nanowires. The multiple network structure largely enhanced gas sensing properties. Compared to single-crystal ZnO nanowire sensors and other nanomaterial

Table 9. Summary on the Gas Sensing Properties of MOS for NO_2

material	structures	particle size (nm)	gas concentration (ppm)	operating temp. (°C)	response time (s)	recovery time (s)	ref
Au−WO$_3$	nanotubes	200	0.2	200	60 ± 6		281
WO$_3$·H$_2$O	hierarchical spheres	1−3 μm	10	120			282
WO$_3$	film	10−30	0.6	174	468	600	283
polythiophene−WO$_3$	nanocrystalline powders	20−30	10	70			284
WO$_3$	lamellar	20−50	0.05−1	200	150−280	4−11 min	285
WO$_3$	nanoplates	192	0.5	300	80−300	30−50	286
WO$_3$	hollow microspheres	226 ± 41	0.5−2.5	300			287
WO$_3$	nanorods	<100	1	350	3 min		288
WO$_3$	nanowires	20−30	0.25	150			289
WO$_3$	nanowire	1 ± 0.1	0.05	150			274
ZnO	film	10	0.01	RT	4 min		275
Co$_3$O$_4$−ZnO	nanowire	80−100	5	200			276
ZnO	nanowire	20−100	1−10	300	310 ± 31	560 ± 56	279
ZnO	nanorods	30−120	0.1−1	200	60	20	290
amine-terminated SnO$_2$	nanowire	47 ± 8	0.25	RT	110	75	280
SnO$_2$	nanoslab	1 μm × 1 μm × 100 nm	0.5	300			291
In$_2$O$_3$	mesoporous ribbons	5.7	5	300	160	5 min	292
reduced graphene oxide−Cu$_2$O	nanowire	80−110	0.064	RT			278
reduced graphene oxide-Co$_3$O$_4$	film	50	60	RT	1 min	2 min	277
Cr$_2$O$_3$	nanoparticle	189	1	200	9 min	40 min	293
In$_2$O$_3$	macroporous powder	~100 μm	0.1−100	250	10 min		294
MoO$_3$−SnO$_2$	film	120−130	100−400	170	2s		295
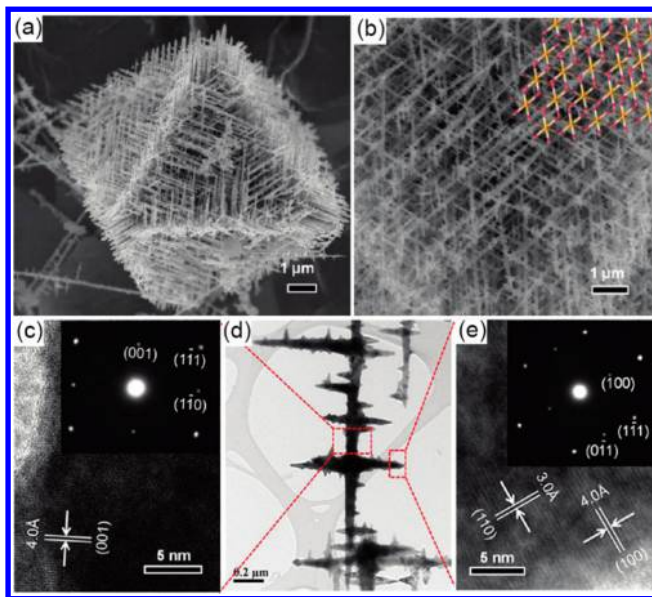
Figure 73. FESEM images of octahedron Cu$_2$O nanowire mesocrystals. (a) Octahedron Cu$_2$O mesocrystal along the view, and (b) interior morphology with overlaid hexapod grid. TEM image of a fragment of the nanowire mesocrystal. (c, e) HRTEM images of stem and branch nanowire indicated in panel d, respectively. (Insets) Corresponding SAED patterns.

sensors reported previously, nanograined ZnO nanowires showed substantially higher electrical responses, shorter response, and recovery time. Hoffmann et al.[280] designed a highly selective and sensitive NO$_2$ gas sensor through electronic structure calculations. On the basis of a systematic organic surface design strategy, an ultraselective NO$_2$ sensor is realized, which used self-assembled monolayer-modified semiconductor nanowire material. The sensor is capable of detecting very low NO$_2$ concentrations in the parts per billion range qualitatively and quantitatively with relatively fast response and recovery time at room temperature.

4.1.4. Sensors for SO$_2$. Das et al.[296] produced films of vanadium-doped SnO$_2$ which have good sensitivity toward SO$_2$ at concentrations down to 5 ppm. Hidalgo et al., Table 10,[297] reported a sensor based on NiO−SnO$_2$ film. The sensor could detect low SO$_2$ concentrations (<32 ppm) at room temperature. Lee et al.[298] reported a SnO$_2$-based thick film, mixing both 5 wt % MgO and 2 wt % V$_2$O$_5$. It shows a high sensor response and excellent recovery properties. The sensor showed a response of approximately 20% even at a level of 0.1 ppm. Liang et al.[299] improved the V$_2$O$_5$-doped TiO$_2$ solid-state potentiometric SO$_2$ sensor. In order to reduce the size of the sensor, a thick film of NASICON was formed on the outer surface of a small Al$_2$O$_3$ tube; furthermore, a thin layer of V$_2$O$_5$-doped TiO$_2$ with nanometer size was attached on the NASICON as a sensing electrode. The sensor attached with 5 wt % V$_2$O$_5$-doped TiO$_2$ sintered at 600 °C exhibited excellent sensing properties to 1−50 ppm of SO$_2$ in air at 200−400 °C.

4.1.5. Sensors for Other Gases. *4.1.5.1. H$_2$.* Hydrogen (H$_2$), the most potential clean and renewable energy source, is widely used in various fields such as environment protection, biomedical and daily chemical industry with a low minimum ignition energy (0.017 mJ), high heat of combustion (142 kJ/g^{-1}), low density (0.0899 kg/m^{-3}), and wide flammable range (4−75%). Therefore, reliable H$_2$ sensors are important for monitoring H$_2$ in different measuring environments. Nowadays, the metal oxide semiconductor, which is employed as a sensing material for H$_2$ sensors, is well studied. As a whole, SnO$_2$ and ZnO are the main two sensing materials. It is also found that doping, noble metal decoration, and morphological change are

Table 10. Summary on the Gas Sensing Properties of MOS for SO₂

material	structures	particle size (nm)	gas concentration (ppm)	operating temp. (°C)	response time (s)	recovery time (s)	ref
V−SnO₂	film	14−17	5	250−450			296
Ni−SnO₂	film (nanopowder)	180	<32	RT	240	900	297
SnO₂(P)Mg₅V₂	film	20−40	<1	350−450	230	625	298
V−TiO₂	film	20	1−50	200−400	10	35	299

Table 11. Summary on the Gas Sensing Properties of MOS for Hydrogen

material	structures	particle size (nm)	gas concentration (ppm)	operating temp. (°C)	response time (s)	recovery time (s)	ref
SnO₂	nanorods	10−45	100	25−350			300
SnO₂	nanofilms	~20	500−10000	550	16−78		306
Pd/SnO₂	nanofibers	70	20−1000	RT	4−13	3−9	301
Ni/SnO₂	nanowires		$3.2-6.4 \times 10^{-2}$ Pa	350	131.7−253.2		307
Pt/SnO₂	nanofibers	210 ± 35	0.125−2.5	100−450			308
Co/SnO₂	nanofibers	100	100	330	2	3	309
Co/SnO₂	nanoparticles	17	40	120−480			310
NiO/SnO₂	nanofibers	100−200	5	320	3	3	311
In₂O₃/SnO₂	nanofilms	30	1000	300	5		312
ZnSnO₃	nanocubes	250−400	50	375	1	12	313
ZnO	nanorods	60	200−3000	200	0.8−79.7		314
ZnO	nanowires	200	2500	RT	55		315
Pd/ZnO	nanorods	30−150	10−500	RT		20	302
Pt/ZnO	nanofilms	40−170	500	RT		<20	303
ZnO/CuO	nanowires	30	200				316
ZnO/CuO	nanofilms	34	3000	30−300	60		317
Au/NiO/ZnO	nanofilms	50−100	300	200	2.5 min		318
CuO	urchin-like nanofibers	3000	10−500	200−250			304
	nanorods			80	0.8 min	0.95 min	
Pd/SiO₂	nanoparticles	30	2.13−10100	RT	<20 min		319
TiO₂	nanofilms	100	$10^{-4}-10^{-2}$ atm	700 k	1		320
MoOₓ/TiOₓ			360−1000	237−329			321
TiO₂/Nb₂O₅	nanofilms	50−130	10−8000	100−300			322
Pd/LaAlO₃/SrTiO₃	nanocrystals		2−14	RT	7.3 min	36.7 min	323
NiO	nanocrystals	20	1000−3000	175	67−134	117−788	324
NiO	nanofilms	50	500−10000	300−650	20 min		325
WO₃	nanofilms	100−200	0.06−1.0%	100	<100	<100	326
WO₃	nanoclusters	3−5	20000	80	<1	60	327
α-MoO₃	nanoflakes	5−85	0.06−1.0%	50−300	7−30	24−130	328
Pd/In₂O₃	nanofilms		0.05−3 vol %	RT	28	32	305
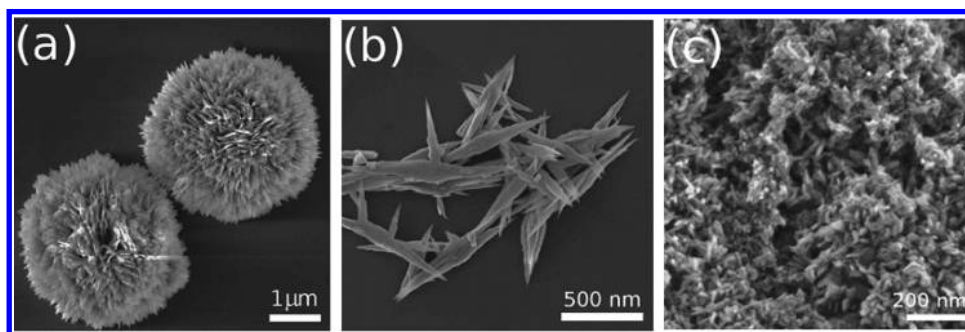
Figure 74. FESEM images of as-prepared CuO-based gas sensor materials with (a) urchin-like structures, (b) fiber-like structures, and (c) nanorods. Reprinted with permission from ref 304. Copyright 2013 WILEY-VCH Verlag GmbH & Co. KGaA, Weinheim.

effective methods for enhancing sensing performance. MOS sensors for H₂ are summarized in Table 11.

SnO₂ single-nanorod sensor was reported to detect 100 ppm of H₂ at room temperature by Huang et al.[300] However, the best sensing performance of the sensor was achieved at around 250 °C, and the response to H₂ will last hundreds of seconds.

To enhance the sensitivity to H₂ at room temperature, Wang et al. synthesized Pd⁰-loaded SnO₂ nanofibers with different Pd-loaded levels via the electrospinning process, sintering technology, and in situ reduction.[301] The gas sensor showed great sensing performance with an ultralow limit of detection (20 ppb), a fast response (4−13 s), and recovery (3−9 s) at

Table 12. Summary on the Gas Sensing Properties of MOS for Ammonia

material	structures	particle size (nm)	gas concentration (ppm)	operating temp. (°C)	response time (s)	recovery time (s)	ref
ZnO	nanocrystals	40	12−50		<500		334
ZnO	nanorods	~150	50−800	RT		300−1800	335
RuO_2/ZnO	nanofilms		1000	250			336
Fe_2O_3−ZnO	nanoparticles	10	0.4	RT	<20	<20	337
ZnO/SiO_2	nanofilms		30−90	RT	13−38	5−54	338
Zn/NiO	dendritic crystals	60−200	5−150	RT	5−8	30−5	330
SnO_2/CuO	nanowires	60	1%	RT	9/10	6	333
SnO_2/MWCNTs	thin film	10−100	60−800	RT	<300	<300	339
$SiO_2/SnO_x/AgO_y$	nanofilms	60−100	20−250	20−50	10−30	300−720	340
WO_3	nanowires	70	9.7−1500	250	7	8	341
Pt/WO_3	nanofilms		15−4000	250−450	<60		342
$PANI/TiO_2$	microfibers	600	50−200 ppt	RT			332
$PANI/TiO_2$	thin film		23−141	RT	2	20−60	331
InTiO	thin film	26.6 ± 2	30−1000	150	73	104	343
CNT/In_2O_3	nanotubes	20−60	5−25	RT	<20	<20	329
CuO	nanowires	100−200	<100	150−300	300	1800	344
$CrNbO_4$	nanocrystals	25	150−800	275	85	65	345
NiV_2O_6	nanorods	30	100	120	10	30	346
$LaCo_{0.8}Fe_{0.2}O_3$	thin film	30	200−1000	260	8	20	347
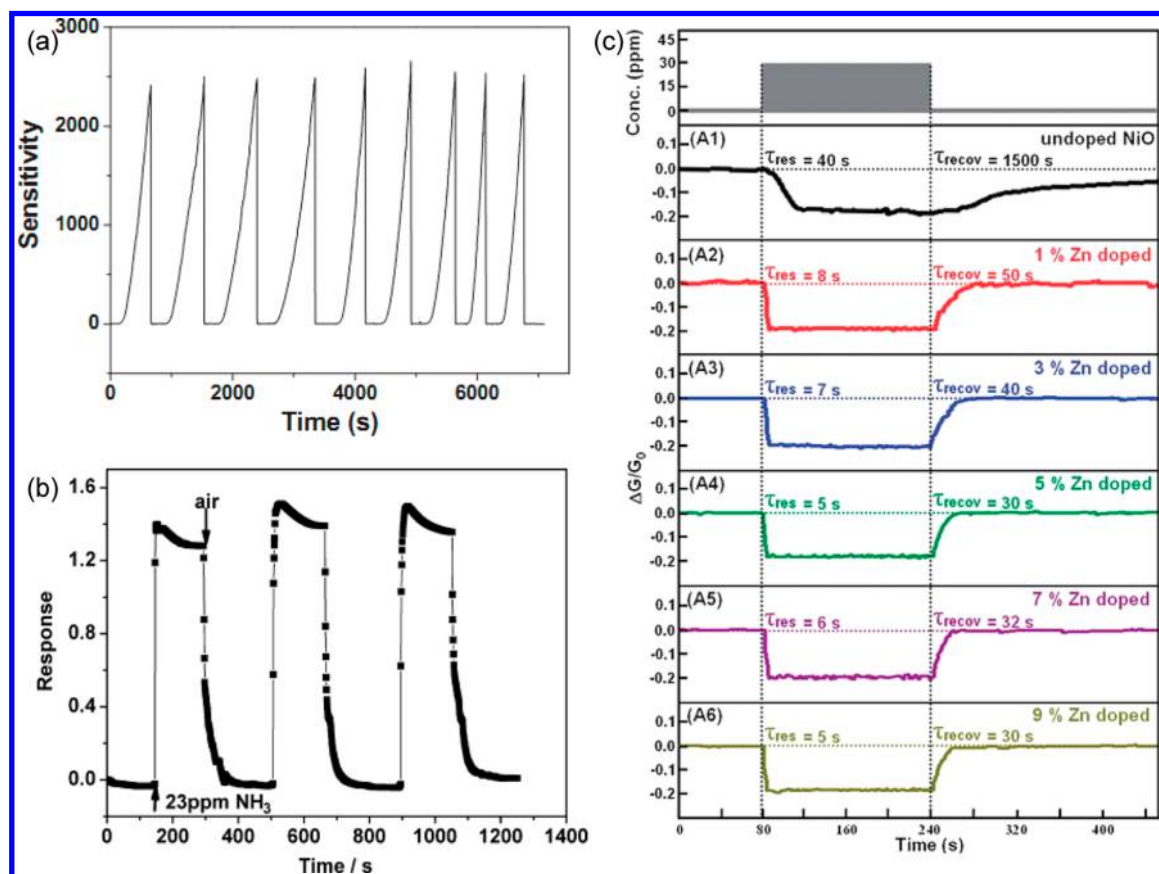
Figure 75. (a) Sensitivity response of the gas sensor based on broken In_2O_3 nanotubes versus the time for a concentration of NH_3 of 20 ppm at room temperature. Reprinted with permission from ref 329. Copyright 2007 WILEY-VCH Verlag GmbH & Co. KGaA, Weinheim. (b) Sensing reproducibility of $PANI/TiO_2$ in the presence of 23 ppm of NH_3 at room temperature. Reprinted with permission from ref 330. Copyright 2012 Royal Society of Chemistry. (c) Sensing performance of the gas sensors based Zn-doped NiO dendritic crystals. Reprinted with permission from ref 331. Copyright 2008 Elsevier B.V. All rights reserved.

room temperature through adjusting Pd^0-loaded levels. Pearton et al. also prepared ZnO nanorods[302] and ZnO nanofilms[303] by doping Pd and Pt, respectively, which could exhibit the ability to detect the parts per million concentrations of H_2 at room temperature, and the recovery time is reduced to 20 s.

Besides SnO_2 and ZnO, some other MOS such as CuO, In_2O_3, NiO, WO_3, and VO_2 can also be used as sensing materials for detecting H_2. Tuller et al. introduced a microwave-assisted synthesis method in preparing p-type semiconductor gas sensors based on copper(II) oxide (CuO).[304] The CuO-

Table 13. Gas Sensing Properties of MOS for Oxygen

material	structures	particle size (nm)	gas concentration	operating temp. (°C)	response time (s)	recovery time (s)	ref
ZnO	nanowires	70–80	8–11%	50	35	55	351
ZnO	nanowires	800	16 Torr oxygen pressure	RT			350
Cr/ZnO	nanofilms	220–280		250			352
Mn/ZnO	nanorods	60	5–15 ppm	RT	120–150	60–90	353
Nb/TiO$_2$	nanofilms	60	10 ppm	300–600	<60	90	349
Pd/TiO$_2$	nanofilms		100 ppm	300	120	1800	354
SrTiO$_3$	nanofilms	27.5–70.5		40			355
ZrO$_2$	nanofilms	10 mm	0.21–1 ppm	450	2		356
Ce$_{1-x}$Zr$_x$O$_2$	nanofilms	100	10^{-7}–10^5 Pa	600–800	9–20 ms/1–2 ms		348

Table 14. Summary on the Gas Sensing Properties of MOS for CO

material	structures	particle size (nm)	gas concentration (ppm)	sensing temp. (°C)	response time (s)	recovery time (s)	ref
SnO$_2$	nanowires	40–300	50	250–350			362
SnO$_2$	nanofilms		114 mTorr	250–325			357
Pd/SnO$_2$	nanoparticle		25–300	150	5	22	363
Pt/SnO$_2$	nanoparticles	10–50	1–40	450			364
Pt/SnO$_2$	nanoparticles	10	1	350			365
Pt/SnO$_2$	nanosolid		100	RT	144	882	358
V–SnO$_2$	nanopowders	3.8–8.2	50–500	175	143.8–8.2–19	18 min	366
In/Pd–SnO$_2$	nanocrystals	10	1	140	15	20	367
CNT/SnO$_2$	nanoparticles		1–100	RT	2	10 min	368
CNT/Co$_3$O$_4$ –SnO$_2$			20–1000	RT	21	37	359
Co$_3$O$_4$	nanorods	6–8	6.55–50	250	3–4	5–6	369
ZnO	nanorods	100	30–200	400	46	27	370
CeO$_2$/ZnO	thin films	45	500	380	40–50	40–50	371
Pt/ZnO-CuO			100–1000	RT	81	81	372
AlGaN/GaN/ZnO	nanowires	80	400–1600	RT			361
In$_2$O$_3$	nanofibers	150–200	100	300			373
Au/CoOH–WO$_3$	nanocomposites	10–40	30–1000	RT	90	95	374
TiO$_2$/Ti^{3+}	nanocrystals		100–10000	RT	<10	<30	360
PdO–NiO	nanosheets	500	5–100	180	3	3	375

based chemiresistor exhibited different morphologies including urchin-like structures, fiber-like structures, and nanorods (Figure 74). Furthermore, it was found urchin-like structures were the most effective for H$_2$ detection in the range of parts per million at 200 °C with 300-fold larger response than the previously best reported values for CuO single-phase gas sensors. Meanwhile, the authors proposed that the large particle size and particle–particle contacts were likely the main reasons for enhanced performance.

In addition, a H$_2$ sensor based on porous In$_2$O$_3$ decorated by Pd was reported by Wang et al.[305] for the first time. Due to the catalytic effect of Pd and Schottky contact, when treated with 1 vol % in ambient air at room temperature, the sensor revealed an ultrahigh sensitivity of 4.6×10^7. Otherwise, the response and recovery time were only 28 and 32 s, respectively.

4.1.5.2. NH$_3$. Due to its wide use, ammonia (NH$_3$) detection by MOS gas sensors has attracted a lot of research attention. Thus, NH$_3$ sensors based on various sensing materials such as SnO$_2$, WO$_3$, ZnO, TiO$_2$, and V$_2$O$_5$ were reported. Unlike sensors for other gases, many sensors for NH$_3$ work at room temperature. MOS sensors for NH$_3$ are summarized in Table 12.

A promising NH$_3$ sensor based on In$_2$O$_3$ was synthesized by Yang et al. using layer-by-layer (LBL) assembly on the CNT templates in combination with subsequent calcination.[329] This sensor showed superior sensitivity response versus NH$_3$ concentration (5–25 ppm). Also, the porous In$_2$O$_3$ nanotubes

offer a response and recovery time of less than 20 s (Figure 75a).

Zhang et al. also introduced a Zn-doped NiO which had a shorter response time (5–8 s) upon exposure to 30 ppm of NH$_3$ gas at room temperature.[330] The sensor with doped NiO dendritic crystals exhibits about 5–8 times faster responses and 30–50 times faster recovery speeds than the one with pristine NiO dendritic crystals for the existence of many tiny ZnO nanocrystallites (Figure 75c).

Besides the metal element, various conducting polymers were also introduced to further enhance the response/recovery kinetics of the sensing materials. Thus, Yu et al. prepared polyaniline/titanium dioxide (PANI/TiO$_2$) nanocomposite thin film which gave an outstanding response time of 2 s in the presence of NH$_3$ in the range of 23–141 ppm (Figure 75b).[331] Deng et al. synthesized an ultrasensitive NH$_3$ sensor based on PANI/TiO$_2$.[332] The encased PANI nanograins on the surface of the TiO$_2$ microfibers could turn off the current circuit when in contact with NH$_3$. For this reason, this sensor could detect 50 ppb of NH$_3$ in air.

In recent years, a heterojunction is gradually adopted by researchers in improving the sensing properties. Lu et al. enhanced the gas sensing properties of CuO nanowires for the electronic interaction between p-type CuO nanowires and n-type SnO$_2$ nanocrystals.[333] Due to the nanosized p–n conjunctions, the response and recovery times were cut to 9/10 and 6 s when exposed to 1% NH$_3$ at room temperature.

Table 15. Gas Sensing Properties of MOS for H$_2$S

materials	structures	particle size (nm)	gas concentration (ppm)	operating temp. (°C)	response time (s)	recovery time (s)	ref
CuO	nanosheets	200	0.03−1.2	240	4	9	379
CuO	hollow spheres	2−4 μm	0.03−1.35	90−300	3	9	376
CuO	nanowires	50−70	2.5	25−420	42 min	20 min	380
CuO	nanofilms		0.1−50	RT	60	90	381
CuO	nanowires	150	0.5	160			382
Pd/CuO	nanorods		100	300	670−700	80−120	383
CuO-BSST	nanofilms	0.25−1.0 μm	0.004−0.01	RT	10	60	384
CuO/SnO$_2$	nanofilms	90	20	150	14	481	385
CuO/SnO$_2$	nanorods	10	10	60	30	30	386
RGO−SnO$_2$	nanofibers	370 ± 65	1−5	150−400	<3.3 min	<1.9 min	377
SnO$_2$	nanofilms		20−50	200−400			387
ZnSnO$_3$	nanocages	200−400	17.6−50	310	<20	<50	388
ZnO	nanowires	400	100−300	RT			389
ZnO	nanorods	1 μm	50	<500			390
In$_2$O$_3$	nanocrystals	50−80	50	268.5	2	7	391
In$_2$O$_3$	nanocrystals		0.2	RT	2−3.5 min		378
β-AgVO$_3$	nanowires	100−700	50−400	250	<20	<20	392
TiO$_2$	nanowires	300	10−80	RT-160	705		393

4.1.5.3. O$_2$. Oxygen (O$_2$) is the one thing that people cannot live without. Nevertheless, it will cause convulsions and other health problems when O$_2$ reaches elevated partial pressures, usually more than 50 kPa. Besides, it can promote rapid combustion and the formation of fire, explosion hazards. O$_2$ sensors using MOS were earlier used in chemical processing, environment, transportation, medicine, agriculture, etc. MOS sensors for O$_2$ are summarized in Table 13.

In the early stages, Izu et al. prepared nanosized Zr-doped ceria powders by a precipitation method in which conventional carbon powder is used.[348] In the paper, powders with a Zr concentration of 0−20 mol % were studied. The amazing response time was 1−2 ms in the case of an oxygen partial pressure change from low to high, while it had a longer time (9−20 ms) in the case of the change from high to low at 800 °C. Actually, the high operating temperature restricts the applications of these sensors in many aspects. Therefore, nanofilms based on doping TiO$_2$ were investigated for detecting O$_2$, such as Pd- and Nb-doped TiO$_2$. Sotter and co-workers synthesized Nb-doped TiO$_2$ nanofilms via the sol−gel method and were calcined at temperatures between 600 and 900 °C.[349] Compared with pure TiO$_2$, the Nb-doped TiO$_2$ exhibited lower operating temperature in the presence of 10 ppm of O$_2$ due to the defects offered by Nb foreign ions that help oxygen to be absorbed offered by Nb foreign ions.

Later, flexible ZnO nanowires were demonstrated by Wang et al.[350] On account of its strong effect on the carrier transport properties, a piezoelectric potential (piezopotential) is created in ZnO nanowires by applying a strain. Also, this gave the sensor excellent performance in sensing O$_2$ at room temperature with a relative current change of 87.3% from 16 to 500 Torr.

4.2. Sensors for Highly Toxic Gases

4.2.1. Sensors for CO. CO, the colorless and odorless toxic gas, is always produced from automotive emissions, natural gas manufacturing, industrial activities, as well as numerous other fires. Thus, real-time monitoring of CO is urgent for security reasons.

MOS sensors for CO are summarized in Table 14. Among these sensors, SnO$_2$-based ones have become a main type for its high response to CO. George et al. reported ultrathin tin oxide films that were deposited on flat hot plate templates using atomic layer deposition (ALD) techniques with SnCl$_4$ and H$_2$O$_2$ as the reactants at 250 °C.[357] Also, the maximum sensor response for CO gas sensing was observed at a SnO$_x$ ALD film thickness of 26.2 Å. Furthermore, the temperature-dependent response to CO (P_{CO} = 20 mTorr) showed the gas sensor displayed the best sensing performance at temperatures between 250 and −325 °C. In order to enhance the sensitivity and purse moderate operating temperature, Pt, Pd, Au, V, and In are doped to SnO$_2$ for catalytic oxidation reactions. In consideration of this, Liang et al. fabricated a kind of CO gas sensor by calcining Pt-loaded SnO$_2$ PNS in different atmospheres.[358] The sensor calcined in N$_2$ exhibited a high response and selectivity to 100 ppm of CO at room temperature. At the same time, the response and recovery times of this sensor reached 144 and 882 s, respectively. Wu's group developed sensing materials of the Co$_3$O$_4$−SnO$_2$ system and found the mixture with a Co$_3$O$_4$−SnO$_2$ ratio of 1:4 had the highest sensor response among various ratios of Co$_3$O$_4$−SnO$_2$ at room temperature.[359] The sensing materials of 1:4 Co$_3$O$_4$−SnO$_2$ showed the fastest response to 600 ppm of CO with a response time of 21 s. By doping 0.1% carbon nanotube (CNT) into Co$_3$O$_4$−SnO$_2$, the CO response was improved and the detection limit of the gas sensor reached 20 ppm.

Recently, Chen et al. prepared a CO sensor based on porous titania through a novel "self-doping" strategy.[360] Due to the Ti^{3+} dopant in TiO$_2$, the activity of surface reaction was greatly enhanced by increasing the chemisorbed oxygen species on the TiO$_2$ surface. Therefore, the relatively fast response and recovery times (<10 s, <30 s) were achieved at room temperature in the presence of 5000 ppm of CO. A CO sensor, based on ZnO nanowires gated by GaN/AlGaN, was synthesized by Hung et al.[361] The high electron mobility transistors (HEMTs) enable the sensor to operate at room temperature by enhancing the electron transfer rate.

4.2.2. Sensors for H$_2$S. Hydrogen sulfide (H$_2$S), a malodorous, toxic, and flammable gas, can induce people's loss of consciousness at a low concentration. Therefore, it is crucial to detect H$_2$S as low as tens of parts per million to even parts per billion. MOS sensors for H$_2$S are summarized in Table 15. Among these sensors, CuO has an essential role in

Table 16. Gas Sensing Properties of MOS for Ozone

materials	structures	particle size (nm)	gas concentration (ppm)	operating temp. (°C)	response time	recovery time	ref
WO_3	nanofilms	20	0–0.8	200–350			398
WO_3	nanofilms	50	0–0.8	300			399
WO_3	nanofilms	20	0.8	150–400			400
WO_3	nanofilms		0.013–0.068	530			401
WO_3	nanofilms	17	0.1–0.8	350	<10 s		394
WO_3	nanofilms	40	0.8				402
WO_3	nanofilms	20	0–0.8	150–400			403
Co/WO_3	nanofilms	20	0.8	250			404
α-Ag_2WO_4	nanorods	100	0.08–0.93	300	3–7 s	13–16s	395
SnO_2	nanofilms	30–200	~1	200–350	5–10 s		405
SnO_2	nanofilms		0.058–0.217	20–350			406
SnO_2	nanofilms	260	0.05–0.135	350			407
Au/SnO_2	nanocomposites	100	1	150			408
In_2O_3	nanocrystals	3.5–8.5	0.060–0.3	100–300	7 min		409
In_2O_3	nanocrystals	4–10	0.06	RT–300			396
CuO	nanofilms	25	0.05–0.6	250	820 s		410
$CuCrO_2$	nanofilms	70	100	RT	4 min	2 min	411
$CuCrO_2$	nanocrystals	10–80	50–200	RT			397
$SmFeO_3$			<1	>240			412
$SmFe_{1-x}Co_xO_3$			0.4	250			413
$SrTi_{1-x}Fe_xO_3$	nanofilms	70	75–600	250	<2 min	<5 min	414
ZnO	nanorods	500–800	1	RT			415

sensing materials with its p-type semiconductor properties. Yang et al. prepared CuO hollow spheres with hierarchical pores.[376] On account of this special nanostructure, a synergetic effect of the hierarchical structure of the unique CuO spheres was realized. Thus, the H_2S sensor exhibited excellent performance with a low concentration limit of 2 ppb. The response and recovery times were shortened to 3 and 9 s at 190 °C.

Recently, SnO_2 was used as a sensing material as well. For example, SnO_2 nanofibers functionalized with reduced graphene oxide nanosheets were fabricated by Kim and co-workers.[377] Its optimal temperature is about 350 °C. Although the detection limit is believed to be 1 ppm with relatively good response (<3.3 min) and recovery times (1.9 min), the sensor also appeared to be responsive to acetone.

An appealing improvement was reported by Kaur et al.,[378] in which In_2O_3 whiskers and bipyramidal nanocrystals can sense H_2S at room temperature. The single-crystal whiskers revealed a large number of defects compared with bipyramids. Thus, the sensor based on In_2O_3 whiskers was found to be a high response to 200 ppb of H_2S. It was gratifying that the response time still needs to be 2–3.5 min.

4.2.3. Sensors for O_3. Although ozone (O_3) is widely used in purification, it will do harm to human health if the concentration is above the normal level. Thus, more and more semiconductor gas sensors are used for monitoring the concentration of O_3. MOS sensors for O_3 are summarized in Table 16. Among the sensing materials, WO_3 has attracted the most attention. However, the operating temperature of O_3 sensors based on WO_3 is always above 200 °C. For instance, Khatko et al. prepared WO_3 sensing films deposited by rf sputtering onto silicon micromachined substrates.[394] Also, the maximal operating temperature is 350 °C when exposed to 0.1–0.8 ppm of O_3. Silva et al. synthesized an ozone gas sensor based on α-Ag_2WO_4 nanorod-like structures as well.[395] The sensor exhibited good sensitivity and short response (6–7 s)

and recovery times (13–16 s) with ozone concentrations from 80 to 930 ppb.

In recent years, big progress has been achieved to lower the operation temperature with new materials. A In_2O_3-based O_3 sensor was prepared by Epifani's group which could sense O_3 of 60 ppb at room temperature.[396] However, the best operating temperature is still at about 200 °C. Fang et al. synthesized delafossite-type oxide $CuCrO_2$ nanocrystals by the hydrothermal method.[397] Also, the O_3 sensor resistance decreased upon exposure to 50–200 ppm ozone at room temperature with short response and recovery time. They also prepared a thin-film sensor based on $CuCrO_2$ which is selective and has a reversible response to ozone at room temperature as well. We can deduce that $CuCrO_2$ is another promising material as a semiconductor room-temperature ozone sensor.

5. CONCLUSIONS AND FUTURE PERSPECTIVES

Methods for the detection and quantification of gases using specific chemosensors are needed in studies aimed at gaining an understanding and for monitoring a variety of environmental and biological phenomena. In this review we summarized from a holistic perspective the results of recent studies carried out in this area along with a detailed discussion of the design strategies, sensing performances and mechanisms, and applications. The discussion of this topic was divided into sections which focus on fluorescent organic molecules, semiconducting oxides, and nanomaterial-based sensors. Moreover, the coverage also highlighted the different types of gases for which sensors have been devised, including those involved mainly in environment exhausts (CO_2, SO_2, NOx, VOCs), biological signaling (H_2S, NO, $^1O_2$), and toxic uses (nerve gases, sulfur mustard). We hope that the review stimulates new research in this rapidly expanding multidisciplinary field. For example, sensors based on nanomaterials and oxide semiconductors have already found applications in gas detection, especially under some extreme conditions. Moreover, fluorescent probes have proved to be an ideal tool to help people in

understanding those biological events. However, although numerous chemosensors for gases have been developed and applied in biological studies, a big challenge remains to construct those that display high selectivities, sensitivities, and biocompatibilities and can be employed for real-time imaging and nondestructive detection of gases.

AUTHOR INFORMATION

Corresponding Authors

*E-mail: zcxu@dicp.ac.cn.
*E-mail: jyoon@ewha.ac.kr.

Notes

The authors declare no competing financial interest.

Biographies
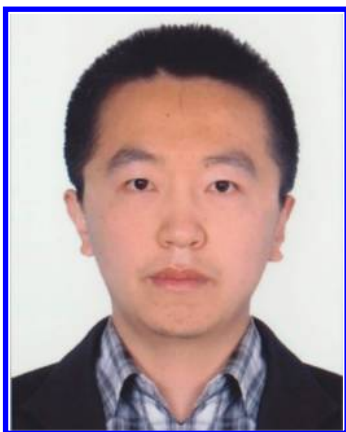
Xin Zhou was born in P. R. China in 1986. He received his Ph.D. degree from Yanbian University in 2014 under the supervision of Xue Wu. Currently, he is a major member of the Research Centre for Chemical Biology in Yanbian University. In 2013 he joined Juyoung Yoon's group at Ewha Womans University (Korea). His current research interests focus on construction of novel fluorescent platforms and development of fluorescent sensors for recognition of biological important molecules and exploring their usage in biology.

Songyi Lee got received her B.S. degree of Chemistry at Ewha Womans University in 2011 and subsequently obtained her M.S. degree in Organic Chemistry from Ewha Womans University in 2013. She pursuing doctoral studies in Juyoung Yoon's laboratory at Ewha Womans University.

Zhaochao Xu was born in Qingdao, China, in 1979. He received his Ph.D. degree in 2006 from Dalian University of Technology under the supervision of Xuhong Qian. Subsequently, he joined the group of Juyoung Yoon at Ewha Womans University as a postdoctoral researcher. In October 2008, he was a Herchel Smith Research Fellow at the University of Cambridge. In 2011, he moved to Dalian Institute of Chemical Physics, CAS, where he is currently a professor. His research is focusing on the development of molecule probes for the selective recognition and fluorescent imaging of biologically important species. In particular, he is interested in the constructions of fluorescent probes for metal ions, anions, protein labeling, and cancer cells.

Juyoung Yoon received his Ph.D. degree (1994) from The Ohio State University. After completing postdoctoral research at UCLA and Scripps Research Institute, he joined the faculty at Silla University in 1998. In 2002, he moved to Ewha Womans University, where he is currently a professor in the Department of Chemistry and Nano Science and the Department of Bioinspired Science. His research interests include investigations of fluorescent chemosensors, molecular recognition, and organofunctional materials.

ABBREVIATIONS

AIE aggregation-induced emission
BINOL 1,1′-bi-2-naphthol
BODIPY boron dipyrromethene difluoride
CA carbamic acid
CGC critical gelation concentration

CNT carbon nanotube
CIL carbamate ionic liquid
CWA chemical-warfare agents
DCP diethylchlorophosphate
DFP diisopropyl fluorophosphate
ESIPT excited-state intramolecular proton transfer
FRET fluorescence resonance energy transfer
HPTS 1-hydroxypyrene-3,6,8-trisulfonate
ICT intramolecular charge transfer
LMWG low molecular weight gel
MOS metal oxide semiconductors
NHC N-heterocyclic carbenes
NIR near-infrared
NMR nuclear magnetic resonance
OP organophosphates
OPD o-phenylenediamine
PBS phosphate-buffered saline
PET photoinduced electron transfer
ROS/RNS reactive oxygen/nitrogen species
RIR restriction of intramolecular rotations
SM sulfur mustard
SQ squaraine dye
TBAF tetrabutylammonium fluoride
TNT trinitrotoluene
VOC volatile organic compound

REFERENCES

(1) Chen, X.; Pradhan, T.; Wang, F.; Kim, J. S.; Yoon, J. *Chem. Rev.* **2012**, *112*, 1910.
(2) Zhang, X.; Yin, J.; Yoon, J. *Chem. Rev.* **2014**, *114*, 4918.
(3) Zhou, Y.; Zhang, J. F.; Yoon, J. *Chem. Rev.* **2014**, *114*, 5511.
(4) Kim, S. K.; Lee, D. H.; Hong, J. I.; Yoon, J. *Acc. Chem. Res.* **2009**, *42*, 23.
(5) Chen, X.; Tian, X.; Shin, I.; Yoon, J. *Chem. Soc. Rev.* **2011**, *40*, 4783.
(6) Chen, X.; Zhou, G.; Peng, X.; Yoon, J. *Chem. Soc. Rev.* **2012**, *41*, 4610.
(7) Chen, X.; Zhou, Y.; Peng, X.; Yoon, J. *Chem. Soc. Rev.* **2010**, *39*, 2120.
(8) Guo, Z.; Park, S.; Yoon, J.; Shin, I. *Chem. Soc. Rev.* **2014**, *43*, 16.
(9) Jung, H. S.; Chen, X.; Kim, J. S.; Yoon, J. *Chem. Soc. Rev.* **2013**, *42*, 6019.
(10) Xu, Z.; Chen, X.; Kim, H. N.; Yoon, J. *Chem. Soc. Rev.* **2010**, *39*, 127.
(11) Zhang, J. F.; Zhou, Y.; Yoon, J.; Kim, J. S. *Chem. Soc. Rev.* **2011**, *40*, 3416.
(12) Zhou, Y.; Xu, Z.; Yoon, J. *Chem. Soc. Rev.* **2011**, *40*, 2222.
(13) Zhou, Y.; Yoon, J. *Chem. Soc. Rev.* **2012**, *41*, 52.
(14) Kim, H. N.; Guo, Z.; Zhu, W.; Yoon, J.; Tian, H. *Chem. Soc. Rev.* **2011**, *40*, 79.
(15) Kim, H. N.; Lee, M. H.; Kim, H. J.; Kim, J. S.; Yoon, J. *Chem. Soc. Rev.* **2008**, *37*, 1465.
(16) Kim, H. N.; Ren, W. X.; Kim, J. S.; Yoon, J. *Chem. Soc. Rev.* **2012**, *41*, 3210.
(17) Ko, S. K.; Chen, X.; Yoon, J.; Shin, I. *Chem. Soc. Rev.* **2011**, *40*, 2120.
(18) Wang, F.; Wang, L.; Chen, X.; Yoon, J. *Chem. Soc. Rev.* **2014**, *43*, 4312.
(19) Xu, Z.; Kim, S. K.; Yoon, J. *Chem. Soc. Rev.* **2010**, *39*, 1457.
(20) Xu, Z.; Yoon, J.; Spring, D. R. *Chem. Soc. Rev.* **2010**, *39*, 1996.
(21) Yoon, J.; Kim, S. K.; Singh, N. J.; Kim, K. S. *Chem. Soc. Rev.* **2006**, *35*, 355.
(22) Anslyn, E. V. *J. Org. Chem.* **2007**, *72*, 687.
(23) Diehl, K. L.; Anslyn, E. V. *Chem. Soc. Rev.* **2013**, *42*, 8596.
(24) Hargrove, A. E.; Nieto, S.; Zhang, T.; Sessler, J. L.; Anslyn, E. V. *Chem. Rev.* **2011**, *111*, 6603.
(25) Joyce, L. A.; Shabbir, S. H.; Anslyn, E. V. *Chem. Soc. Rev.* **2010**, *39*, 3621.
(26) Leung, D.; Kang, S. O.; Anslyn, E. V. *Chem. Soc. Rev.* **2012**, *41*, 448.
(27) Stewart, S.; Ivy, M. A.; Anslyn, E. V. *Chem. Soc. Rev.* **2014**, *43*, 70.
(28) Wenger, O. S. *Chem. Rev.* **2013**, *113*, 3686.
(29) Patel, S. V.; Mlsna, T. E.; Fruhberger, B.; Klaassen, E.; Cemalovic, S.; Baselt, D. R. *Sens. Actuators, B: Chem.* **2003**, *96*, 541.
(30) Peng, G.; Tisch, U.; Adams, O.; Hakim, M.; Shehada, N.; Broza, Y. Y.; Billan, S.; Abdah-Bortnyak, R.; Kuten, A.; Haick, H. *Nat. Nanotechnol.* **2009**, *4*, 669.
(31) Machado, R. F.; Laskowski, D.; Deffenderfer, O.; Burch, T.; Zheng, S.; Mazzone, P. J.; Mekhail, T.; Jennings, C.; Stoller, J. K.; Pyle, J.; Duncan, J.; Dweik, R. A.; Erzurum, S. C. *Am. J. Respir. Crit. Care Med.* **2005**, *171*, 1286.
(32) Haick, H.; Broza, Y. Y.; Mochalski, P.; Ruzsanyi, V.; Amann, A. *Chem. Soc. Rev.* **2014**, *43*, 1423.
(33) Bencic-Nagale, S.; Sternfeld, T.; Walt, D. R. *J. Am. Chem. Soc.* **2006**, *128*, 5041.
(34) Dale, T. J.; Rebek, J., Jr. *J. Am. Chem. Soc.* **2006**, *128*, 4500.
(35) Diaz de Grenu, B.; Moreno, D.; Torroba, T.; Berg, A.; Gunnars, J.; Nilsson, T.; Nyman, R.; Persson, M.; Pettersson, J.; Eklind, I.; Wasterby, P. *J. Am. Chem. Soc.* **2014**, *136*, 4125.
(36) Lei, Z.; Yang, Y. *J. Am. Chem. Soc.* **2014**, *136*, 6594.
(37) Xu, Q.; Lee, S.; Cho, Y.; Kim, M. H.; Bouffard, J.; Yoon, J. *J. Am. Chem. Soc.* **2013**, *135*, 17751.
(38) Ishida, M.; Kim, P.; Choi, J.; Yoon, J.; Kim, D.; Sessler, J. L. *Chem. Commun.* **2013**, *49*, 6950.
(39) Zhang, X.; Lee, S.; Liu, Y.; Lee, M.; Yin, J.; Sessler, J. L.; Yoon, J. *Sci. Rep.* **2014**, *4*, 4593.
(40) Plaza, M.; Santoyo, S.; Jaime, L.; Garcia-Blairsy Reina, G.; Herrero, M.; Senorans, F. J.; Ibanez, E. *J. Pharm. Biomed. Anal.* **2010**, *51*, 450.
(41) Tomás-Barberán, F. A.; Gil, M. I.; Cremin, P.; Waterhouse, A. L.; Hess-Pierce, B.; Kader, A. A. *J. Agric. Food Chem.* **2001**, *49*, 4748.
(42) Ashley, D. L.; Bonin, M. A.; Cardinali, F. L.; McCraw, J. M.; Holler, J. S.; Needham, L. L.; Patterson, D. G. *Anal. Chem.* **1992**, *64*, 1021.
(43) Potyrailo, R. A.; Surman, C.; Nagraj, N.; Burns, A. *Chem. Rev.* **2011**, *111*, 7315.
(44) Llobet, E. *Sens. Actuators, B: Chem.* **2013**, *179*, 32.
(45) Arafat, M. M.; Dinan, B.; Akbar, S. A.; Haseeb, A. S. *Sensors (Basel)* **2012**, *12*, 7207.
(46) Arshak, K.; Moore, E.; Lyons, G. M.; Harris, J.; Clifford, S. *Sensor Rev.* **2004**, *24*, 181.
(47) Tricoli, A.; Righettoni, M.; Teleki, A. *Angew. Chem., Int. Ed.* **2010**, *49*, 7632.
(48) Ho, G. W. *Sci. Adv. Mater.* **2011**, *3*, 150.
(49) Lin, V. S.; Chang, C. J. *Curr. Opin. Chem. Biol.* **2012**, *16*, 595.
(50) Schrag, D. P. *Science* **2007**, *315*, 812.
(51) Tian, T.; Chen, X.; Li, H.; Wang, Y.; Guo, L.; Jiang, L. *Analyst* **2013**, *138*, 991.
(52) Dansby-Sparks, R. N.; Jin, J.; Mechery, S. J.; Sampathkumaran, U.; Owen, T. W.; Yu, B. D.; Goswami, K.; Hong, K.; Grant, J.; Xue, Z. L. *Anal. Chem.* **2010**, *82*, 593.
(53) Jiang, Y.; Wang, Y.; Hua, J.; Qu, S.; Qian, S.; Tian, H. *J. Polym. Sci., Part A: Polym. Chem.* **2009**, *47*, 4400.
(54) Zhao, Q.; Li, F.; Huang, C. *Chem. Soc. Rev.* **2010**, *39*, 3007.
(55) Schutting, S.; Borisov, S. M.; Klimant, I. *Anal. Chem.* **2013**, *85*, 3271.
(56) Hampe, E. M.; Rudkevich, D. M. *Chem. Commun.* **2002**, *38*, 1450.
(57) Han, Y.; Pacheco, K.; Bastiaansen, C. W.; Broer, D. J.; Sijbesma, R. P. *J. Am. Chem. Soc.* **2010**, *132*, 2961.
(58) Jessop, P. G.; Heldebrant, D. J.; Li, X.; Eckert, C. A.; Liotta, C. L. *Nature* **2005**, *436*, 1102.
(59) Ning, Z.; Chen, Z.; Zhang, Q.; Yan, Y.; Qian, S.; Cao, Y.; Tian, H. *Adv. Funct. Mater.* **2007**, *17*, 3799.

(60) Zhao, Z.; Wang, Z.; Lu, P.; Chan, C. Y.; Liu, D.; Lam, J. W.; Sung, H. H.; Williams, I. D.; Ma, Y.; Tang, B. Z. *Angew. Chem., Int. Ed.* **2009**, *48*, 7608.

(61) An, B. K.; Kwon, S. K.; Jung, S. D.; Park, S. Y. *J. Am. Chem. Soc.* **2002**, *124*, 14410.

(62) Gunnlaugsson, T.; Kruger, P. E.; Jensen, P.; Pfeffer, F. M.; Hussey, G. M. *Tetrahedron Lett.* **2003**, *44*, 8909.

(63) Guo, Z.; Song, N. R.; Moon, J. H.; Kim, M.; Jun, E. J.; Choi, J.; Lee, J. Y.; Bielawski, C. W.; Sessler, J. L.; Yoon, J. *J. Am. Chem. Soc.* **2012**, *134*, 17846.

(64) Wood, T. E.; Thompson, A. *Chem. Rev.* **2007**, *107*, 1831.

(65) Lee, M.; Moon, J. H.; Swamy, K. M. K.; Jeong, Y.; Kim, G.; Choi, J.; Lee, J. Y.; Yoon, J. *Sens. Actuators, B: Chem.* **2014**, *199*, 369.

(66) Li, G.; Sang, N. *Ecotoxicol. Environ. Saf.* **2009**, *72*, 236.

(67) Choi, M. G.; Hwang, J.; Eor, S.; Chang, S. K. *Org. Lett.* **2010**, *12*, 5624.

(68) Sun, Y. Q.; Liu, J.; Zhang, J.; Yang, T.; Guo, W. *Chem. Commun.* **2013**, *49*, 2637.

(69) Wu, M. Y.; He, T.; Li, K.; Wu, M. B.; Huang, Z.; Yu, X. Q. *Analyst* **2013**, *138*, 3018.

(70) Wu, M. Y.; Li, K.; Li, C. Y.; Hou, J. T.; Yu, X. Q. *Chem. Commun.* **2014**, *50*, 183.

(71) Liu, Z.; Guo, S.; Piao, J.; Zhou, X.; Wu, X. *RSC Adv.* **2014**, *4*, 54554.

(72) Babior, B. M.; Takeuchi, C.; Ruedi, J.; Gutierrez, A.; Wentworth, P., Jr. *Proc. Natl. Acad. Sci. U.S.A.* **2003**, *100*, 3031.

(73) Criegee, R. *Angew. Chem., Int. Ed.* **1975**, *14*, 745.

(74) Willand-Charnley, R.; Fisher, T. J.; Johnson, B. M.; Dussault, P. H. *Org. Lett.* **2012**, *14*, 2242.

(75) Garner, A. L.; St Croix, C. M.; Pitt, B. R.; Leikauf, G. D.; Ando, S.; Koide, K. *Nat. Chem.* **2009**, *1*, 316.

(76) Zhang, Y.; Shi, W.; Li, X.; Ma, H. *Sci. Rep.* **2013**, *3*, 2830.

(77) Fukumura, D.; Kashiwagi, S.; Jain, R. K. *Nat. Rev. Cancer* **2006**, *6*, 521.

(78) Kojima, H.; Nakatsubo, N.; Kikuchi, K.; Kawahara, S.; Kirino, Y.; Nagoshi, H.; Hirata, Y.; Nagano, T. *Anal. Chem.* **1998**, *70*, 2446.

(79) Kojima, H.; Urano, Y.; Kikuchi, K.; Higuchi, T.; Hirata, Y.; Nagano, T. *Angew. Chem., Int. Ed.* **1999**, *38*, 3209.

(80) Kojima, H.; Hirotani, M.; Nakatsubo, N.; Kikuchi, K.; Urano, Y.; Higuchi, T.; Hirata, Y.; Nagano, T. *Anal. Chem.* **2001**, *73*, 1967.

(81) Gabe, Y.; Urano, Y.; Kikuchi, K.; Kojima, H.; Nagano, T. *J. Am. Chem. Soc.* **2004**, *126*, 3357.

(82) Sasaki, E.; Kojima, H.; Nishimatsu, H.; Urano, Y.; Kikuchi, K.; Hirata, Y.; Nagano, T. *J. Am. Chem. Soc.* **2005**, *127*, 3684.

(83) Helmchen, F.; Denk, W. *Nat. Methods* **2005**, *2*, 932.

(84) Dong, X.; Heo, C. H.; Chen, S.; Kim, H. M.; Liu, Z. *Anal. Chem.* **2014**, *86*, 308.

(85) Yu, H.; Xiao, Y.; Jin, L. *J. Am. Chem. Soc.* **2012**, *134*, 17486.

(86) Seo, E. W.; Han, J. H.; Heo, C. H.; Shin, J. H.; Kim, H. M.; Cho, B. R. *Chemistry* **2012**, *18*, 12388.

(87) Zheng, H.; Shang, G. Q.; Yang, S. Y.; Gao, X.; Xu, J. G. *Org. Lett.* **2008**, *10*, 2357.

(88) Sun, Y. Q.; Liu, J.; Zhang, H.; Huo, Y.; Lv, X.; Shi, Y.; Guo, W. *J. Am. Chem. Soc.* **2014**, *136*, 12520.

(89) Franz, K. J.; Singh, N.; Lippard, S. J. *Angew. Chem., Int. Ed.* **2000**, *39*, 2120.

(90) Hilderbrand, S. A.; Lippard, S. J. *Inorg. Chem.* **2004**, *43*, 4674.

(91) Tsuge, K.; DeRosa, F.; Lim, M. D.; Ford, P. C. *J. Am. Chem. Soc.* **2004**, *126*, 6564.

(92) Lim, M. H.; Xu, D.; Lippard, S. J. *Nat. Chem. Biol.* **2006**, *2*, 375.

(93) Hu, X.; Wang, J.; Zhu, X.; Dong, D.; Zhang, X.; Wu, S.; Duan, C. *Chem. Commun.* **2011**, *47*, 11507.

(94) Mondal, B.; Kumar, P.; Ghosh, P.; Kalita, A. *Chem. Commun.* **2011**, *47*, 2964.

(95) Hu, X.; Zhang, X.; Song, H.; He, C.; Bao, Y.; Tang, Q.; Duan, C. *Tetrahedron* **2012**, *68*, 8371.

(96) Zhou, Y.; Liu, K.; Li, J. Y.; Fang, Y.; Zhao, T. C.; Yao, C. *Org. Lett.* **2011**, *13*, 1290.

(97) Apfel, U. P.; Buccella, D.; Wilson, J. J.; Lippard, S. J. *Inorg. Chem.* **2013**, *52*, 3285.

(98) Yang, Y.; Seidlits, S. K.; Adams, M. M.; Lynch, V. M.; Schmidt, C. E.; Anslyn, E. V.; Shear, J. B. *J. Am. Chem. Soc.* **2010**, *132*, 13114.

(99) Lv, X.; Wang, Y.; Zhang, S.; Liu, Y.; Zhang, J.; Guo, W. *Chem. Commun.* **2014**, *50*, 7499.

(100) Ryter, S. W.; Alam, J.; Choi, A. M. K. *Physiol. Rev.* **2006**, *86*, 583.

(101) Esteban, J.; Ros-Lis, J. V.; Martinez-Manez, R.; Marcos, M. D.; Moragues, M.; Soto, J.; Sancenon, F. *Angew. Chem., Int. Ed.* **2010**, *49*, 4934.

(102) Michel, B. W.; Lippert, A. R.; Chang, C. J. *J. Am. Chem. Soc.* **2012**, *134*, 15668.

(103) Moragues, M. E.; Toscani, A.; Sancenon, F.; Martinez-Manez, R.; White, A. J.; Wilton-Ely, J. D. *J. Am. Chem. Soc.* **2014**, *136*, 11930.

(104) Li, L.; Rose, P.; Moore, P. K. *Annu. Rev. Pharmacol. Toxicol.* **2011**, *51*, 169.

(105) Culotta, E.; Koshland, D. *Science* **1992**, *258*, 1862.

(106) Szabo, C. *Nat. Rev. Drug Discovery* **2007**, *6*, 917.

(107) Papapetropoulos, A.; Pyriochou, A.; Altaany, Z.; Yang, G.; Marazioti, A.; Zhou, Z.; Jeschke, M. G.; Branski, L. K.; Herndon, D. N.; Wang, R.; Szabo, C. *Proc. Natl. Acad. Sci. U.S.A.* **2009**, *106*, 21972.

(108) Chen, Y. H.; Yao, W. Z.; Geng, B.; Ding, Y. L.; Lu, M.; Zhao, M. W.; Tang, C. S. *Chest* **2005**, *128*, 3205.

(109) Yang, C.; Yang, Z.; Zhang, M.; Dong, Q.; Wang, X.; Lan, A.; Zeng, F.; Chen, P.; Wang, C.; Feng, J. *PLoS One* **2011**, *6*, e21971.

(110) Zanardo, R. C.; Brancaleone, V.; Distrutti, E.; Fiorucci, S.; Cirino, G.; Wallace, J. L. *FASEB J.* **2006**, *20*, 2118.

(111) Eto, K.; Asada, T.; Arima, K.; Makifuchi, T.; Kimura, H. *Biochem. Biophys. Res. Commun.* **2002**, *293*, 1485.

(112) Fiorucci, S.; Antonelli, E.; Mencarelli, A.; Orlandi, S.; Renga, B.; Rizzo, G.; Distrutti, E.; Shah, V.; Morelli, A. *Hepatology* **2005**, *42*, 539.

(113) Yang, W.; Yang, G.; Jia, X.; Wu, L.; Wang, R. *J. Physiol.* **2005**, *569*, 519.

(114) Blackstone, E.; Morrison, M.; Roth, M. B. *Science* **2005**, *308*, 518.

(115) Lippert, A. R.; New, E. J.; Chang, C. J. *J. Am. Chem. Soc.* **2011**, *133*, 10078.

(116) Montoya, L. A.; Pluth, M. D. *Chem. Commun.* **2012**, *48*, 4767.

(117) Yu, F.; Li, P.; Song, P.; Wang, B.; Zhao, J.; Han, K. *Chem. Commun.* **2012**, *48*, 2852.

(118) Denk, W.; Strickler, J. H.; Webb, W. W. *Science* **1990**, *248*, 73.

(119) Das, S. K.; Lim, C. S.; Yang, S. Y.; Han, J. H.; Cho, B. R. *Chem. Commun.* **2012**, *48*, 8395.

(120) Bae, S. K.; Heo, C. H.; Choi, D. J.; Sen, D.; Joe, E. H.; Cho, B. R.; Kim, H. M. *J. Am. Chem. Soc.* **2013**, *135*, 9915.

(121) Mao, G. J.; Wei, T. T.; Wang, X. X.; Huan, S. Y.; Lu, D. Q.; Zhang, J.; Zhang, X. B.; Tan, W.; Shen, G. L.; Yu, R. Q. *Anal. Chem.* **2013**, *85*, 7875.

(122) Qian, Y.; Karpus, J.; Kabil, O.; Zhang, S. Y.; Zhu, H. L.; Banerjee, R.; Zhao, J.; He, C. *Nat. Commun.* **2011**, *2*, 495.

(123) Liu, C.; Pan, J.; Li, S.; Zhao, Y.; Wu, L. Y.; Berkman, C. E.; Whorton, A. R.; Xian, M. *Angew. Chem., Int. Ed.* **2011**, *50*, 10327.

(124) Liu, C.; Peng, B.; Li, S.; Park, C. M.; Whorton, A. R.; Xian, M. *Org. Lett.* **2012**, *14*, 2184.

(125) Wang, X.; Sun, J.; Zhang, W.; Ma, X.; Lv, J.; Tang, B. *Chem. Sci.* **2013**, *4*, 2551.

(126) Zhang, J.; Sun, Y. Q.; Liu, J.; Shi, Y.; Guo, W. *Chem. Commun.* **2013**, *49*, 11305.

(127) Xu, Z.; Xu, L.; Zhou, J.; Xu, Y.; Zhu, W.; Qian, X. *Chem. Commun.* **2012**, *48*, 10871.

(128) Chen, Y.; Zhu, C.; Yang, Z.; Chen, J.; He, Y.; Jiao, Y.; He, W.; Qiu, L.; Cen, J.; Guo, Z. *Angew. Chem., Int. Ed.* **2013**, *52*, 1688.

(129) Sasakura, K.; Hanaoka, K.; Shibuya, N.; Mikami, Y.; Kimura, Y.; Komatsu, T.; Ueno, T.; Terai, T.; Kimura, H.; Nagano, T. *J. Am. Chem. Soc.* **2011**, *133*, 18003.

(130) Hou, F.; Huang, L.; Xi, P.; Cheng, J.; Zhao, X.; Xie, G.; Shi, Y.; Cheng, F.; Yao, X.; Bai, D.; Zeng, Z. *Inorg. Chem.* **2012**, *51*, 2454.

(131) Hou, F.; Cheng, J.; Xi, P.; Chen, F.; Huang, L.; Xie, G.; Shi, Y.; Liu, H.; Bai, D.; Zeng, Z. *Dalton Trans.* **2012**, *41*, 5799.

(132) Choi, M. G.; Cha, S.; Lee, H.; Jeon, H. L.; Chang, S. K. *Chem. Commun.* **2009**, *45*, 7390.

(133) Wang, M. Q.; Li, K.; Hou, J. T.; Wu, M. Y.; Huang, Z.; Yu, X. Q. *J. Org. Chem.* **2012**, *77*, 8350.

(134) Cao, X.; Lin, W.; He, L. *Org. Lett.* **2011**, *13*, 4716.

(135) Umezawa, N.; Tanaka, K.; Urano, Y.; Kikuchi, K.; Higuchi, T.; Nagano, T. *Angew. Chem., Int. Ed.* **1999**, *38*, 2899.

(136) Tanaka, K.; Miura, T.; Umezawa, N.; Urano, Y.; Kikuchi, K.; Higuchi, T.; Nagano, T. *J. Am. Chem. Soc.* **2001**, *123*, 2530.

(137) Flors, C.; Fryer, M. J.; Waring, J.; Reeder, B.; Bechtold, U.; Mullineaux, P. M.; Nonell, S.; Wilson, M. T.; Baker, N. R. *J. Exp. Bot.* **2006**, *57*, 1725.

(138) Song, B.; Wang, G.; Tan, M.; Yuan, J. *J. Am. Chem. Soc.* **2006**, *128*, 13442.

(139) Song, B.; Wang, G.; Yuan, J. *Chem. Commun.* **2005**, *41*, 3553.

(140) Sidell, F. R.; Borak, J. *Ann. Emerg. Med.* **1992**, *21*, 865.

(141) Zhang, S. W.; Swager, T. M. *J. Am. Chem. Soc.* **2003**, *125*, 3420.

(142) Han, S.; Xue, Z.; Wang, Z.; Wen, T. B. *Chem. Commun.* **2010**, *46*, 8413.

(143) Wu, X.; Wu, Z.; Han, S. *Chem. Commun.* **2011**, *47*, 11468.

(144) Wu, W. H.; Dong, J. J.; Wang, X.; Li, J.; Sui, S. H.; Chen, G. Y.; Liu, J. W.; Zhang, M. *Analyst* **2012**, *137*, 3224.

(145) Xuan, W.; Cao, Y.; Zhou, J.; Wang, W. *Chem. Commun.* **2013**, *49*, 10474.

(146) Barba-Bon, A.; Costero, A. M.; Gil, S.; Harriman, A.; Sancenon, F. *Chemistry* **2014**, *20*, 6339.

(147) Jang, Y. J.; Murale, D. P.; Churchill, D. G. *Analyst* **2014**, *139*, 1614.

(148) Davis, K. G.; Aspera, G. *Ann. Emerg. Med.* **2001**, *37*, 653.

(149) Takeshima, Y.; Inai, K.; Bennett, W. P.; Metcalf, R. A.; Welsh, J. A.; Yonehara, S.; Hayashi, Y.; Fujihara, M.; Yamakido, M.; Akiyama, M.; Tokuoka, S.; Land, C. E.; Harris, C. C. *Carcinogenesis* **1994**, *15*, 2075.

(150) Pathak, U.; Raza, S. K.; Kulkarni, A. S.; Vijayaraghvan, R.; Kumar, P.; Jaiswal, D. K. *J. Med. Chem.* **2004**, *47*, 3817.

(151) Kim, K.; Tsay, O. G.; Atwood, D. A.; Churchill, D. G. *Chem. Rev.* **2011**, *111*, 5345.

(152) Kumar, V.; Anslyn, E. V. *J. Am. Chem. Soc.* **2013**, *135*, 6338.

(153) Kumar, V.; Anslyn, E. V. *Chem. Sci.* **2013**, *4*, 4292.

(154) Raghavender Goud, D.; Purohit, A. K.; Tak, V.; Dubey, D. K.; Kumar, P.; Pardasani, D. *Chem. Commun.* **2014**, *50*, 12363.

(155) Moon, R. J.; Martini, A.; Nairn, J.; Simonsen, J.; Youngblood, J. *Chem. Soc. Rev.* **2011**, *40*, 3941.

(156) Leng, B.; Jiang, J.; Tian, H. *AIChE J.* **2010**, *56*, 2957.

(157) Zou, Q.; Zou, L.; Tian, H. *J. Mater. Chem.* **2011**, *21*, 14441.

(158) Yanai, N.; Kitayama, K.; Hijikata, Y.; Sato, H.; Matsuda, R.; Kubota, Y.; Takata, M.; Mizuno, M.; Uemura, T.; Kitagawa, S. *Nat. Mater.* **2011**, *10*, 787.

(159) Yao, Z.; Hu, X.; Huang, B.; Zhang, L.; Liu, L.; Zhao, Y.; Wu, H. C. *ACS Appl. Mater. Interfaces* **2013**, *5*, 5783.

(160) Lee, H. J.; Park, K. K.; Kupnik, M.; Melosh, N. A.; Khuri-Yakub, B. T. *Anal. Chem.* **2012**, *84*, 3063.

(161) Esser, B.; Swager, T. M. *Angew. Chem., Int. Ed.* **2010**, *49*, 8872.

(162) Hyakutake, T.; Okura, I.; Asai, K.; Nishide, H. *J. Mater. Chem.* **2008**, *18*, 917.

(163) Payne, S. J.; Fiore, G. L.; Fraser, C. L.; Demas, J. N. *Anal. Chem.* **2010**, *82*, 917.

(164) Tian, Y.; Shumway, B. R.; Meldrum, D. R. *Chem. Mater.* **2010**, *22*, 2069.

(165) Lipatov, A.; Varezhnikov, A.; Wilson, P.; Sysoev, V.; Kolmakov, A.; Sinitskii, A. *Nanoscale* **2013**, *5*, 5426.

(166) Yoon, B.; Park, I. S.; Shin, H.; Park, H. J.; Lee, C. W.; Kim, J. M. *Macromol. Rapid Commun.* **2013**, *34*, 731.

(167) Sarkar, T.; Srinives, S.; Sarkar, S.; Haddon, R. C.; Mulchandani, A. *J. Phys. Chem. C* **2014**, *118*, 1602.

(168) Qian, N.; Duan, Z.; Zhu, Y.; Xiang, Q.; Xu, J. *J. Phys. Chem. C* **2014**, *118*, 1879.

(169) Jeon, H.; Lee, J.; Kim, M. H.; Yoon, J. *Macromol. Rapid Commun.* **2012**, *33*, 972.

(170) Lv, Y.-Y.; Wu, J.; Xu, Z.-K. *Sens. Actuators, B: Chem.* **2010**, *148*, 233.

(171) Feng, L.; Musto, C. J.; Suslick, K. S. *J. Am. Chem. Soc.* **2010**, *132*, 4046.

(172) Lee, G. S.; Lee, C.; Choi, H.; Ahn, D. J.; Kim, J.; Gila, B. P.; Abernathy, C. R.; Pearton, S. J.; Ren, F. *Phys. Status Solidi A* **2007**, *204*, 3556.

(173) Gu, Y.; Huang, J. *Colloids Surf., A: Physicochem. Eng. Aspects* **2013**, *433*, 166.

(174) Soga, T.; Jimbo, Y.; Suzuki, K.; Citterio, D. *Anal. Chem.* **2013**, *85*, 8973.

(175) Liao, Y.; Zhang, C.; Zhang, Y.; Strong, V.; Tang, J.; Li, X. G.; Kalantar-Zadeh, K.; Hoek, E. M.; Wang, K. L.; Kaner, R. B. *Nano Lett.* **2011**, *11*, 954.

(176) Lin, H.; Jang, M.; Suslick, K. S. *J. Am. Chem. Soc.* **2011**, *133*, 16786.

(177) Zou, X.; Wang, J.; Liu, X.; Wang, C.; Jiang, Y.; Wang, Y.; Xiao, X.; Ho, J. C.; Li, J.; Jiang, C.; Fang, Y.; Liu, W.; Liao, L. *Nano Lett.* **2013**, *13*, 3287.

(178) Offermans, P.; Crego-Calama, M.; Brongersma, S. H. *Nano Lett.* **2010**, *10*, 2412.

(179) Khalap, V. R.; Sheps, T.; Kane, A. A.; Collins, P. G. *Nano Lett.* **2010**, *10*, 896.

(180) Kim, H. J.; Lee, J. H.; Lee, H.; Lee, J. H.; Lee, J. H.; Jung, J. H.; Kim, J. S. *Adv. Funct. Mater.* **2011**, *21*, 4035.

(181) Chulvi, K.; Gavina, P.; Costero, A. M.; Gil, S.; Parra, M.; Gotor, R.; Royo, S.; Martinez-Manez, R.; Sancenon, F.; Vivancos, J. L. *Chem. Commun.* **2012**, *48*, 10105.

(182) Li, M.; Myers, E. B.; Tang, H. X.; Aldridge, S. J.; McCaig, H. C.; Whiting, J. J.; Simonson, R. J.; Lewis, N. S.; Roukes, M. L. *Nano Lett.* **2010**, *10*, 3899.

(183) Kwon, O. S.; Park, S. J.; Lee, J. S.; Park, E.; Kim, T.; Park, H. W.; You, S. A.; Yoon, H.; Jang, J. *Nano Lett.* **2012**, *12*, 2797.

(184) Yildirim, A.; Budunoglu, H.; Deniz, H.; O. Guler, M.; Bayindir, M. *ACS Appl. Mater. Interfaces* **2010**, *2*, 2892.

(185) Xu, P.; Yu, H.; Li, X. *Anal. Chem.* **2011**, *83*, 3448.

(186) Germain, M. E.; Knapp, M. J. *J. Am. Chem. Soc.* **2008**, *130*, 5422.

(187) Seiyama, T.; Kato, A.; Fujiishi, K.; Nagatani, M. *Anal. Chem.* **1962**, *34*, 1502.

(188) Jaaniso, R.; Tan, O. K. *Semiconductor Gas Sensors*; Woodhead Publishing Ltd.: Cambridge, U.K., 2013.

(189) Bârsan, N.; Weimar, U. *J. Phys.: Condens. Matter* **2003**, *15*, R813.

(190) Wetchakun, K.; Samerjai, T.; Tamaekong, N.; Liewhiran, C.; Siriwong, C.; Kruefu, V.; Wisitsoraat, A.; Tuantranont, A.; Phanichphant, S. *Sens. Actuators, B: Chem.* **2011**, *160*, 580.

(191) Kim, H.-J.; Lee, J.-H. *Sens. Actuators, B: Chem.* **2014**, *192*, 607.

(192) Kanan, S. M.; El-Kadri, O. M.; Abu-Yousef, I. A.; Kanan, M. C. *Sensors (Basel)* **2009**, *9*, 8158.

(193) Fine, G. F.; Cavanagh, L. M.; Afonja, A.; Binions, R. *Sensors (Basel)* **2010**, *10*, 5469.

(194) Sun, Y. F.; Liu, S. B.; Meng, F. L.; Liu, J. Y.; Jin, Z.; Kong, L. T.; Liu, J. H. *Sensors (Basel)* **2012**, *12*, 2610.

(195) Asefa, T.; Duncan, C. T.; Sharma, K. K. *Analyst* **2009**, *134*, 1980.

(196) Ren, Z.; Guo, Y.; Liu, C. H.; Gao, P. X. *Front Chem.* **2013**, *1*, 18.

(197) Ramgir, N.; Datta, N.; Kaur, M.; Kailasaganapathi, S.; Debnath, A. K.; Aswal, D. K.; Gupta, S. K. *Colloids Surf., A: Physicochem. Eng. Aspects* **2013**, *439*, 101.

(198) Comini, E.; Baratto, C.; Faglia, G.; Ferroni, M.; Vomiero, A.; Sberveglieri, G. *Prog. Mater. Sci.* **2009**, *54*, 1.

(199) Gu, H.; Wang, Z.; Hu, Y. *Sensors (Basel)* **2012**, *12*, 5517.

(200) Chiu, S. W.; Tang, K. T. *Sensors (Basel)* **2013**, *13*, 14214.

(201) Bedford, K. R.; Nolan, S. L.; Onrust, R.; Siegers, J. D. *Forensic Sci. Int.* **1987**, *34*, 197.

(202) Liu, Y.; Koep, E.; Liu, M. *Chem. Mater.* **2005**, *17*, 3997.

(203) Li, K.-M.; Li, Y.-J.; Lu, M.-Y.; Kuo, C.-I.; Chen, L.-J. *Adv. Funct. Mater.* **2009**, *19*, 2453.

(204) Bie, L.-J.; Yan, X.-N.; Yin, J.; Duan, Y.-Q.; Yuan, Z.-H. *Sens. Actuators, B: Chem.* **2007**, *126*, 604.

(205) Hsueh, T.-J.; Hsu, C.-L.; Chang, S.-J.; Chen, I. C. *Sens. Actuators, B: Chem.* **2007**, *126*, 473.

(206) Xiangfeng, C.; Dongli, J.; Djurišic, A. B.; Leung, Y. H. *Chem. Phys. Lett.* **2005**, *401*, 426.

(207) Hsueh, T.-J.; Chang, S.-J.; Hsu, C.-L.; Lin, Y.-R.; Chen, I. C. *Appl. Phys. Lett.* **2007**, *91*, 053111.

(208) Lin, Y.-H.; Hsueh, Y.-C.; Lee, P.-S.; Wang, C.-C.; Wu, J. M.; Perng, T.-P.; Shih, H. C. *J. Mater. Chem.* **2011**, *21*, 10552.

(209) Wan, Q.; Wang, T. H. *Chem. Commun.* **2005**, *41*, 3841.

(210) Hwang, I. S.; Choi, J. K.; Woo, H. S.; Kim, S. J.; Jung, S. Y.; Seong, T. Y.; Kim, I. D.; Lee, J. H. *ACS Appl. Mater. Interfaces* **2011**, *3*, 3140.

(211) Li, L. M.; Li, C. C.; Zhang, J.; Du, Z. F.; Zou, B. S.; Yu, H. C.; Wang, Y. G.; Wang, T. H. *Nanotechnology* **2007**, *18*, 225504.

(212) Tricoli, A.; Graf, M.; Pratsinis, S. E. *Adv. Funct. Mater.* **2008**, *18*, 1969.

(213) Na, C. W.; Park, S. Y.; Chung, J. H.; Lee, J. H. *ACS Appl. Mater. Interfaces* **2012**, *4*, 6565.

(214) Hernández, P. T.; Naik, A. J. T.; Newton, E. J.; Hailes, S. M. V.; Parkin, I. P. *J. Mater. Chem. A* **2014**, *2*, 8952.

(215) Van Hieu, N.; Kim, H.-R.; Ju, B.-K.; Lee, J.-H. *Sens. Actuators, B: Chem.* **2008**, *133*, 228.

(216) Vallejos, S.; Stoycheva, T.; Umek, P.; Navio, C.; Snyders, R.; Bittencourt, C.; Llobet, E.; Blackman, C.; Moniz, S.; Correig, X. *Chem. Commun.* **2011**, *47*, 565.

(217) Kim, S.-J.; Hwang, I.-S.; Na, C. W.; Kim, I.-D.; Kang, Y. C.; Lee, J.-H. *J. Mater. Chem.* **2011**, *21*, 18560.

(218) Wang, G.; Gou, X.; Horvat, J.; Park, J. *J. Phys. Chem. C* **2008**, *112*, 15220.

(219) Cho, N. G.; Hwang, I.-S.; Kim, H.-G.; Lee, J.-H.; Kim, I.-D. *Sens. Actuators, B: Chem.* **2011**, *155*, 366.

(220) Song, X.; Gao, L.; Mathur, S. *J. Phys. Chem. C* **2011**, *115*, 21730.

(221) Yang, C.; Su, X.; Xiao, F.; Jian, J.; Wang, J. *Sens. Actuators, B: Chem.* **2011**, *158*, 299.

(222) Sun, C.; Rajasekhara, S.; Chen, Y.; Goodenough, J. B. *Chem. Commun.* **2011**, *47*, 12852.

(223) Liu, H.; Du, X.; Xing, X.; Wang, G.; Qiao, S. Z. *Chem. Commun.* **2012**, *48*, 865.

(224) Cho, N. G.; Woo, H. S.; Lee, J. H.; Kim, I. D. *Chem. Commun.* **2011**, *47*, 11300.

(225) Van Hieu, N. *Sens. Actuators, B: Chem.* **2010**, *144*, 425.

(226) Xue, X. Y.; Chen, Y. J.; Wang, Y. G.; Wang, T. H. *Appl. Phys. Lett.* **2005**, *86*, 233101.

(227) Choi, S. H.; Hwang, I. S.; Lee, J. H.; Oh, S. G.; Kim, I. D. *Chem. Commun.* **2011**, *47*, 9315.

(228) Pugh, D. C.; Newton, E. J.; Naik, A. J. T.; Hailes, S. M. V.; Parkin, I. P. *J. Mater. Chem. A* **2014**, *2*, 4758.

(229) Liu, X.; Zhang, J.; Kang, Y.; Wu, S.; Wang, S. *CrystEngComm* **2012**, *14*, 620.

(230) Liu, J.; Wang, X.; Peng, Q.; Li, Y. *Adv. Mater.* **2005**, *17*, 764.

(231) Cao, M.; Wang, Y.; Chen, T.; Antonietti, M.; Niederberger, M. *Chem. Mater.* **2008**, *20*, 5781.

(232) Tian, S.; Ding, X.; Zeng, D.; Wu, J.; Zhang, S.; Xie, C. *RSC Adv.* **2013**, *3*, 11823.

(233) Wang, J.; Zhang, P.; Qi, J.-Q.; Yao, P.-J. *Sens. Actuators, B: Chem.* **2009**, *136*, 399.

(234) Zheng, Y.; Wang, J.; Yao, P. *Sens. Actuators, B: Chem.* **2011**, *156*, 723.

(235) Lee, Y.-I.; Lee, K.-J.; Lee, D.-H.; Jeong, Y.-K.; Lee, H. S.; Choa, Y.-H. *Curr. Appl. Phys.* **2009**, *9*, S79.

(236) Li, Z.; Zhao, Q.; Fan, W.; Zhan, J. *Nanoscale* **2011**, *3*, 1646.

(237) Chu, X.; Chen, T.; Zhang, W.; Zheng, B.; Shui, H. *Sens. Actuators, B: Chem.* **2009**, *142*, 49.

(238) Castro-Hurtado, I.; Malagù, C.; Morandi, S.; Pérez, N.; Mandayo, G. G.; Castaño, E. *Acta Mater.* **2013**, *61*, 1146.

(239) Li, G.; Wang, X.; Ding, H.; Zhang, T. *RSC Adv.* **2012**, *2*, 13018.

(240) Liu, Y.; Zhu, G.; Ge, B.; Zhou, H.; Yuan, A.; Shen, X. *CrystEngComm* **2012**, *14*, 6264.

(241) Yang, W.; Wan, P.; Zhou, X.; Hu, J.; Guan, Y.; Feng, L. *Sens. Actuators, B: Chem.* **2014**, *201*, 228.

(242) Liu, B.; Yang, H.; Zhao, H.; An, L.; Zhang, L.; Shi, R.; Wang, L.; Bao, L.; Chen, Y. *Sens. Actuators, B: Chem.* **2011**, *156*, 251.

(243) Wang, C.; Cheng, X.; Zhou, X.; Sun, P.; Hu, X.; Shimanoe, K.; Lu, G.; Yamazoe, N. *ACS Appl. Mater. Interfaces* **2014**, *6*, 12031.

(244) Kim, H. J.; Yoon, J. W.; Choi, K. I.; Jang, H. W.; Umar, A.; Lee, J. H. *Nanoscale* **2013**, *5*, 7066.

(245) Hong, Y. J.; Yoon, J. W.; Lee, J. H.; Kang, Y. C. *Chemistry* **2014**, *20*, 2737.

(246) Elmi, I.; Zampolli, S.; Cozzani, E.; Mancarella, F.; Cardinali, G. C. *Sens. Actuators, B: Chem.* **2008**, *135*, 342.

(247) Wang, L.; Lou, Z.; Fei, T.; Zhang, T. *J. Mater. Chem.* **2011**, *21*, 19331.

(248) Ma, H.; Xu, Y.; Rong, Z.; Cheng, X.; Gao, S.; Zhang, X.; Zhao, H.; Huo, L. *Sens. Actuators, B: Chem.* **2012**, *174*, 325.

(249) Park, J.; Shen, X.; Wang, G. *Sens. Actuators, B: Chem.* **2009**, *136*, 494.

(250) Suematsu, K.; Shin, Y.; Hua, Z.; Yoshida, K.; Yuasa, M.; Kida, T.; Shimanoe, K. *ACS Appl. Mater. Interfaces* **2014**, *6*, 5319.

(251) Cao, J.; Wang, Z.; Wang, R.; Zhang, T. *CrystEngComm* **2014**, *16*, 7731.

(252) Sun, C.; Su, X.; Xiao, F.; Niu, C.; Wang, J. *Sens. Actuators, B: Chem.* **2011**, *157*, 681.

(253) Vomiero, A.; Bianchi, S.; Comini, E.; Faglia, G.; Ferroni, M.; Sberveglieri, G. *Cryst. Growth Des.* **2007**, *7*, 2500.

(254) Nguyen, H.; El-Safty, S. A. *J. Phys. Chem. C* **2011**, *115*, 8466.

(255) Song, P.; Wang, Q.; Yang, Z. *Sens. Actuators, B: Chem.* **2012**, *173*, 839.

(256) Sun, P.; Cai, Y.; Du, S.; Xu, X.; You, L.; Ma, J.; Liu, F.; Liang, X.; Sun, Y.; Lu, G. *Sens. Actuators, B: Chem.* **2013**, *182*, 336.

(257) David, S.; Patrik, Š.; Anthony, A. F.; Fahmy, H.; Gordon, A. A. F. *J. Breath Res.* **2011**, *5*, 022001.

(258) Ryabtsev, S. V.; Shaposhnick, A. V.; Lukin, A. N.; Domashevskaya, E. P. *Sens. Actuators, B: Chem.* **1999**, *59*, 26.

(259) Shin, J.; Choi, S.-J.; Lee, I.; Youn, D.-Y.; Park, C. O.; Lee, J.-H.; Tuller, H. L.; Kim, I.-D. *Adv. Funct. Mater.* **2013**, *23*, 2357.

(260) Bai, X.; Ji, H.; Gao, P.; Zhang, Y.; Sun, X. *Sens. Actuators, B: Chem.* **2014**, *193*, 100.

(261) Karmakar, M.; Mondal, B.; Pal, M.; Mukherjee, K. *Sens. Actuators, B: Chem.* **2014**, *190*, 627.

(262) Chen, D.; Hou, X.; Li, T.; Yin, L.; Fan, B.; Wang, H.; Li, X.; Xu, H.; Lu, H.; Zhang, R.; Sun, J. *Sens. Actuators, B: Chem.* **2011**, *153*, 373.

(263) Gunawan, P.; Mei, L.; Teo, J.; Ma, J.; Highfield, J.; Li, Q.; Zhong, Z. *Langmuir* **2012**, *28*, 14090.

(264) Trung, D. D.; Toan, L. D.; Hong, H. S.; Lam, T. D.; Trung, T.; Hieu, N. V. *Talanta* **2012**, *88*, 152.

(265) Herrán, J.; Ga Mandayo, G.; Ayerdi, I.; Castaño, E. *Sens. Actuators, B: Chem.* **2008**, *129*, 386.

(266) Herrán, J.; Ga Mandayo, G.; Castaño, E. *Thin Solid Films* **2009**, *517*, 6192.

(267) Michel, C. R.; López-Contreras, N. L.; Martínez-Preciado, A. H. *Sens. Actuators, B: Chem.* **2013**, *177*, 390.

(268) Michel, C. R.; Martínez-Preciado, A. H.; Contreras, N. L. L. *Sens. Actuators, B: Chem.* **2013**, *184*, 8.

(269) Jinesh, K. B.; Dam, V. A. T.; Swerts, J.; de Nooijer, C.; van Elshocht, S.; Brongersma, S. H.; Crego-Calama, M. *Sens. Actuators, B: Chem.* **2011**, *156*, 276.

(270) Chapelle, A.; Oudrhiri-Hassani, F.; Presmanes, L.; Barnabé, A.; Tailhades, P. *Appl. Surf. Sci.* **2010**, *256*, 4715.

(271) Fan, K.; Qin, H.; Wang, L.; Ju, L.; Hu, J. *Sens. Actuators, B: Chem.* **2013**, *177*, 265.

(272) Jinesh, K. B.; Dam, V. A. T.; Swerts, J.; de Nooijer, C.; van Elshocht, S.; Brongersma, S. H.; Crego-Calama, M. *Sens. Actuators B: Chem.* **2011**, *156*, 276.

(273) Michel, C. R.; López Contreras, N. L.; López-Alvarez, M. A.; Martínez-Preciado, A. H. *Sens. Actuators, B: Chem.* **2012**, *171−172*, 686.

(274) Polleux, J.; Gurlo, A.; Barsan, N.; Weimar, U.; Antonietti, M.; Niederberger, M. *Angew. Chem., Int. Ed.* **2005**, *45*, 261.

(275) Andringa, A.-M.; Meijboom, J. R.; Smits, E. C. P.; Mathijssen, S. G. J.; Blom, P. W. M.; de Leeuw, D. M. *Adv. Funct. Mater.* **2011**, *21*, 100.

(276) Na, C. W.; Woo, H. S.; Kim, I. D.; Lee, J. H. *Chem. Commun.* **2011**, *47*, 5148.

(277) Chen, N.; Li, X.; Wang, X.; Yu, J.; Wang, J.; Tang, Z.; Akbar, S. A. *Sens. Actuators, B: Chem.* **2013**, *188*, 902.

(278) Deng, S.; Tjoa, V.; Fan, H. M.; Tan, H. R.; Sayle, D. C.; Olivo, M.; Mhaisalkar, S.; Wei, J.; Sow, C. H. *J. Am. Chem. Soc.* **2012**, *134*, 4905.

(279) Park, S.; An, S.; Ko, H.; Jin, C.; Lee, C. *ACS Appl. Mater. Interfaces* **2012**, *4*, 3650.

(280) Hoffmann, M. W. G.; Prades, J. D.; Mayrhofer, L.; Hernandez-Ramirez, F.; Järvi, T. T.; Moseler, M.; Waag, A.; Shen, H. *Adv. Funct. Mater.* **2014**, *24*, 595.

(281) Artzi-Gerlitz, R.; Benkstein, K. D.; Lahr, D. L.; Hertz, J. L.; Montgomery, C. B.; Bonevich, J. E.; Semancik, S.; Tarlov, M. J. *Sens. Actuators, B: Chem.* **2009**, *136*, 257.

(282) Bai, S.; Zhang, K.; Luo, R.; Li, D.; Chen, A.; Liu, C.-C. *Mater. Lett.* **2013**, *111*, 32.

(283) Breedon, M.; Spizzirri, P.; Taylor, M.; du Plessis, J.; McCulloch, D.; Zhu, J.; Yu, L.; Hu, Z.; Rix, C.; Wlodarski, W.; Kalantar-zadeh, K. *Cryst. Growth Des.* **2010**, *10*, 430.

(284) Hua, Z.; Wang, Y.; Wang, H.; Dong, L. *Sens. Actuators, B: Chem.* **2010**, *150*, 588.

(285) Kida, T.; Nishiyama, A.; Yuasa, M.; Shimanoe, K.; Yamazoe, N. *Sens. Actuators, B: Chem.* **2009**, *135*, 568.

(286) Kim, S.-J.; Hwang, I.-S.; Choi, J.-K.; Lee, J.-H. *Thin Solid Films* **2011**, *519*, 2020.

(287) Lee, C.-Y.; Kim, S.-J.; Hwang, I.-S.; Lee, J.-H. *Sens. Actuators, B: Chem.* **2009**, *142*, 236.

(288) Liu, Z.; Miyauchi, M.; Yamazaki, T.; Shen, Y. *Sens. Actuators, B: Chem.* **2009**, *140*, 514.

(289) Ma, S.; Hu, M.; Zeng, P.; Li, M.; Yan, W.; Li, C. *Mater. Lett.* **2013**, *112*, 12.

(290) Öztürk, S.; Kılınç, N.; Öztürk, Z. Z. *J. Alloys Compd.* **2013**, *581*, 196.

(291) Maeng, S.; Kim, S. W.; Lee, D. H.; Moon, S. E.; Kim, K. C.; Maiti, A. *ACS Appl. Mater. Interfaces* **2014**, *6*, 357.

(292) Wagner, T.; Kohl, C. D.; Morandi, S.; Malagu, C.; Donato, N.; Latino, M.; Neri, G.; Tiemann, M. *Chemistry* **2012**, *18*, 8216.

(293) Stanoiu, A.; Simion, C. E.; Diamandescu, L.; Tarabasanu-Mihaila, D.; Feder, M. *Thin Solid Films* **2012**, *522*, 395.

(294) Hyodo, T.; Inoue, H.; Motomura, H.; Matsuo, K.; Hashishin, T.; Tamaki, J.; Shimizu, Y.; Egashira, M. *Sens. Actuators, B: Chem.* **2010**, *151*, 265.

(295) Kaur, J.; Vankar, V. D.; Bhatnagar, M. C. *Thin Solid Films* **2010**, *518*, 3982.

(296) Das, S.; Chakraborty, S.; Parkash, O.; Kumar, D.; Bandyopadhyay, S.; Samudrala, S. K.; Sen, A.; Maiti, H. S. *Talanta* **2008**, *75*, 385.

(297) Hidalgo, P.; Castro, R. H. R.; Coelho, A. C. V.; Gouvêa, D. *Chem. Mater.* **2005**, *17*, 4149.

(298) Lee, S. C.; Hwang, B. W.; Lee, S. J.; Choi, H. Y.; Kim, S. Y.; Jung, S. Y.; Ragupathy, D.; Lee, D. D.; Kim, J. C. *Sens. Actuators, B: Chem.* **2011**, *160*, 1328.

(299) Liang, X.; Zhong, T.; Quan, B.; Wang, B.; Guan, H. *Sens. Actuators, B: Chem.* **2008**, *134*, 25.

(300) Hui, H.; Lee, Y. C.; Tan, O. K.; Zhou, W.; Peng, N.; Zhang, Q. *Nanotechnology* **2009**, *20*, 115501.

(301) Wang, Z.; Li, Z.; Jiang, T.; Xu, X.; Wang, C. *ACS Appl. Mater. Interfaces* **2013**, *5*, 2013.

(302) Wang, H. T.; Kang, B. S.; Ren, F.; Tien, L. C.; Sadik, P. W.; Norton, D. P.; Pearton, S. J.; Lin, J. *Appl. Phys. Lett.* **2005**, *86*, 243503.

(303) Tien, L. C.; Sadik, P. W.; Norton, D. P.; Voss, L. F.; Pearton, S. J.; Wang, H. T.; Kang, B. S.; Ren, F.; Jun, J.; Lin, J. *Appl. Phys. Lett.* **2005**, *87*, 222106.

(304) Volanti, D. P.; Felix, A. A.; Orlandi, M. O.; Whitfield, G.; Yang, D.-J.; Longo, E.; Tuller, H. L.; Varela, J. A. *Adv. Funct. Mater.* **2013**, *23*, 1759.

(305) Liu, B.; Cai, D.; Liu, Y.; Li, H.; Weng, C.; Zeng, G.; Li, Q.; Wang, T. *Nanoscale* **2013**, *5*, 2505.

(306) Choi, Y.-H.; Hong, S.-H. *Sens. Actuators, B: Chem.* **2007**, *125*, 504.

(307) Sysoev, V. V.; Button, B. K.; Wepsiec, K.; Dmitriev, S.; Kolmakov, A. *Nano Lett.* **2006**, *6*, 1584.

(308) Jang, B.-H.; Landau, O.; Choi, S.-J.; Shin, J.; Rothschild, A.; Kim, I.-D. *Sens. Actuators, B: Chem.* **2013**, *188*, 156.

(309) Liu, L.; Guo, C.; Li, S.; Wang, L.; Dong, Q.; Li, W. *Sens. Actuators, B: Chem.* **2010**, *150*, 806.

(310) Oleksenko, L. P.; Maksymovych, N. P.; Buvailo, A. I.; Matushko, I. P.; Dollahon, N. *Sens. Actuators, B: Chem.* **2012**, *174*, 39.

(311) Wang, Z.; Li, Z.; Sun, J.; Zhang, H.; Wang, W.; Zheng, W.; Wang, C. *J. Phys. Chem. C* **2010**, *114*, 6100.

(312) Yoo, K. S.; Park, S. H.; Kang, J. H. *Sens. Actuators, B: Chem.* **2005**, *108*, 159.

(313) Wadkar, P.; Bauskar, D.; Patil, P. *Talanta* **2013**, *105*, 327.

(314) Öztürk, S.; Kılınç, N.; Torun, İ.; Kösemen, A.; Şahin, Y.; Öztürk, Z. Z. *Int. J. Hydrogen Energy* **2014**, *39*, 5194.

(315) Das, S. N.; Kar, J. P.; Choi, J.-H.; Lee, T. I.; Moon, K.-J.; Myoung, J.-M. *J. Phys. Chem. C* **2010**, *114*, 1689.

(316) Park, W. J.; Choi, K. J.; Kim, M. H.; Koo, B. H.; Lee, J. L.; Baik, J. M. *ACS Appl. Mater. Interfaces* **2013**, *5*, 6802.

(317) Mridha, S.; Basak, D. *Semicond. Sci. Technol.* **2006**, *21*, 928.

(318) Della Gaspera, E.; Guglielmi, M.; Martucci, A.; Giancaterini, L.; Cantalini, C. *Sens. Actuators, B: Chem.* **2012**, *164*, 54.

(319) Tan, S.-W.; Tsai, J.-H.; Lai, S.-W.; Lo, C.; Lour, W.-S. *Int. J. Hydrogen Energy* **2011**, *36*, 15446.

(320) Kozhushner, M. A.; Trakhtenberg, L. I.; Landerville, A. C.; Oleynik, I. I. *J. Phys. Chem. C* **2013**, *117*, 11562.

(321) Archanjo, B. S.; Silveira, G. V.; Goncalves, A. M.; Alves, D. C.; Ferlauto, A. S.; Lacerda, R. G.; Neves, B. R. *Langmuir* **2009**, *25*, 602.

(322) Hyodo, T.; Shibata, H.; Shimizu, Y.; Egashira, M. *Sens. Actuators, B: Chem.* **2009**, *142*, 97.

(323) Chan, N. Y.; Zhao, M.; Huang, J.; Au, K.; Wong, M. H.; Yao, H. M.; Lu, W.; Chen, Y.; Ong, C. W.; Chan, H. L.; Dai, J. *Adv. Mater.* **2014**, *26*, 5962.

(324) Soleimanpour, A. M.; Khare, S. V.; Jayatissa, A. H. *ACS Appl. Mater. Interfaces* **2012**, *4*, 4651.

(325) Steinebach, H.; Kannan, S.; Rieth, L.; Solzbacher, F. *Sens. Actuators, B: Chem.* **2010**, *151*, 162.

(326) Yaacob, M. H.; Breedon, M.; Kalantar-zadeh, K.; Wlodarski, W. *Sens. Actuators, B: Chem.* **2009**, *137*, 115.

(327) Zhao, M.; Ong, C. W. *Sens. Actuators, B: Chem.* **2012**, *174*, 65.

(328) Alsaif, M. M. Y. A.; Balendhran, S.; Field, M. R.; Latham, K.; Wlodarski, W.; Ou, J. Z.; Kalantar-zadeh, K. *Sens. Actuators, B: Chem.* **2014**, *192*, 196.

(329) Du, N.; Zhang, H.; Chen, B. D.; Ma, X. Y.; Liu, Z. H.; Wu, J. B.; Yang, D. R. *Adv. Mater.* **2007**, *19*, 1641.

(330) Wang, J.; Wei, L.; Zhang, L.; Zhang, J.; Wei, H.; Jiang, C.; Zhang, Y. *J. Mater. Chem.* **2012**, *22*, 20038.

(331) Tai, H.; Jiang, Y.; Xie, G.; Yu, J.; Chen, X.; Ying, Z. *Sens. Actuators, B: Chem.* **2008**, *129*, 319.

(332) Gong, J.; Li, Y.; Hu, Z.; Zhou, Z.; Deng, Y. *J. Phys. Chem. C* **2010**, *114*, 9970.

(333) Mashock, M.; Yu, K.; Cui, S.; Mao, S.; Lu, G.; Chen, J. *ACS Appl. Mater. Interfaces* **2012**, *4*, 4192.

(334) Hou, Y.; Jayatissa, A. H. *Appl. Surf. Sci.* **2014**, *309*, 46.

(335) Minh, V. A.; Tuan, L. A.; Huy, T. Q.; Hung, V. N.; Quy, N. V. *Appl. Surf. Sci.* **2013**, *265*, 458.

(336) Wagh, M. S.; Jain, G. H.; Patil, D. R.; Patil, S. A.; Patil, L. A. *Sens. Actuators, B: Chem.* **2006**, *115*, 128.

(337) Tang, H.; Yan, M.; Zhang, H.; Li, S.; Ma, X.; Wang, M.; Yang, D. *Sens. Actuators, B: Chem.* **2006**, *114*, 910.

(338) Tang, Y.-L.; Li, Z.-J.; Ma, J.-Y.; Guo, Y.-J.; Fu, Y.-Q.; Zu, X.-T. *Sens. Actuators, B: Chem.* **2014**, *201*, 114.

(339) Van Hieu, N.; Thuy, L. T. B.; Chien, N. D. *Sens. Actuators, B: Chem.* **2008**, *129*, 888.

(340) Petrov, V. V.; Nazarova, T. N.; Korolev, A. N.; Kopilova, N. F. *Sens. Actuators, B: Chem.* **2008**, *133*, 291.

(341) Hieu, N. V.; Quang, V. V.; Hoa, N. D.; Kim, D. *Curr. Appl. Phys.* **2011**, *11*, 657.

(342) Srivastava, V.; Jain, K. *Sens. Actuators, B: Chem.* **2008**, *133*, 46.

(343) Lin, C.-W.; Chen, H.-I.; Chen, T.-Y.; Huang, C.-C.; Hsu, C.-S.; Liu, R.-C.; Liu, W.-C. *Sens. Actuators, B: Chem.* **2011**, *160*, 1481.

(344) Shao, F.; Hernández-Ramírez, F.; Prades, J. D.; Fàbrega, C.; Andreu, T.; Morante, J. R. *Appl. Surf. Sci.* **2014**, *311*, 177.

(345) Balamurugan, C.; Bhuvanalogini, G.; Subramania, A. *Sens. Actuators, B: Chem.* **2012**, *168*, 165.

(346) Balamurugan, C.; Lee, D. W. *Sens. Actuators, B: Chem.* **2014**, *192*, 414.

(347) Chaudhari, G. N.; Jagtap, S. V.; Gedam, N. N.; Pawar, M. J.; Sangawar, V. S. *Talanta* **2009**, *78*, 1136.

(348) Izu, N.; Oh-hori, N.; Itou, M.; Shin, W.; Matsubara, I.; Murayama, N. *Sens. Actuators, B: Chem.* **2005**, *108*, 238.

(349) Sotter, E.; Vilanova, X.; Llobet, E.; Vasiliev, A.; Correig, X. *Sens. Actuators, B: Chem.* **2007**, *127*, 567.

(350) Niu, S.; Hu, Y.; Wen, X.; Zhou, Y.; Zhang, F.; Lin, L.; Wang, S.; Wang, Z. L. *Adv. Mater.* **2013**, *25*, 3701.

(351) Minaee, H.; Mousavi, S. H.; Haratizadeh, H.; de Oliveira, P. W. *Thin Solid Films* **2013**, *545*, 8.

(352) Al-Hardan, N.; Abdullah, M. J.; Abdul Aziz, A.; Ahmad, H. *Appl. Surf. Sci.* **2010**, *256*, 3468.

(353) Ahmed, F.; Arshi, N.; Anwar, M. S.; Danish, R.; Koo, B. H. *Curr. Appl. Phys.* **2013**, *13*, S64.

(354) Castañeda, L. *Mater. Sci. Eng., B* **2007**, *139*, 149.

(355) Hu, Y.; Tan, O. K.; Pan, J. S.; Huang, H.; Cao, W. *Sens. Actuators, B: Chem.* **2005**, *108*, 244.

(356) Kaneko, H.; Okamura, T.; Taimatsu, H.; Matsuki, Y.; Nishida, H. *Sens. Actuators, B: Chem.* **2005**, *108*, 331.

(357) Du, X.; George, S. M. *Sens. Actuators, B: Chem.* **2008**, *135*, 152.

(358) Wang, K.; Zhao, T.; Lian, G.; Yu, Q.; Luan, C.; Wang, Q.; Cui, D. *Sens. Actuators, B: Chem.* **2013**, *184*, 33.

(359) Wu, R.-J.; Wu, J.-G.; Yu, M.-R.; Tsai, T.-K.; Yeh, C.-T. *Sens. Actuators, B: Chem.* **2008**, *131*, 306.

(360) Su, J.; Zou, X. X.; Zou, Y. C.; Li, G. D.; Wang, P. P.; Chen, J. S. *Inorg. Chem.* **2013**, *52*, 5924.

(361) Hung, S. C.; Chen, C. W.; Shieh, C. Y.; Chi, G. C.; Fan, R.; Pearton, S. J. *Appl. Phys. Lett.* **2011**, *98*, 223504.

(362) Gerhard, T.; Stefan, B.; Elise, B.; Giorgio, C. M.; Stephan, S.; Anton, K.; Paolo, E. B.; Clemens, H. *Nanotechnology* **2013**, *24*, 315501.

(363) Li, W.; Shen, C.; Wu, G.; Ma, Y.; Gao, Z.; Xia, X.; Du, G. *J. Phys. Chem. C* **2011**, *115*, 21258.

(364) Tricoli, A.; Graf, M.; Mayer, F.; Kuühne, S.; Hierlemann, A.; Pratsinis, S. E. *Adv. Mater.* **2008**, *20*, 3005.

(365) Mädler, L.; Roessler, A.; Pratsinis, S. E.; Sahm, T.; Gurlo, A.; Barsan, N.; Weimar, U. *Sens. Actuators, B: Chem.* **2006**, *114*, 283.

(366) Wang, C.-T.; Chen, M.-T. *Sens. Actuators, B: Chem.* **2010**, *150*, 360.

(367) Zhang, T.; Liu, L.; Qi, Q.; Li, S.; Lu, G. *Sens. Actuators, B: Chem.* **2009**, *139*, 287.

(368) Yang, Z.; Shumao, C.; Jingbo, C.; Leonidas, E. O.; Junhong, C. *Nanotechnology* **2013**, *24*, 025503.

(369) Patil, D.; Patil, P.; Subramanian, V.; Joy, P. A.; Potdar, H. S. *Talanta* **2010**, *81*, 37.

(370) Khoang, N. D.; Hong, H. S.; Trung, D. D.; Duy, N. V.; Hoa, N. D.; Thinh, D. D.; Hieu, N. V. *Sens. Actuators, B: Chem.* **2013**, *181*, 529.

(371) Al-Kuhaili, M. F.; Durrani, S. M. A.; Bakhtiari, I. A. *Appl. Surf. Sci.* **2008**, *255*, 3033.

(372) Yu, M.-R.; Wu, R.-J.; Chavali, M. *Sens. Actuators, B: Chem.* **2011**, *153*, 321.

(373) Lim, S. K.; Hwang, S.-H.; Chang, D.; Kim, S. *Sens. Actuators, B: Chem.* **2010**, *149*, 28.

(374) Wu, R.-J.; Chang, W.-C.; Tsai, K.-M.; Wu, J.-G. *Sens. Actuators, B: Chem.* **2009**, *138*, 35.

(375) Wang, L.; Lou, Z.; Wang, R.; Fei, T.; Zhang, T. *Sens. Actuators, B: Chem.* **2012**, *171−172*, 1180.

(376) Qin, Y.; Zhang, F.; Chen, Y.; Zhou, Y.; Li, J.; Zhu, A.; Luo, Y.; Tian, Y.; Yang, J. *J. Phys. Chem. C* **2012**, *116*, 11994.

(377) Choi, S. J.; Jang, B. H.; Lee, S. J.; Min, B. K.; Rothschild, A.; Kim, I. D. *ACS Appl. Mater. Interfaces* **2014**, *6*, 2588.

(378) Kaur, M.; Jain, N.; Sharma, K.; Bhattacharya, S.; Roy, M.; Tyagi, A. K.; Gupta, S. K.; Yakhmi, J. V. *Sens. Actuators, B: Chem.* **2008**, *133*, 456.

(379) Zhang, F.; Zhu, A.; Luo, Y.; Tian, Y.; Yang, J.; Qin, Y. *J. Phys. Chem. C* **2010**, *114*, 19214.

(380) Li, X.; Wang, Y.; Lei, Y.; Gu, Z. *RSC Adv.* **2012**, *2*, 2302.

(381) Ramgir, N. S.; Ganapathi, S. K.; Kaur, M.; Datta, N.; Muthe, K. P.; Aswal, D. K.; Gupta, S. K.; Yakhmi, J. V. *Sens. Actuators, B: Chem.* **2010**, *151*, 90.

(382) Chen, J.; Wang, K.; Hartman, L.; Zhou, W. *J. Phys. Chem. C* **2008**, *112*, 16017.

(383) Kim, H.; Jin, C.; Park, S.; Kim, S.; Lee, C. *Sens. Actuators, B: Chem.* **2012**, *161*, 594.

(384) Jain, G. H.; Patil, L. A. *Sens. Actuators, B: Chem.* **2007**, *123*, 246.

(385) Chowdhuri, A.; Singh, S. K.; Sreenivas, K.; Gupta, V. *Sens. Actuators, B: Chem.* **2010**, *145*, 155.

(386) Xue, X.; Xing, L.; Chen, Y.; Shi, S.; Wang, Y.; Wang, T. *J. Phys. Chem. C* **2008**, *112*, 12157.

(387) Kersen, Ü.; Holappa, L. *Anal. Chim. Acta* **2006**, *562*, 110.

(388) Zeng, Y.; Zhang, K.; Wang, X.; Sui, Y.; Zou, B.; Zheng, W.; Zou, G. *Sens. Actuators, B: Chem.* **2011**, *159*, 245.

(389) Liao, L.; Lu, H. B.; Li, J. C.; Liu, C.; Fu, D. J.; Liu, Y. L. *Appl. Phys. Lett.* **2007**, *91*, 173110.

(390) Kim, J.; Yong, K. *J. Phys. Chem. C* **2011**, *115*, 7218.

(391) Xu, J.; Wang, X.; Shen, J. *Sens. Actuators, B: Chem.* **2006**, *115*, 642.

(392) Mai, L.; Xu, L.; Gao, Q.; Han, C.; Hu, B.; Pi, Y. *Nano Lett.* **2010**, *10*, 2604.

(393) Munz, M.; Langridge, M. T.; Devarapally, K. K.; Cox, D. C.; Patel, P.; Martin, N. A.; Vargha, G.; Stolojan, V.; White, S.; Curry, R. J. *ACS Appl. Mater. Interfaces* **2013**, *5*, 1197.

(394) Vallejos, S.; Khatko, V.; Aguir, K.; Ngo, K. A.; Calderer, J.; Gràcia, I.; Cané, C.; Llobet, E.; Correig, X. *Sens. Actuators, B: Chem.* **2007**, *126*, 573.

(395) da Silva, L. F.; Catto, A. C.; Avansi, W., Jr.; Cavalcante, L. S.; Andres, J.; Aguir, K.; Mastelaro, V. R.; Longo, E. *Nanoscale* **2014**, *6*, 4058.

(396) Epifani, M.; Comini, E.; Arbiol, J.; Pellicer, E.; Siciliano, P.; Faglia, G.; Morante, J. R. *J. Phys. Chem. C* **2007**, *111*, 13967.

(397) Zhou, S.; Fang, X.; Deng, Z.; Li, D.; Dong, W.; Tao, R.; Meng, G.; Wang, T. *Sens. Actuators, B: Chem.* **2009**, *143*, 119.

(398) Guérin, J.; Aguir, K.; Bendahan, M.; Lambert-Mauriat, C. *Sens. Actuators, B: Chem.* **2005**, *104*, 289.

(399) Labidi, A.; Jacolin, C.; Bendahan, M.; Abdelghani, A.; Guerin, J.; Aguir, K.; Maaref, M. *Sens. Actuators, B: Chem.* **2005**, *106*, 713.

(400) Guérin, J.; Aguir, K.; Bendahan, M. *Sens. Actuators, B: Chem.* **2006**, *119*, 327.

(401) Utembe, S. R.; Hansford, G. M.; Sanderson, M. G.; Freshwater, R. A.; Pratt, K. F. E.; Williams, D. E.; Cox, R. A.; Jones, R. L. *Sens. Actuators, B: Chem.* **2006**, *114*, 507.

(402) Boulmani, R.; Bendahan, M.; Lambert-Mauriat, C.; Gillet, M.; Aguir, K. *Sens. Actuators, B: Chem.* **2007**, *125*, 622.

(403) Guérin, J.; Bendahan, M.; Aguir, K. *Sens. Actuators, B: Chem.* **2008**, *128*, 462.

(404) Belkacem, W.; Labidi, A.; Guérin, J.; Mliki, N.; Aguir, K. *Sens. Actuators, B: Chem.* **2008**, *132*, 196.

(405) Korotcenkov, G.; Blinov, I.; Ivanov, M.; Stetter, J. R. *Sens. Actuators, B: Chem.* **2007**, *120*, 679.

(406) Gaddari, A.; Berger, F.; Amjoud, M.; Sanchez, J. B.; Lahcini, M.; Rhouta, B.; Mezzane, D.; Mavon, C.; Beche, E.; Flaud, V. *Sens. Actuators, B: Chem.* **2013**, *176*, 811.

(407) Berry, L.; Brunet, J. *Sens. Actuators, B: Chem.* **2008**, *129*, 450.

(408) Korotcenkov, G.; Cho, B. K.; Gulina, L.; Tolstoy, V. *Sens. Actuators, B: Chem.* **2009**, *138*, 512.

(409) Epifani, M.; Comini, E.; Arbiol, J.; Diaz, R.; Sergent, N.; Pagnier, T.; Siciliano, P.; Faglia, G.; Morante, J. *Sens. Actuators, B: Chem.* **2008**, *130*, 483.

(410) Bejaoui, A.; Guerin, J.; Zapien, J. A.; Aguir, K. *Sens. Actuators, B: Chem.* **2014**, *190*, 8.

(411) Deng, Z.; Fang, X.; Li, D.; Zhou, S.; Tao, R.; Dong, W.; Wang, T.; Meng, G.; Zhu, X. *J. Alloys Compd.* **2009**, *484*, 619.

(412) Hosoya, Y.; Itagaki, Y.; Aono, H.; Sadaoka, Y. *Sens. Actuators, B: Chem.* **2005**, *108*, 198.

(413) Mori, M.; Itagaki, Y.; Sadaoka, Y. *Sens. Actuators, B: Chem.* **2012**, *163*, 44.

(414) Mastelaro, V. R.; Zílio, S. C.; da Silva, L. F.; Pelissari, P. I.; Bernardi, M. I. B.; Guerin, J.; Aguir, K. *Sens. Actuators, B: Chem.* **2013**, *181*, 919.

(415) Kenanakis, G.; Vernardou, D.; Koudoumas, E.; Kiriakidis, G.; Katsarakis, N. *Sens. Actuators, B: Chem.* **2007**, *124*, 187.